Günther Bauernfeind

Using Functional Near-Infrared Spectroscopy (fNIRS) for Optical Brain-Computer Interface (oBCI) Applications

Dissertation

Institute of Medical Engineering

Graz University of Technology
Kronesgasse 5/II, 8010 Graz, Austria

Supervisor: Ao.Univ.-Prof. Dipl.-Ing. Dr.techn. Hermann Scharfetter

Graz, March 2012

EIDESSTATTLICHE ERKLÄRUNG

Ich erkläre an Eides statt, dass ich die vorliegende Arbeit selbstständig verfasst, andere als die angegebenen Quellen/Hilfsmittel nicht benutzt und die den benutzten Quellen wörtlich und inhaltlich entnommenen Stellen als solche kenntlich gemacht habe.

Graz, am …… ……..
(Unterschrift)

STATUTORY DECLARATION

I declare that I have authored this thesis independently, that I have not used other than the declared sources / resources and that I have explicitly marked all material which has been quoted either literally or by content from the used sources.

…… ……..
date (signature)

Abstract

Functional near-infrared spectroscopy (fNIRS) is a non-invasive technique that can reveal hemodynamic and metabolic changes during cortical activation. In recent years fNIRS has been used mainly to study hemodynamic responses (changes of oxygenated (oxy-Hb) and deoxygenated hemoglobin (deoxy-Hb)) to cognitive, visual and motor tasks. A few years ago fNIRS was proposed as a novel approach in the field of brain-computer interface (BCI) research. Since that time, only a few research groups have investigated different concepts using fNIRS as an alternative to, or in combination with, traditional EEG-based systems for BCI communication. Therefore, there is still ongoing research needed to investigate the full potential of fNIRS.

This thesis consists of two primary parts. Part one focuses on exploring the usefulness of mental arithmetic (MA) as a control strategy for optical BCI (oBCI) systems. The focus of part two is to use operand conditioning, train subjects to influence their hemodynamic signals volitionalyl and use this control for an oBCI.

In the first part special emphasis is put on the investigation of brain patterns caused by the performance of a simple mental MA task and whether these patterns can be classified reasonably well in a single-trial approach. In detail, this part consists of three interrelated studies whereby the goal of the first and second study is to investigate the spatial and temporal nature of activation responses and to examine if these responses are stable and reproducible over multiple subjects. Different experiments were performed using custom made one-channel and commercial multi-channel fNIRS systems. Similar results in both studies could be achieved and give evidence that the activation responses caused by the performance of a simple MA task may be suitable for an oBCI. Therefore, the focus of study three lies on the single-trial classification of these responses by means of cue-based BCI off-line simulations. The offline simulation results confirmed the hypothesis that patterns, caused by the performance of a simple MA, can be classified with approximately 80% accuracy and therefore are a suitable control strategy for oBCI applications.

In the second part investigations are performed on an operand conditioning, which is also known as "biofeedback", approach. In general, in this approach specific parameters of the recorded brain signals are presented to the user, for example in the form of a feedback bar. The user learns, by a trial-and-error strategy, to influence the presented parameter volitionally. In detail, this part consists of two interrelated studies whereby in the first study the focus lies on fNIRS-based feedback-training. Subjects were trained to influence their prefrontal oxy-Hb concentration volitionally and use it finally as a control signal for an oBCI. Out of this investigation, in a preliminary feasibility study, the worldwide first realization of an asynchronous fNIRS based hybrid BCI system is shown and evaluated with a single subject. To do this, the above mentioned oBCI system is combined with a traditional EEG-based BCI system to control an electrical hand orthosis. In this study the subject gained perfect control (100% accuracy) after a short period of training. This result provides evidence that the combination of an oBCI and an EEG-based BCI within a hybrid BCI system may be a suitable control interface.

Kurzfassung

Die funktionelle Nahinfrarotspektroskopie (fNIRS) ist eine nichtinvasive Methode, welche die Detektion von, durch kortikale Aktivierungen induzierten, hämodynamischen und metabolischen Mustern ermöglicht. In den letzten Jahren wurde die fNIRS hauptsächlich zur Untersuchung dieser Muster (Änderungen in der Konzentration von oxygeniertem (oxy-Hb) und deoxygeniertem (deoxy-Hb) Hämoglobin) bei kognitiven, visuellen oder motorischen Tasks verwendet. Vor einiger Zeit wurde auch die Anwendung der fNIRS im Bereich der Brain-Computer Interface (BCI) Forschung als ein weiterer, vielversprechender Ansatz angedacht. Seitdem haben jedoch nur einige wenige Forschungsgruppen Konzepte zur alternativen oder kombinierten Verwendung der fNIRS Methode untersucht, sodass in diesem Bereich noch grundlegende Forschungsarbeit notwendig ist, um das volle Potential der fNIRS auszuschöpfen.

Diese Dissertation besteht aus zwei Hauptteilen. Der erste Teil fokussiert die Verwendung von mentaler Arithmetik (MA) als Kontrollstrategie für optische BCI (oBCI) Systeme. Der Fokus des zweiten Teils wiederum liegt auf der Verwendung des sogenannten "Operand Conditioning" - Ansatzes. Dabei werden Versuchspersonen darauf trainiert ihre hämodynamischen Muster willentlich zu beeinflussen um diese in weiterer Folge als Steuersignale für ein oBCI verwenden zu können.

Im ersten Teil dieser Arbeit liegt der Schwerpunkt im Speziellen auf der Untersuchung von hämodynamischen Aktivierungsmustern welche durch die Ausführung von einfachen MA Aufgaben entstehen. Des weiteren wird die Klassifizierbarkeit dieser Muster auf "Single-Trial"-Basis untersucht. Detaillierter dargestellt, besteht der erste Teil dieser Dissertation aus drei zusammenhängenden Studien, wobei das Hauptaugenmerk in der ersten und zweiten Studie auf der Untersuchung der räumlichen und zeitlichen Eigenschaften der Aktivierungsmuster sowie auf deren Stabilität und Reproduzierbarkeit über mehrere Probanden liegt. Dazu wurden verschiedene Experimente mit einem selbst etwickelten Einkanalsystem sowie einem kommerziell erhältlichen Multikanalsystem durchgeführt. Dabei wurden mit beiden Systemen vergleich-

bare Ergebnisse erzielt, welche darauf hinweisen, dass die durch MA entstehenden Aktivierungsmuster als Kontrollstrategie in einem oBCI System geeignet sind. Demzufolge lag der Schwerpunkt der dritten Studie auf der Single-Trial-Klassifizierung dieser Muster auf Basis einer BCI Offline-Simulation. Es konnte festgestellt werden, dass die durch MA entstehenden Aktivierungsmuster mit einer Genauigkeit von annähernd 80% detektierbar sind und sich somit als Kontrollstrategie für optische BCI (oBCI) Systeme eignen.

Im zweiten Teil dieser Dissertation werden Untersuchungen unter Verwendung des Operand Conditioning Ansatzes, auch als "Biofeedback"-Ansatz bekannt, durchgeführt. Im Allgemeinen werden bei einem solchen Ansatz spezielle Parameter der aufgezeichneten Hirnsignale dem Anwender, zum Beispiel in Form eines Feedback-Balken, rückgemeldet. Der Anwender lernt nun durch praktisches Ausprobieren ("Trial-and-Error"), den präsentierten Parameter willentlich zu beinflussen. Detaillierter dargestellt, besteht der zweite Teil dieser Dissertation aus zwei zusammenhängenden Studien wobei in der ersten Studie der Fokus auf fNIRS basiertem Anwendertraining liegt. Dazu wurden Versuchspersonen darauf trainiert die präfrontale oxy-Hb Konzentration willentlich zu beeinflussen um diese schlussendlich als Kontrollsignal für ein oBCI zu verwenden. Ausgehend von dieser Studie wurde in einer nachfolgenden Machbarkeitsstudie die Realisierung des weltweit ersten, auf fNIRS basierenden, asynchronen hybriden BCI Systems gezeigt, sowie an einer Versuchsperson evaluiert. Dazu wurde das oBCI System mit einem traditionellen, auf EEG basierenden, BCI kombiniert um eine elektrische Handorthese zu steuern. Unter Verwendung des hybriden BCIs war es der Versuchsperson nach kurzer Zeit möglich, die Orthese mit 100%-iger Genauigkeit zu kontrollieren. Dieses Ergebnis gibt Hinweise, dass auch die Kombination von oBCI und traditionellem EEG-basierten BCI in einem hybriden BCI System ein adäquates Kontrollinterface darstellt.

Acknowledgments

Without the help and support of many persons it would not have been possible to complete this work.

First of all, I want to thank my supervisor Prof. Hermann Scharfetter for continous help and advice. Thanks also to Prof. Gert Pfurtscheller, Prof. Christa Neuper and Prof. Gernot R. Müller-Putz for granting me the opportunity to work in the Laboratory of Brain-Computer Interfaces at the Institute for Knowledge Discovery and to write my doctoral thesis. Further thanks to all my colleagues for all the enlightening conversations and the excellent working atmosphere. Also I would like to thank Brendan Z. Allison, Ian Daly and Selina C. Wriessnegger for proofreading and special thanks to my reviewers and examiners Prof. Gerhard Litscher and Prof. Gernot R. Müller-Putz. I also have to acknowledge the support of the Styrian government (project A3-22.N-13/2009-8).

Finally, I would like to thank my parents and my sweetheart Heike for all their support and love.

Contents

List of Abbreviations

BCI	Brain-computer interface
BOLD	Blood oxygen level dependent
BP	Blood pressure
BPdia	Diastolic blood pressure
CAR	Common average reference
CBF	Cerebral blood flow
CBV	Cerebral blood volume
$CMRO_2$	Cerebral metabolic rate of oxygenation
CSP	Common spacial patterns
CW	Continuous wave
Cyt. c ox.	Cytochrome c oxidase
Deoxy-Hb	Deoxygenated hemoglobin
DLPFC	Dorsolateral prefrontal cortex
EEG	Electroencephalography
ERD	Event-related desynchronization
ERDS	Event-related desynchronization and synchronization
ERS	Event-related synchronization
FDT	Frequency-domain technique
fMRI	Functional magnetic resonance imaging
fNIRS	Functional near-infrared spectroscopy
FP	False positive
Hb	Hemoglobin
HMM	Hidden Markov model
ICA	Independent component analysis
LDA	Linear discriminant analysis
MA	Mental arithmetic
Mb	Myoglobin
MEG	Magnetoencephalography
MC	Monte Carlo simulation
MI	Motor imagery
NIR	Near-infrared

NIRI	Near-infrared imaging
NIRS	Near-infrared spectroscopy
OD	Optical density
OT	Optical topography
Oxy-Hb	Oxygenated hemoglobin
PCA	Principal component analysis
PFC	Prefrontal cortex
PET	Positron emission tomography
QDA	Quadratic discriminant analysis
SCP	Slow cortical potential
SSAEP	Steady-state auditory evoked potential
SSEP	Steady-state evoked potential
SSSEP	Steady-state somatosensory evoked potential
SSVEP	Steady-state visual evoked potential
SMR	Sensorimotor rhythm
SQUID	Superconducting quantum interference device
SVM	Support vector machine
TF	Transfer function
TP	True positive
TPSF	Temporal point spread function
TRS	Time-resolved spectroscopy
VLPFC	Ventrolateral prefrontal cortex

List of Tables

List of Figures

Chapter 1

Introduction

> ***"We had discovered the possible existence of an optical window into the body ... if we could now prove its practicality for obtaining significant information about the ongoing metabolic reactions!"***
>
> Frans F. Jöbsis (1999)

1.1 General

Near-infrared spectroscopy (NIRS) is an emerging non-invasive optical technique for the in-vivo assessment of cerebral oxygenation. In recent years multichannel NIRS has been used to study functional activity of the human cerebral cortex to cognitive, visual and motor tasks (e.g. [60, 66, 67, 73, 151, 165, 186]) and appears to be becoming an established diagnostic tool in neonatology (e.g. [70, 166, 169, 182]), pediatrics [26, 170], psychiatry [38, 61, 81] and neurorehabilitation (for a review see [1, 109]). In addition to studying brain functions, NIRS is also an increasingly popular technology used alternatively to [36, 118, 155, 164], or in combination with, electroencephalography (EEG) [54, 128] for brain computer interfaces systems (optical and hybrid BCIs).

The concept of using optical techniques to monitor changes of biological tissues is not new. For example, changes in the optical properties in single myelinated nerve fibers or nerve trunk during repetitive stimulation were already reported at the end of the forties of the last century [68, 97, 98]. However, the foundation stone for the modern non-invasive in-vivo monitoring of cerebral oxygenation with near-infrared light was laid by Frans F. Jöbsis in

1977 [80]. In his pioneering work *"Noninvasive, infrared monitoring of cerebral and myocardial oxygen sufficiency and circulatory parameters"* Jöbsis introduces an optical window (wavelengths around 700 to 1300 nm) in the near-infrared (NIR) spectrum of the light in which the radiation can be effectively transmitted through biological materials over longer distances. He used these findings to monitor, for the first time, oxygen sufficiency and cerebral circulation on cats and the human brain by near-infrared transillumination. Since this time NIRS studies have been performed, in the majority of cases, in neonates (e.g. [22, 31, 32]) using the transcranial cerebral oximetry (for an overview see [96]). A few studies also investigated the usability of NIR light reflected from the cortex to study the adult brain (e.g. [50, 57], but it took more than 15 years before the progress in the NIRS technology allowed researchers to monitor functional activation of the human cerebral cortex. First investigations in this field were performed by Villringer et al. [175], Hoshi and Tamura [77, 78] and Kato et al. [84]. Hoshi and Tamura were also the first who performed multichannel NIRS measurements [78]. They recorded brain activity over frontal, temporal and occipital region of the left and right hemisphere during visual and auditory stimulation as well as in response to various mental tasks by using five commercial NIRS systems in parallel.

This research in the direction of functional mapping of human brain activity with NIR light (called functional NIRS (fNIRS), NIR imaging (NIRI) or optical topography (OT)) was motivated by its simplicity of application compared to other imaging techniques such as functional magnetic resonance imaging (fMRI) or positron emission tomography (PET) [78]. The fNIRS signals are strongly correlated to the fMRI Blood-Oxygen-Level-Dependent (BOLD) signal [157, 160], but compared to fMRI, NIRS has a limited penetration depth (about 25 mm, [124]) and a lower spatial resolution, however, fNIRS exhibits a higher temporal resolution [37]. Compared to PET, fNIRS has a higher temporal resolution and nearly the same spatial resolution and no exogenous contrast medium is necessary. In general the fNIRS devices are smaller and moveable, less expensive, safe for long term use and less susceptible to motion artifacts then the alternatives. This flexibility allows bedside monitoring and recording during a huge number of different tasks.

A few years ago fNIRS was proposed as a novel approach in the field of brain-computer communication. A brain-computer interface (BCI) provides the user with artificial output channels to control external devices by the regulation of brain activity [14]. Coyle et al. [35] were the first to investigate the suitability of fNIRS systems for next-generation BCIs, the so called optical BCI (oBCI) systems. Since that time, a few research groups have investigated

different concepts using fNIRS alternatively to, or in combination with, traditional EEG-based systems for BCI communication [8, 9, 35, 36, 118, 155, 164]. However, there is still ongoing research needed to investigate the full potential of fNIRS in this field. For example, previous studies not only show the feasibility of using motor imagery [35, 36, 155] for oBCI systems, but also other mental tasks, such as mental arithmetic (MA) [8, 9, 118, 139] and music imagery [139, 140], exhibit potential as suitable control tasks. Therefore, it is of interest to investigate the activity patterns during the performance of these types of mental tasks, which areas are involved during the performance, and how the activity of the areas changes over time. Furthermore, a common challenge for BCIs is a stable and reliable classification of single-trial data, especially for mental tasks. For this it is essential to improve the signal to noise ratio (SNR) and to reduce false classifications which may occur in the case of fNIRS primarily due to misclassification of physiological noise [34].

In the following section BCI basics and the necessary components of a BCI system are briefly discussed. Subsequently, a detailed description of the basics and principles of the fNIRS technique is given. A review of the underlying neurophysiological phenomena is followed by a section describing the technical background of fNIRS recordings and the possible approaches (Continuous Wave (CW), Time-resolved spectroscopy (TRS) and Frequency-domain technique (FDT)).

1.2 Brain-computer interfaces

A brain-computer interface (BCI), sometimes also called direct brain interface or brain-machine interface, is a system which provides the user with an artificial output channel that utilizes the information from neuronal activity of the brain and which does not rely on the normal output pathways of peripheral nerves and muscles (for reviews see e.g. [14, 92, 110, 119, 135, 184]). The concept of BCI systems is not new, the first attempt to evaluate the feasibility and practicality of brain computer communication was published more than 30 years ago by Jacques J. Vidal[1] [173]. Since this time a multitude of publications in the field of BCI research from different research groups have emerged. However, the underlying principles and basics are universal.

[1]The author would like to thank Jacques J. Vidal for his impressive talk and enlightening conversation at the 5^{th} international BCI conference held 2011 in Graz, Austria.

In general a BCI system is composed of the following five components (see Figure 1.1).

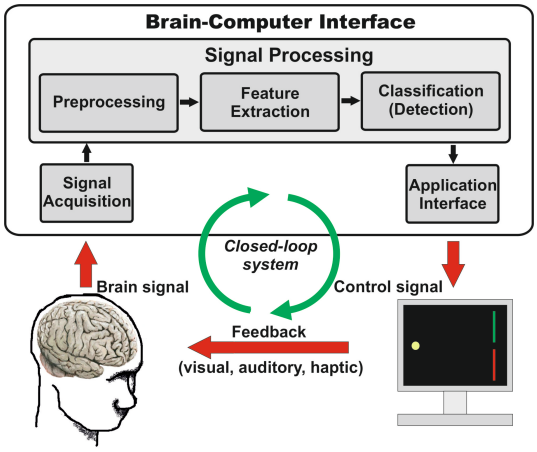

Figure 1.1: General scheme of the different components of a BCI system. This scheme can be found (slightly modified) in numerous articles about BCIs. (Modified from [63].)

Signal acquisition: This component is responsible for the recording of the brain signal(s) used (for details see section 1.2.1) and provides the input signal for the signal processing. Depending on the signal acquisition method used, the signal(s) are amplified and digitized accordingly.

Preprocessing: With the aim to provide optimal data for the subsequent components, this component includes artifact reduction such as reducing / removing signals arising from muscle activity and eye movement or physiological noise (in the case of fNIRS), or canceling out the line-frequency with 50/60 Hz notch filters. Further filtering in the frequency domain, i.e. low-pass or high-pass filtering, spatial filtering (bipolar, Laplacian, Common average reference (CAR)) or more sohisticated methods, like independent component analysis (ICA), principal component analysis (PCA), common spatial patterns (CSP) or tranfer function models, can be applied.

Feature extraction: In this component features, describing important signal properties, are extracted from the data. This step is necessary to find an appropriate representation of the data and to simplify the information, contained in the data, for the next component. Common

features are, for example, amplitude measures, autoregressive parameters, the power in certain frequency bands (band power), wavelets and coupling measures.

Classification (Detection): Provided features from the feature extraction are used to assign the brain signal to a category. Several classification schemes are usable. Popular classifiers are, for example, Fisher's linear discriminant analysis (LDA), the quadratic discriminant analysis (QDA), support vector machines (SVM) and Hidden Markov models (HMM).

Application interface: This component of the BCI system transforms the output of the classifier into a control signal for application devices (e.g. a cursor position on a monitor, the hand position of a hand orthosis or a sound signal) and provides the user with feedback about the assignment of the recorded brain signal to a category. With this feedback the control loop of the BCI system is closed (closed-loop system).

1.2.1 Signals and signal acquisition methods

Typically, a BCI detects voluntary changes in electroencephalography (EEG) signals and translates different brain states into appropriate commands for communication and control [184]. Additionally, other neurophysiological signal types are suitable for extracting information from the brain. The methods can be distinguished, in a first step, by the necessary signal recording technologies into non-invasive and invasive.

Non-invasive technologies

The non-invasive signal acquisition can be further divided into direct and indirect methods. Direct methods, like EEG and magnetoencephalography (MEG) measure activity directly related to the summation of ionic current flows in syncronously working neurons. Signals recorded non-invasively have a limited spatial (especially in the case of EEG) and, partly, temporal resolution when compared to invasively recorded signals. This phenomenon is caused by the scalp, the scull, the cerebrospinal fluid and finally the meninges of the brain which attenuate the electromagnetic signals created by the neurons. Although the activity signals are attenuated, the EEG is the most commonly used signal acquisition method for BCI systems.

Two different neurophysiological phenomena (event-related potentials (ERP) and event-related oscillations) of the EEG are suitable for BCI control. ERPs, including the P300 wave (a component typically induced by an

infrequent task-related stimulus over the parietal cortex) [53, 163], slow cortical potentials (SCP, positive or negative potential shifts in the EEG) [15, 17] and steady-state evoked potentials (SSEP: visual (SSVEP) [108, 115, 144], auditory (SSAEP) [138] or somatosensory (SSSEP) [117] stimuli) are time- and phase-locked responses. In contrast to ERPs, event-related oscillations are only time-locked but not phase-locked to the stimulus and can be seen as changes in the functional connectivity of neuronal networks produced by thalamocortical circuits [39, 120]. This phenomenon was already observed by the neurologist Hans Berger in the early thirties of the last century [12] for alpha EEG activity (8-12 Hz). Berger reported that different events can block the ongoing alpha EEG activity. Additionally, primary sensory or motor areas display oscillations in the frequency range of 8 to 13 Hz (the so-called sensorimotor rhythm (SMR) or mu-rhythm) when they are not activated (e.g. not performing motor execution or motor imagery (MI)). Intensive computer-based investigations on this phenomenon were performend by Pfurtscheller and colleagues in the late seventies [127, 129, 134]. Further, the mu-rhythms can be associated with beta-rhythms in the frequency range of 18 to 26 Hz [131, 133]. Applying these features, the method of event-related desynchronisation (ERD) and event-related synchronisation (ERS) [129, 133] are useful for EEG-based communication [20, 135, 183].

The second method to investigate the electrical activity of the brain in a direct way, is to detect the weak magnetic fields caused by the ionic current flows with MEG. With this technique small fields in the range of pT to fT can be measured with superconducting quantum interference devices (SQUIDs) in a shielded enviroment. Although this technique combines excellent temporal and good spatial resolution, a practical application is unrewarding because of the hardware requirements and operating expenses. Nevertheless, the use of MEG as a signal acquisition method for BCI systems was investigated [19, 85].

In contrast to the direct methods which detect the electrical activity, indirect methods, like fMRI and fNIRS, measure localised changes of the blood-supply related to the neuronal activity (for details see section 1.3.1). In the case of fMRI for BCI [178, 179] the activation of brain regions is mapped in real-time onto a high-resolution brain model of the subject. However, the use of real-time fMRI for BCI requires high performance magnetic resonance scanners and computers as well as techniques for faster acquisition, processing and analysis of magnetic resonance images [153] and therefore a practical application is, like for MEG-based BCI systems, not really preexisting. Just as in the case of fMRI the fNIRS technique measures the metabolic changes in the brain, but in contrast to fMRI the fNIRS devices (for details see section 2.1) are smaller and moveable, less expensive, safe for long term use

and less susceptible to motion artifacts. They are, therefore, more suitable for BCI systems than MEG or fMRI.

Invasive technologies

Different invasive methods like the electrocorticogram (ECoG), where small electrodes are placed directly on the surface of the cortex [94, 149], or implanted intracortically (small electrode arrays are inserted into the cortex) [71, 105], are possible and produce very good results. However, their invasiveness limits the applicability and acceptance.

In conclusion, none of the mentioned (non-)invasive methods (EEG, MEG, fMRI, fNIRS, ECoG, ...) are perfect for signal acquisition, and all have their advantages and disadvantages. However, beside the EEG, which is at the moment the most commonly used signal acquisition method for BCI systems, the fNIRS method also seems to be a promising technique for BCI signal aquisition.

1.2.2 Approaches to BCI Control: The experimental strategy

There exist two different strategies to gain BCI control. The first approach is the so called "operand conditioning" the second approach is the "machine learning" approch.

During operant conditioning, also known as "biofeedback approach" [89], specific parameters (features) of the recorded brain signals are presented to the user, for example, in the form of a feedback bar. The user learns by a trial-and-error strategy to control the presented parameter volitionally. Therefore, the user receives continuous information about the alteration of the parameter. Since feedback is provided, after repeated training different brain states can be reproduced by the user and are suitable for use as control commands [17]. Investigations based on this approach are presented in chapter 4.

In the second approach the training is transferred from the user to the BCI system. To train and adapt the system to a user a sufficient amount of training data is necessary. During training the user is required to repeatedly produce specific brain patterns. From this data, features, describing important signal properties, are extracted offline and used to train and optimize a classifier (e.g. LDA) which can distinguish the specific brain patterns in

an optimal way. The trained classifier is then used online in a subsequent feedback session. Investigations based on this approach are presented in chapter 3.

1.3 Basic concept of fNIRS

1.3.1 Neurophysiological background: The principle of neurovascular coupling

Neurovascular coupling is a term for the interaction between the neuronal (electrical) activity and the consequential changes in the regional cortical blood circulation and metabolism of the brain tissue. The relationship between localised changes of the blood-supply and neural activity (first introduced by Roy and Sherrington in 1890 [146]) is not only the basis for fNIRS recording, but also for other recording techniques (e.g. fMRI or PET) based on vascular responses [102, 174]. However, all these techniques map activity indirectly via hemodynamic changes, for instance changes in the concentration of (de)oxygenated hemoglobin ((de)oxy-Hb)[2] in the case of fNIRS, and therefore, an understanding of this coupling mechanism is essential for interpretation [44].

All human cells, including brain cells, require oxygen (via oxy-Hb) and different essential nutrients to work properly (cellular metabolism). Therefore, the brain tissue is well supplied with blood through a closely intertwined network of blood vessels (arteriols, capillaries and venules). The exhcange of oxygen and nutrients occurs at the capillaries and postcapillary venules which carry metabolic products and the [deoxy-Hb] back to the heart. This *"metabolic activity of the brain is remarkably constant over time"* [143]. The brain represents only 2% of the body weight but requires about 20% of the oxygen and nutrients [18, 29, 143]. Each additional activity of a specific brain region increases the metabolic activity: more oxygen is consumed, the cerebral metabolic rate of oxygenation ($CMRO_2$) changes and therefore triggers a focal increase in the cerebral blood flow (CBF). Such an increase is required because *"ionic gradients degraded by neural activity must be restored and neurotransmitter molecules repackaged"* [24].

However, there is a discrepancy between the $CMRO_2$ and the CBF. Fox and Raichle [58] found that during the resting state an excellent correlation

[2]In the following sections the concentration of oxy-Hb and deoxy-Hb is denoted as [oxy-Hb] and [deoxy-Hb]

between CBF and $CMRO_2$ exists, but during neuronal activation an *"uncoupling"* between both factors occurs. They hypothesized that *"dynamic, physiological regulation of CBF by a mechanism (neuronal or biochemical) dependent on neuronal firing per se, but independent of the cerebral metabolic rate of oxygen"* occurs [58]. These findings, and the results of a follow up study on nonoxidative glucose consumption during neural activity [59], prompted further important studies on basic principles of neurovascular coupling mechanisms.

For example, Malonek and Grinvald [103] investigated the spatiotemporal characteristics of the interactions between neuronal activity and cortical microcirculation by optical imaging spectroscopy (measuring [(de)oxy-Hb]) and reported a sequence of three different physiological events after activation. First, they found a highly localised initial increase in [deoxy-Hb] which occured within 2 s after activation onset. This *"initial dip"* [103] indicates that neuronal activity is accompanied by aerobic metabolism (as a change in the $CMRO_2$). In contrast to the clear occurrence of the increase in [deoxy-Hb] they found only a weak (barely measurable) complementary reduction in [oxy-Hb]. This observation led them to the postulation of a second event which accounts for this weak reduction in [oxy-Hb]: Malonek and Grinvald suggested, taking account the findings of Kuschinsky and Paulson [91], that a fast and highly localized redistribution of the cerebral blood volume (CBV) and the CBF may therefore be responsible. As the third event, a delayed increase of [oxy-Hb] and decrease of [deoxy-Hb], caused by large increases of CBV and CBF, was found. Grinvald and colleagues [103, 167] depicted the resulting excess supply of oxygen, caused by this event, in response to the consumption, caused by the neuronal activity, as *"watering the entire garden for the sake of one thirsty flower"* [103].

Summarizing these findings, there exist three main factors which partially occur at the same time and affect the [oxy-Hb] and [deoxy-Hb] and consequently the attenuation of the NIR light (for a detailed description see chapter 1.3.2). These factors are:

- Cerebral metabolic rate of oxygenation ($CMRO_2$)
- Cerebral blood flow (CBF)
- Cerebral blood volume (CBV)

Wolf et al. [181] investigated the isolated influence of $CMRO_2$, CBF and CBV on [oxy-Hb] and [deoxy-Hb] in detail. On the supposition of a one-compartment model they found the following effects which lead, in combination, to a typical activation induced response of [oxy-Hb] and [deoxy-Hb]:

$CMRO_2$: An isolated increase in the $CMRO_2$ causes an increase in the [deoxy-Hb] and a decrease in [oxy-Hb] (depicted in Figure 1.2). These changes occur because the oxygen is consumed without being replaced sufficiently (aerobic metabolism).

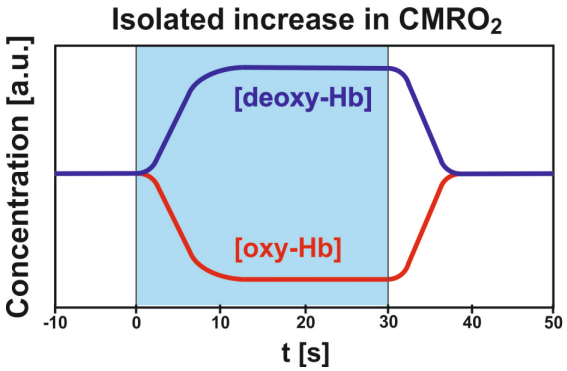

Figure 1.2: Changes of [oxy-Hb] and [deoxy-Hb] related to an isolated increase of the cerebral metabolic rate of oxygenation ($CMRO_2$). (Modified from [181].)

CBF: As shown in Figure 1.3 an increase in the CBF leads to an increase in [oxy-Hb] and a decrease in [deoxy-Hb] because more oxygenated blood will fill the compartment (washout effect) [181].

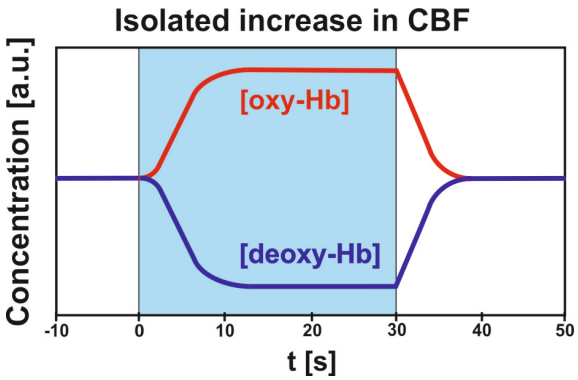

Figure 1.3: Changes of [oxy-Hb] and [deoxy-Hb] related to an isolated increase of the cerebral blood flow (CBF). (Modified from [181].)

CBV: Figure 1.4 shows an increase in both concentrations caused by an increase in the CBV. The difference in [oxy-Hb] and [deoxy-Hb] increase depends on the oxygen saturation of the additional blood [181].

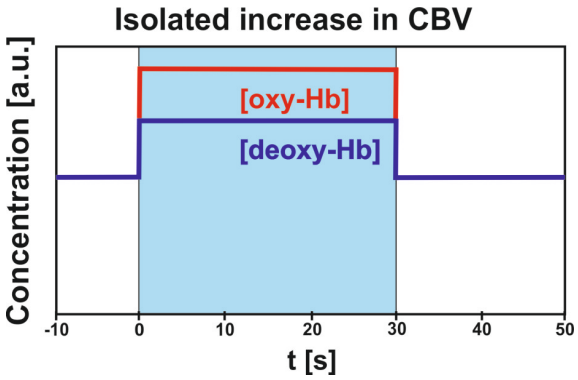

Figure 1.4: Changes of [oxy-Hb] and [deoxy-Hb] related to an isolated increase of the cerebral blood volume (CBV). (Modified from [181].)

Figure 1.5 shows a schematic depiction of the dynamics of a typical activation induced response of [oxy-Hb] and [deoxy-Hb]. As one can see the [deoxy-Hb] response exhibits a biphasic shape [102] during neuronal activation which is, as already mentioned, composed of two factors [103]: An early increase (*"initial dip"*) starting at activity onset (caused by an increase in the $CMRO_2$) is followed by a decrease. This decrease is caused by an increase of CBF and CBV [102]. In contrast the [oxy-Hb] respose exhibits a monophasic shape [102] whereby the [oxy-Hb] increase is dominated by the increases of CBF and CBV. After the end of the activity the [oxy-Hb] and [deoxy-Hb] return to the baseline.

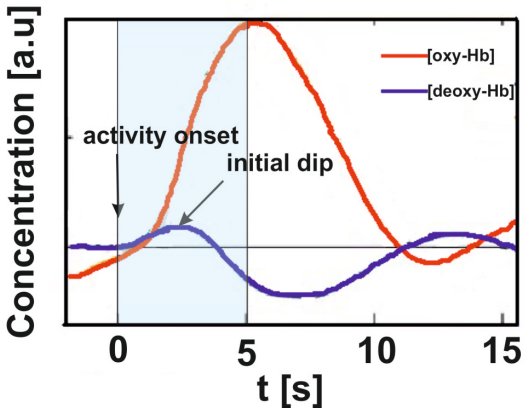

Figure 1.5: Schematic depiction of the typical dynamics of an activation induced response of [oxy-Hb] and [deoxy-Hb].

1.3.2 Technical and physical background

The fNIRS technique uses the optical window in the NIR light spectrum which was found by Jöbsis [80] in 1977. Within this spectral range (wavelengths about 700 to 1300 nm), light can penetrate the cranium and reach sufficient depth [124] to allow an investigation of the metabolism in the cerebral cortex [80].

NIR light, which invades the tissue at a particular place at the head, interacts with the tissue in several ways. The beam becomes diffuse through scattering of the photons in the tissue.

The scattered photons follow a random path through the tissue, resulting in a partial absorption of these photons through compounds in the brain tissue. The interest in fNIRS therefore lies only on a few biological chromophores which exist at reasonable concentrations and which absorb in the given spectral range. Further it is important to differentiate between chromophores (see Figure 1.6[3]) which exist at fixed (e.g. water or lipids), or variable concentrations and, most importantly, which vary their absorbance with the oxidation state (e.g. hemoglobin (Hb) and myoglobin (Mb) or cytochrome c oxidase and other respiratory enzymes). Only these chromophores provide useful information of the changes in the metabolism and consequently on neuronal activity. A detailed description of absorbing componds in the brain tissue and their spectra can be found in the work of Mark Cope [31].

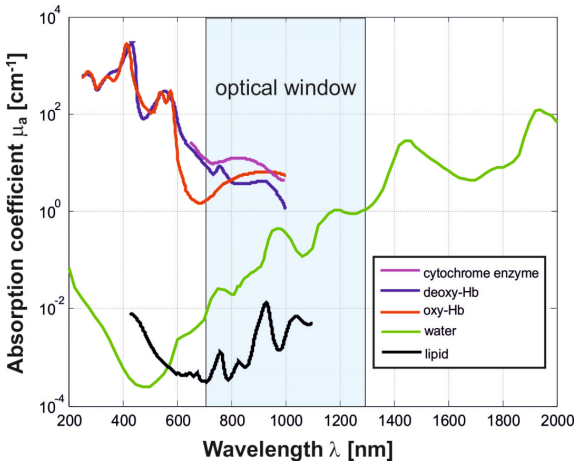

Figure 1.6: Absorption spectra of total tissue cytochrome enzyme, deoxy-Hb, oxy-Hb, water and lipid.

[3]Data for total tissue cytochrome enzyme are taken from [31]; data for deoxy-Hb, oxy-Hb, water and lipid are taken from the Oregon Laser Medical Center (`http://omlc.ogi.edu/spectra/`).

Beside the absorbed photons another part of the photons is back-scattered and leaves the head several centimetre away from the source location [124]. Theoretical (Monte Carlo (MC) simulation) and experimental investigations of Okada et al. [124] have shown that the photons travel in a crescent-shaped path from the source to the detector (see Figure 1.7). If the back-scattered photons are detected over a longer time period it is possible to draw conclusions about metabolic changes in the tissue area that is penetrated by the photons. These changes, such as increased or decreased CBF, CBV or changes in $CMRO_2$ are associated with brain activity (see chapter 1.3.1) and modify the tissue-characteristics. This means that the absorption and scattering of the photons is changed and, hence, affect the detected light. Therefore qualitative measures of brain activity can be obtained by measuring the optical attenuation changes at various wavelengths (λ_i) [175].

While these underlying principles are universal, different approaches for NIRS instruments (Continuous wave (CW), Time-resolved spectroscopy (TRS) and Frequency-domain technique) are useable.

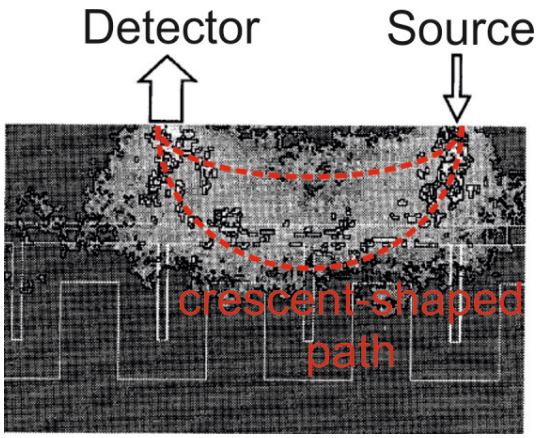

Figure 1.7: Photons travel in a crescent-shaped path from the source to the detector. The figure shows an MC-calculated spatial sensitivity profile (sophisticated brain model) for a source-detector spacing of 30 mm. (Modified from [124].)

Continuous wave (CW) technique

The CW technique is the simplest method for NIRS instruments. All instruments used in this work are based on this technique, therefore a more detailed description is given.

Changes in the transmitted NIR light intensity (see Figure 1.8) are used to calculate relative concentration changes in the chromophores, realized by utilizing Beer-Lambert's law (equation 1.1).

$$A = \log\left(\frac{I_0}{I}\right) = \alpha \cdot c \cdot d, \tag{1.1}$$

A is the attenuation (also known in the literature as optical density (OD)), I_0 [mW] is the light intensity entering the tissue, I [mW] is the light intensity exiting the tissue, α [l/(mol · m)] is the specific extinction coefficient of the absorber (data taken from [31]), c [mol/l] is the concentration of the absorber in the natural unit of Molar concentration [M] and d [m] is the geometrical distance between emitter and detector.

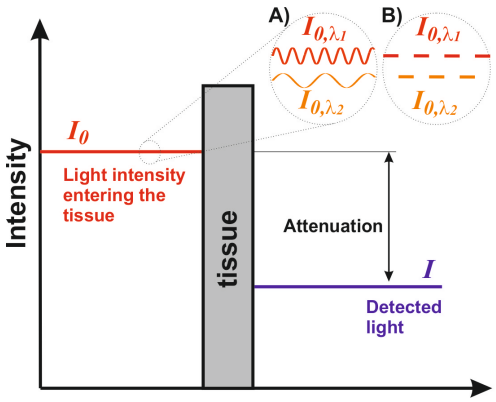

Figure 1.8: Schematic illustration of the CW technique. Light intensity attenuation by the tissue is used to calculate the concentration. If two or more light sources are used, the soures have to be A) modulated with a sine oscillation (see chapter 2.1) or B) multiplexed, in order to separate the light emitted from the sources. (Modified from [42].)

However, as already mentioned biological tissue is a highly scattering medium. Therefore, the photons' path length increases, compared to a transparent medium, as a result of scattering events. This elongated path length leads to higher scattering losses. In order to describe the light absorption process the Beer-Lambert Law has to be modified [43] by terms taking into acount this elongated path length (equation 1.2)

$$A = \log\left(\frac{I_0}{I}\right) = \alpha \cdot c \cdot x \cdot d + K. \tag{1.2}$$

The Beer-Lambert Law is extended by a differential path length factor x (estimated factor, based on empirical studies [47]) which takes into account the increased length and a term K takes into account the scattering loss. This term is influenced by the geometry of the measurement and can be seen as time-invariant in a small time interval [33]. Therefore the attenuation change (caused by a concentration change Δc) between two time points (t_1 and t_2, $t_1 < t_2$) can be expressed by the following equation:

$$\Delta A = \log\left(\frac{I_0}{I(t_2)}\right) - \log\left(\frac{I_0}{I(t_1)}\right) = \alpha \cdot \Delta c \cdot d \cdot x. \tag{1.3}$$

To calculate the concentration changes of oxy-Hb and deoxy-Hb two wavelengths (λ_1, λ_2) are necessary. Therefore equation 1.3 has to be extended for two absorbers and two wavelengths (equation 1.4 and 1.5),

$$\frac{\Delta A_{\lambda_1}}{x_{\lambda_1} \cdot d} = \left(\alpha_{(\lambda_1, oxy-Hb)} \cdot \Delta c_{oxy-Hb} + \alpha_{(\lambda_1, deoxy-Hb)} \cdot \Delta c_{deoxy-Hb}\right) \tag{1.4}$$

and

$$\frac{\Delta A_{\lambda_2}}{x_{\lambda_2} \cdot d} = \left(\alpha_{(\lambda_2, oxy-Hb)} \cdot \Delta c_{oxy-Hb} + \alpha_{(\lambda_2, deoxy-Hb)} \cdot \Delta c_{deoxy-Hb}\right). \tag{1.5}$$

By combining both equations, relative concentration changes of oxy-Hb and deoxy-Hb can be calculated (equation 1.6),

$$\Delta \mathbf{C} = \boldsymbol{\alpha}^{-1} \cdot \Delta \mathbf{A} = \boldsymbol{\alpha}^{-1} \cdot \begin{bmatrix} \frac{\Delta A_{\lambda_1}}{x_{\lambda_1} \cdot d} \\ \frac{\Delta A_{\lambda_2}}{x_{\lambda_2} \cdot d} \end{bmatrix}$$

$$= \begin{bmatrix} \alpha_{(\lambda_1, deoxy-Hb)} & \alpha_{(\lambda_1, oxy-Hb)} \\ \alpha_{(\lambda_2, deoxy-Hb)} & \alpha_{(\lambda_2, oxy-Hb)} \end{bmatrix}^{-1} \cdot \begin{bmatrix} \frac{\Delta A_{\lambda_1}}{x_{\lambda_1} \cdot d} \\ \frac{\Delta A_{\lambda_2}}{x_{\lambda_2} \cdot d} \end{bmatrix} = \begin{bmatrix} \Delta c_{deoxy-Hb} \\ \Delta c_{oxy-Hb} \end{bmatrix}. \tag{1.6}$$

Time-resolved spectroscopy (TRS)

For the TRS, ultrashort laser pulses with a duration of picoseconds are used. The emerging light provides a temporal profile about the optical interaction of the photons with the tissue (see Figure 1.9) [28, 42, 43, 126].

With this approach the mean optical path length L (for a given source detector spacing d) and therefore the differential path length factor x can be derived from the transit time (*"time of flight"*, [28]) t of the light, the speed of light c and the refractive index n [21] of the tissue as follows [28, 43],

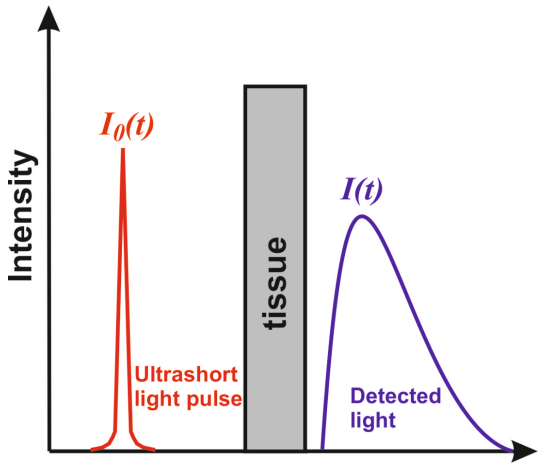

Figure 1.9: Schematic illustration of the temporal profile of an ultrashort (picosecond) pulse, and the emerging intensity. (Modified from [42].)

$$L = x \cdot d = \frac{c \cdot t}{n}. \tag{1.7}$$

By using different wavelengths, absolute concentration values of the absorbers can be calculated. A more detailed description of the TRS technology and the equations used for calculation of absorber concentrations can be found elsewhere [28, 42, 43, 75, 126].

Frequency-domain technique (FDT)

The FDT is a cost-efficient alternative to the TRS method [75]. Theoretically with the FDT the same information as with the TRS can be calculated. For the FDT the NIR light source is modulated with a high frequency oscillation (f, in the range of 100 MHz). The intensity-modulated light passes through the tissue and undergoes an attenuation and an phase shift $\Delta\Phi$ (see Figure 1.10) [42].

For frequencies, f, below 200 MHz this phase shift $\Delta\Phi$ is linearly related to the mean optical path length L [2, 42] which can be calculated, using the speed of light, c, and the refractive index, n, [21] of the tissue, as follows [47],

$$L = \frac{\Delta\Phi \cdot c}{2\pi \cdot f \cdot n}. \tag{1.8}$$

Therefore, with the knowledge of $\Delta\Phi$, a direct conversion of the attenuation into absorber concentration is possible [42]. A detailed description on

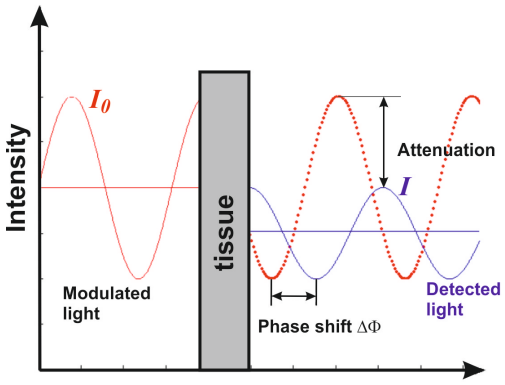

Figure 1.10: Schematic illustration of the Frequency-domain technique (FDT). Attenuation and phase shift are indicated. (Modified from [33, 42].)

the underlying theory, different approaches, and requirements of FDT can be found in [2, 27, 28].

1.4 Aim of this work

The main focus of this work was to explore the usefulness of fNIRS in the field of optical and hybrid brain-computer interfaces. Special emphasis was put on the use of brain patterns caused by the performance of a simple arithmetic task which can be classified reasonably well in a single-trial approach. Further investigations were performed on the biofeedback approach. Out of this approach a preliminary feasibility study was carried out on the use of a hybrid BCI system. This thesis is organized into the following chapters:

Chapter 1 introduces and defines the basics and principles of the fNIRS technique. The underlying neurophysiological phenomena and the technical background of fNIRS recordings are presented in detail. Further BCI basics and the required components of a BCI system are briefly discussed.

Chapter 2 provides a detailed description of the fNIRS systems used in the context of this work. Further signal processing methods used in this thesis are presented. Preprocessing methods to reduce systemic signals which influence the fNIRS recording will be detailed. Finally, feature extraction and classification methods used are discussed.

Chapter 3 describes the concept of using hemodynamic responses caused

by performing MA tasks as a control signal for an oBCI system. This chapter is mainly based on three publications [8, 9, 130].

Chapter 4 describes the realization and evaluation of a real-time feedback system based on a one-channel fNIRS-system for usage as an oBCI. This chapter also includes a case study on using the oBCI system in combination with an SSVEP-based BCI application as a "hybrid" BCI [128].

Chapter 5 contains a summary and conclusion of the present thesis.

Chapter 2

Methods

This chaper provides a detailed description of the fNIRS systems used in the context of this work. Further signal processing methods principally used in this thesis are presented. Preprocessing methods to reduce undesired systemic signals which influence the fNIRS recording will be detailed. Finally, feature extraction and classification methods, which are used in the framework of this thesis, will be briefly discussed.

2.1 Signal acquisition: fNIRS-systems used

2.1.1 One-channel custom-made system

Inspired by the work of Coyle et al. [35] a one-channel fNIRS-system (Figure 2.1) was developed in the framework of a diploma thesis [4, 5]. With this system characteristic hemodynamic responses during cognitive, visual or motor tasks can be measured in real-time. The developed fNIRS-system uses the continuous wave method (chapter 1.3.2) and operates at two different wavelengths. Two light emitting diodes (LEDs) with a wavelength of 670 nm and of 890 nm (L6112-01 and L2656-03, Hamamatsu Photonics K.K., Japan) are used as light sources. Both have a narrow spectral half width (< 50 nm) and a narrow lobe. The LEDs are placed in direct contact with the scalp (see Figure 2.2A). For light detection a single avalanche photodiode (C5460-01, Hamamatsu Photonics K.K., Shizuoka, Japan), connected to the scalp via an optical fiber with a diameter of 2.5 mm, is used. The distance d between LED-sources and detector is 3 cm, which corresponds to a penetration depth of approximately 2.5 cm [124]. In order to separate the light emitted from the two sources, the amplitude of each LED was modulated with a sine oscillation (3 kHz and 7 kHz). A dual lock-in amplifier

(Model 7265, AMETEK Signal Recovery, Oak Ridge, USA) was used to obtain the intensities at the two modulated frequencies. These intensities correspond to the two LED wavelengths. The modulation frequencies have no influence on the absorption coefficients, since they are only determined by the wavelengths of the LED-lights. The output of the lock-in amplifier can be recorded, with different sampling frequencies, by a data acquisition card (NI PCI-6024E, National Instruments, USA). The recording and analysis software is implemented in MATLAB and Simulink (MathWorks) using rtsBCI [147] and BIOSIG (`http://biosig.sf.net`). The fNIRS system measures relative changes of [oxy-Hb] and [deoxy-Hb] (implementation of equation 1.6 in section 1.3.2) in the unit of μmol/l (further denoted as μM) by using an estimated differential path length factor based on empirical studies [47]. For comparison with the commercial multi-channel system the concentrations can also be converted into the unit of mM mm. Since continuous wave systems cannot measure the optical path length [75] the scale unit molar concentration (mmol/l) multiplied by the unknown path length in mm (further denoted as mM mm, for details see chapter 1.3.2) is also prevalent. A picture of the complete setup is given in Figure 2.3.

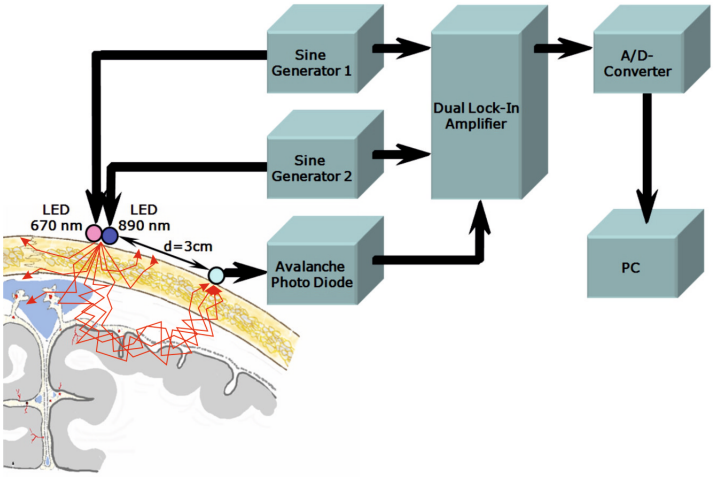

Figure 2.1: Components of the fNIRS-system developed at Graz University of Technology. (Modified from [8].)

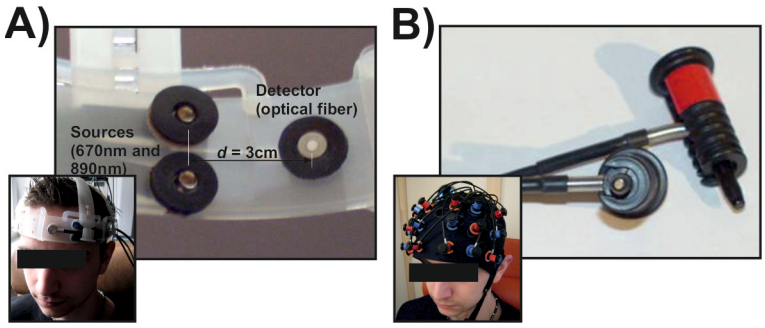

Figure 2.2: A) Optode of the one-channel system and B) of the multi-channel fNIRS-system. Both systems have a source-detector spacing of 3 cm, which corresponds to a penetration depth of approximately 2.5 cm [124]. For further details on the one-channel optode see [4, 5].

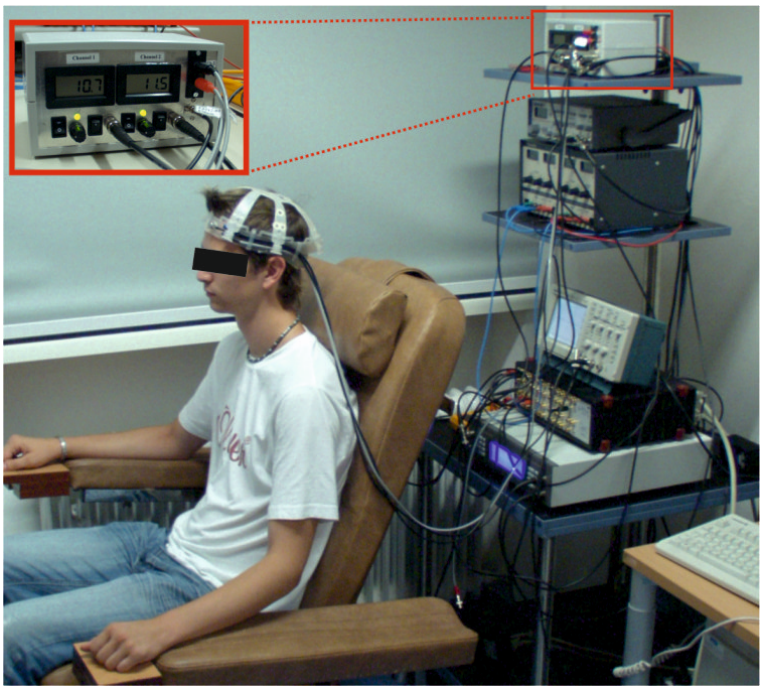

Figure 2.3: Picture of the whole measurement system. The picture in the upper left corner is the main module of the fNIRS system. The hardware tower shows the whole fNIRS setup including the main module, an external signal generator, an external power supply, an oscilloscope for quality check, an ECG amplifier and the lock-in amplifier (from top to bottom). The subject is wearing the helmet used for placing the optodes over the prefrontal cortex. (Modified from [5].)

2.1.2 Commercial multi-channel system

The commercial multi-channel system is an ETG-4000 (Hitachi Medical Co., Osaka, Japan; see Figure 2.4A), also based on the continuous wave principle (section 1.3.2) but using laser diodes as light sources. Different optode probe sets, consisting of a number of photo-detectors and light emitters, resulting in a total of up to 52 channels can be used. Figure 2.5 shows different schematic illustrations of multi-channel arrays and their projections on the cortical surface used for measurements in this thesis (chapter 3.1, 3.2 and 3.3). The system uses two different wavelengths (695 ± 20 nm and 830 ± 20 nm) and its frequency is modulated for wavelengths and channels to prevent crosstalk [168]. The inter-optode distance is equal to the one-channel custom-made system (3 cm), which results in the same penetration depth (approximately 2.5 cm). The fixed sampling rate of the system is 10 Hz. The fNIRS system measures relative changes in oxy-Hb, deoxy-Hb and total Hb concentration in the unit of mM mm.

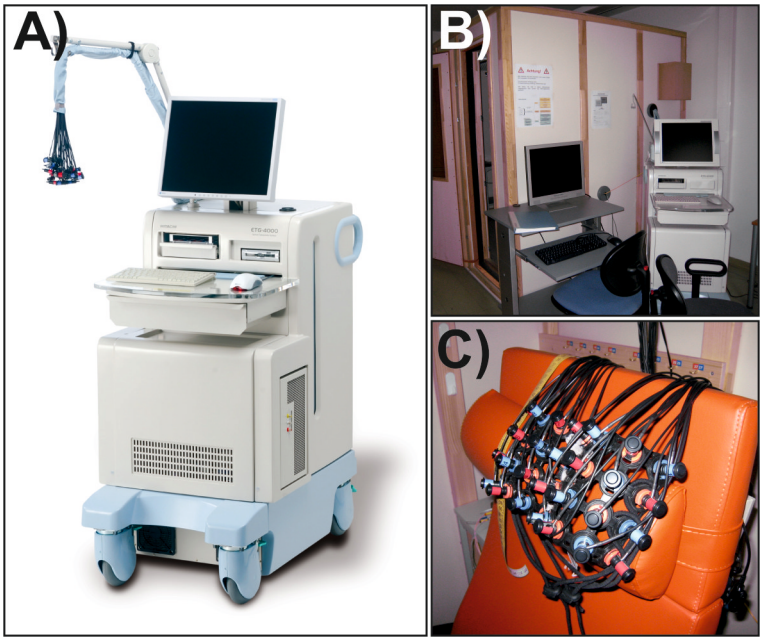

Figure 2.4: A) Picture of the commercial system ETG-4000 (Hitachi Medical Co., Osaka, Japan). B) Recording environment. The system is placed outside a shielded measurement box. C) Multi-channel optode probeset.

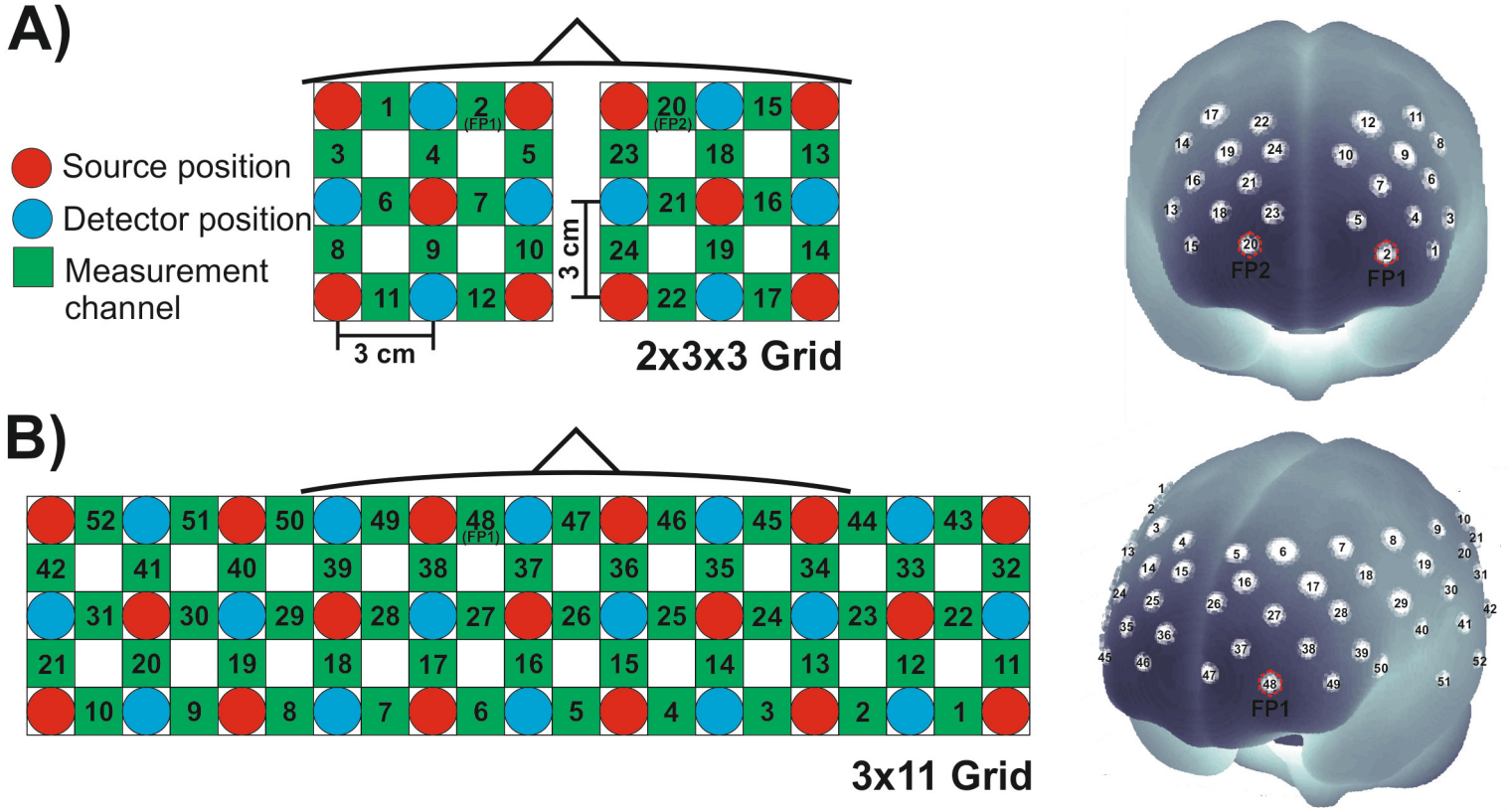

Figure 2.5: Schematic illustration of the multi-channel positional layouts (A) 24 channels, 2x3x3 grid, chapter 3.1 and B) 52 channels, 3x11 grid, chapter 3.2 and 3.3) used in this thesis. The distance between source (colored red) and detector (colored blue) is 3 cm. The recorded channels (colored green) are between neighboring sources and detectors. Furthermore, the projections of the channel positions onto the cortical surface are shown. Positions are overlaid on an MNI-152 compatible canonical brain which is optimized for NIRS analysis [152].

2.2 Signal processing methods

2.2.1 Preprocessing

With fNIRS characteristic hemodynamic changes in [oxy-Hb] and [deoxy-Hb] during cognitive, visual, or motor tasks can be measured (e.g. [60, 67, 66, 73, 151, 165, 186]). For the measurement, the NIR light invades the tissue at a particular place at the head, penetrates the cranium and reaches sufficient depth [124] to interact with the cortical tissue in several ways. Parts of the photons are back-scattered and leave the head several centimeters away from the source location [124]. In order to determine whether the recorded signal is due to a local functional activity of the human cerebral cortex or to global interfering signals of the cardiovascular system, it is essential to identify systemic influences. Figure 2.6 shows a spectral analysis of the recorded [oxy-Hb] signal, revealing various quasi-periodic physiological rhythms. Given the typical time constant of the activation response (about 5 to 10 s, [51, 102]), these rhythms, such as blood pressure (BP), respiratory and cardiovascular rhythms, may influence and superimpose the recorded activation [8, 34, 51, 87].

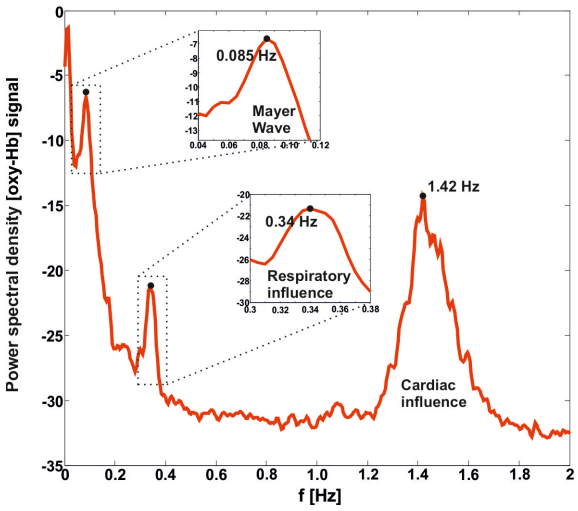

Figure 2.6: Power spectral density of the [oxy-Hb] signal (one subject) showing the influence of pulse waves at frequencies of 1.2-1.7 Hz (equivalent to 72-102 bpm), respiration at around 0.34 Hz (20 breaths/min) and Mayer wave at a frequency of 0.085 Hz.

The frequency of the pulse waves is typically in the range of 1 Hz (60 bpm) to 2 Hz (120 bpm). The respiration frequency lies between 0.2 Hz and 0.4 Hz (around 18 breaths per minute) and the Mayer-Traube-Hering waves

(MTH) [40, 87], which are 3^{rd} order BP waves, occur with a frequency of around 0.1 Hz. The sources of these influences are located in the tissue overlaying the brain as well as in the brain tissue itself. To decrement the influence of these global interfering signals, different methods are suitable. These methods include the usage of different types of low-pass (e.g. [8, 60, 140]) or moving average filters (e.g. [156]) as well as pulse regression [64], peak averaging [36], spatial filtering [130] or more sophisticated methods such as adaptive filtering (e.g. [113, 189]), ICA [52] and PCA [188] (for a review see [104]).

Filters in the frequency domain

Using standard finite impulse response (FIR) or infinite impulse response (IIR) filtering is the simplest approach to improve the signal quality and facilitate the subsequent processing stages. For example, in chapter 3.1 a 0.09 Hz low-pass Butterworth filter of order 4 with 60 dB in the stop band (stop frequency at 0.45 Hz) is used to reduce pulse and respiration related effects. The effects of Mayer waves were not removed with this filter. Furthermore, a 0.01 Hz highpass filter is used to remove baseline drift. Figure 2.7 compares the recorded signal before and after applying the preprocessing step. Further in online studies moving average filters are used to reduce the physiological noise (see chapter 4.1.1 or [156]).

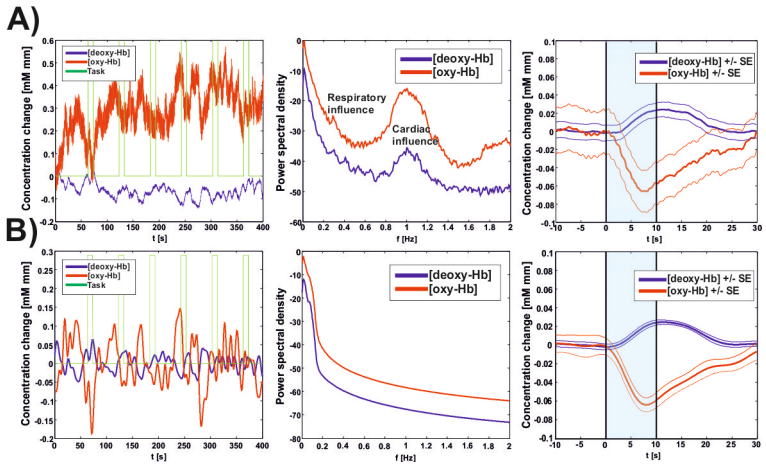

Figure 2.7: Representative case (subject S1, experiment 2, chapter 3.1) of filtering in the frequency domain. A) Time series, power spectral density and averaged response of [oxy-Hb] and [deoxy-Hb] during the performance of an MA task before and B) after applying a 0.09 Hz low-pass and a 0.01 Hz highpass filter.

A disadvantage of such a filtering process is a possible reduction of hemodynamic responses caused by functional activity of the human cerebral cortex as well as the global interfering signals. This is due to the fact that parts of both components may overlap in some frequency bands, especially in the case of Mayer waves, which are located around 0.1 Hz [104, 189]. Therefore other preprocessing procedures might be useful.

Spatial filtering

Some methods to reduce the physiological noise may evolve from approaches used in fMRI or EEG analysis [104, 189]. For example, spatial filters, like bipolar or Laplacian derivation and common average reference (CAR), are used in the analysis of multichannel EEG signals. A new approach, for the first time implemented in [130], is the application of such spatial filters. For example in chapter 3.2 the CAR approach is used to reduce the influence of BP changes in the hemodynamic signal. In EEG recordings CAR is used in order to eliminate the influence of the reference electrode, for fNIRS the idea behind the application of CAR is the fact, that the global interfering signals influence all channels. For this purpose the mean of all channels is calculated and subtracted from each single channel and for every time point. In this way interfering signals should be reduced.

Figure 2.8 shows the application of CAR filtering in the case of a right hand movement task on a representative subject. The measurement grid was arranged above the motor cortex. For fNIRS recording the multichannel continuous wave system (chapter 2.1) was used. Furthermore, the continuous BP signal (CNAP^{TM} Monitor 500, CNSystems Medizintechnik AG, Graz, Austria) and the respiration (resp) were recorded. From the BP signal the diastolic BP (BPdia) was extracted. Figure 2.8A depicts the averaged concentration changes (mean $\pm$ SE) of [oxy-Hb] and [deoxy-Hb] during hand movement execution. As one can see nearly all channels exhibit the same hemodynamic response, which is caused by the performance of the motor task and superimposed by a global BP change (the averaged BPdia response is also shown in the Figure). Additionally, the topographic distribution of the [oxy-Hb] response (calculated for the time range 6 to 8 seconds) indicates an activation pattern over the whole motor cortex. After applying CAR filtering (Figure 2.8B), the global interfering signal is removed and the multichannel map and the topographic distribution of the responses exhibit a clear focal activation pattern, which corresponds to the given task.

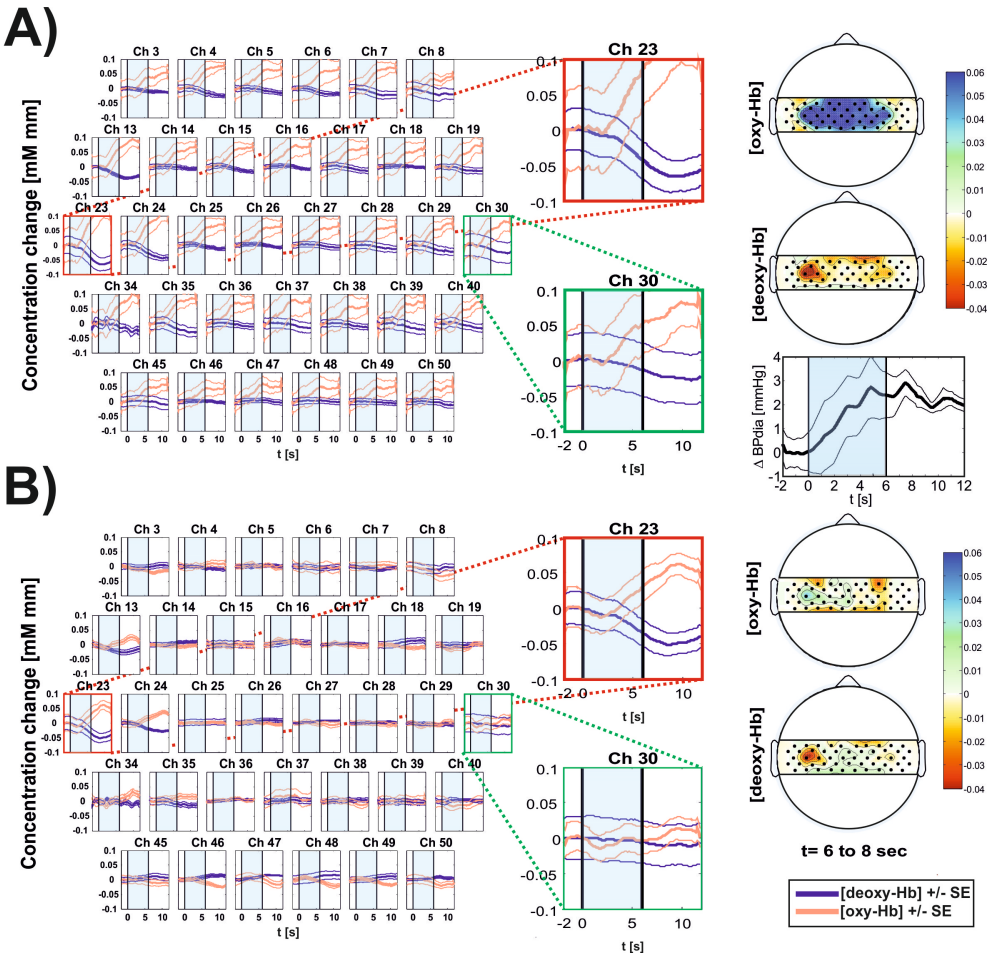

Figure 2.8: An example of applying spatial filtering. A) Averaged concentration changes (mean ± SE) and topographic distribution of [oxy-Hb] and [deoxy-Hb] during hand movement execution (seconds 0 to 6) before and B) after applying CAR filtering. Additionally the averaged BP response which superimposes the hemodynamic activation response is shown.

Other methods currently under investigation

In this section further methods, which are currently under investigation (not used in this thesis), are presented. As mentioned above the application of spatial filters is only usable for multichannel recordings. Therefore other methods, which can be applied on oBCI approaches using only one or two channels (see chapter 3.3 and 4.1) are under investigation by our group. In this part preliminary results on the reduction of physiological rhythms using ICA and transfer function models (TF) are presented. This section is based mainly on one publication [6]:

- **G. Bauernfeind**, I. Daly, and G. R. Müller-Putz. On the removal of physiological artifacts from fNIRS. *Proceedings of the 3rd TOBI Workshop 2012*, 24-25, 2012.

The investigations were carried out on a group of 10 subjects (4 male, 6 female, aged 24.2 ± 4.2 years) who participated in an fNIRS study on the cortical effects of BCI training [7]. In this study the subjects performed sessions of cue-based right hand or feet motor imagery (MI). For fNIRS recordings the multichannel continuous wave system (chapter 2.1) was used. Furthermore, in two of the sessions the continuous BP signal ((CNAP^{TM} Monitor 500, CNSystems Medizintechnik AG, Graz, Austria) and the respiration were recorded. From the BP signal the BPdia was extracted. These two signals (BPdia and resp) were band-pass filtered with 0.07-0.13 Hz and 0.2-0.4 Hz, respectively, and used in the following approaches to reduce the systemic perturbances in the recorded [oxy-Hb] signal.

In the ICA approach[4] the [oxy-Hb] signal is decomposed into independent components (ICs) via SOBI ICA [11]. The coherence between each IC and the BPdia and resp signals is then calculated. ICs for which the coherence with one of the systemic signals is higher than the mean of all the coherence scores with that artifact signal plus 1 standard deviation are flagged for removal. The choice of this threshold is based upon a compromise between removal of the components with the largest coherence with artifact signals and the desire to retain components with small or zero artifact contamination. The remaining ICs not flagged for removal are used to reconstruct the cleaned [oxy-Hb] signals.

[4]Special thanks to Ian Daly for implementing the ICA approach and performing parts of the data analysis.

In the TF approach, by using the BPdia and resp signals, TF models are applied to remove the related perturbation (Figure 2.9 depicts the use of the TF on a representative dataset). These models are in the form of

$$\mathrm{X}[n] = \sum_{u=0}^{m} g_u \mathrm{Y}[n-u] + \mathrm{N}[n], \tag{2.1}$$

where X refers to the time series of the signal and Y to the source of perturbation [55]. The term

$$\sum_{u=0}^{m} g_u \mathrm{Y}[n-u], \tag{2.2}$$

stands for the perturbance and N is the signal without the influence. By minimizing the mean squared error $\mathrm{E}(\mathrm{N}^2[n])$ the parameters g_u of the transfer functions are estimated

$$\gamma_{xy}(-j) = \sum_{u=0}^{m} g_u \gamma_{yy}(u-j), \tag{2.3}$$

with $j = 0, 1, 2, ..., m$ where γ_{xy} is the autocovariance function of $\mathrm{Y}[n]$ and γ_{xy} is the cross-covariance function between $\mathrm{X}[n]$ and $\mathrm{Y}[n]$.
Finally, one needs to find the optimal value of m in equation (2.2). According to [55] the values for m were chosen between 5 and 15. With the calculated parameters of g_u it is now possible to compute the signal without the perturbance

$$\mathrm{N}[n] = \mathrm{X}[n] - \sum_{u=0}^{m} g_u \mathrm{Y}[n-u]. \tag{2.4}$$

For further information on this algorithm see [55].

To compare both approaches the relative [oxy-Hb] power reduction (averaged over the used channels) in the frequency bands between 0.05 and 0.15 Hz, for BP influence (taking into account the frequency roll off of the BPdia processing), and 0.2 and 0.4 Hz, for the respiration, were calculated (Figure 2.10A). Furthermore, the power reduction in the non-influenced bands (0 - 0.05, 0.15 - 0.2 and 0.40 - 0.8 Hz), denoted as stability, was investigated. Good artifact removal will reduce the power in the BP and respiration bands while making no significant changes to the power in the rest of the spectrum. Hence, the lower the stability measure the more accurate the removal of artifacts.

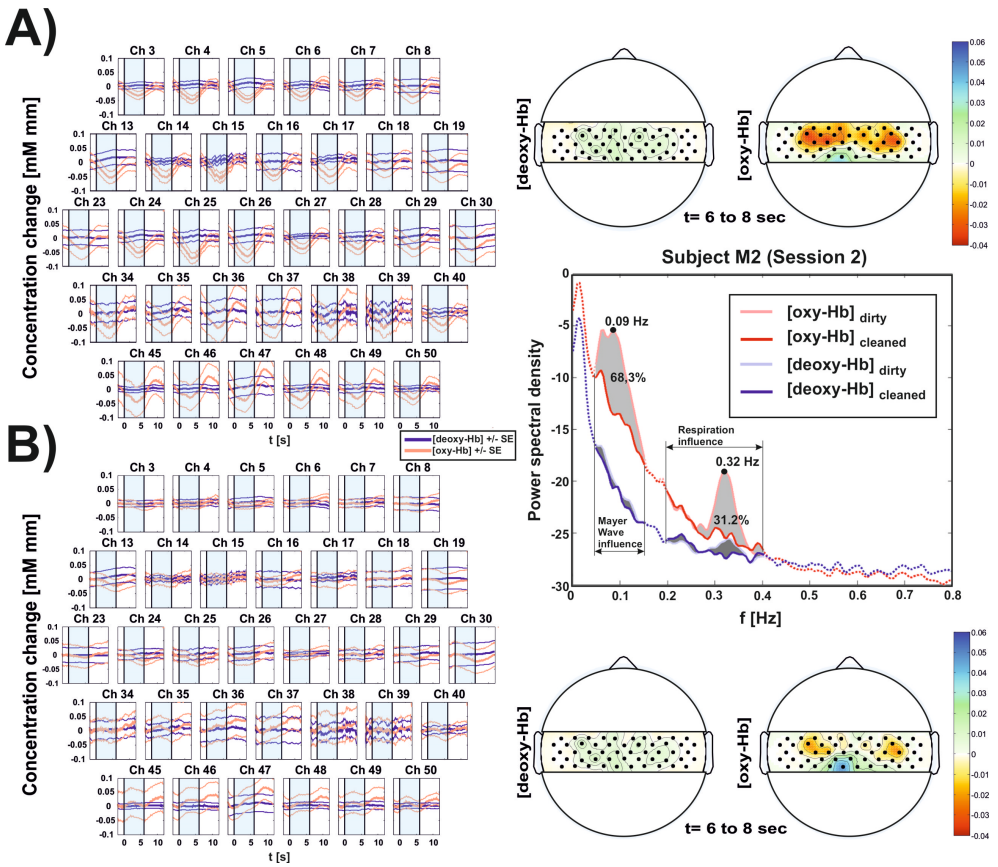

Figure 2.9: Representative case of applying TF models for BP and respiration reduction. A) Averaged concentration changes (mean±SE) and topographic distribution of [oxy-Hb] and [deoxy-Hb] during foot movement imagination (seconds 0 to 6) before and B) after applying TF. Also the power spectrum illustrating percentage reduction in Mayer wave and respiratory rhythms (averaged over all channel) is shown for [oxy-Hb] and [deoxy-Hb].

With TFs a mean reduction of 47% (BP) and 28% (respiration) was possible (Table 2.1). No significant difference (for details see Figure 2.10B) was found between TF and ICA (44% (BP), 18% (respiration)) using Student's t-test. Comparing the stability a significant difference ($t_{(19)}$=-6.11; p<0.01) between ICA (24%) and TFs (0.3%) can be found.

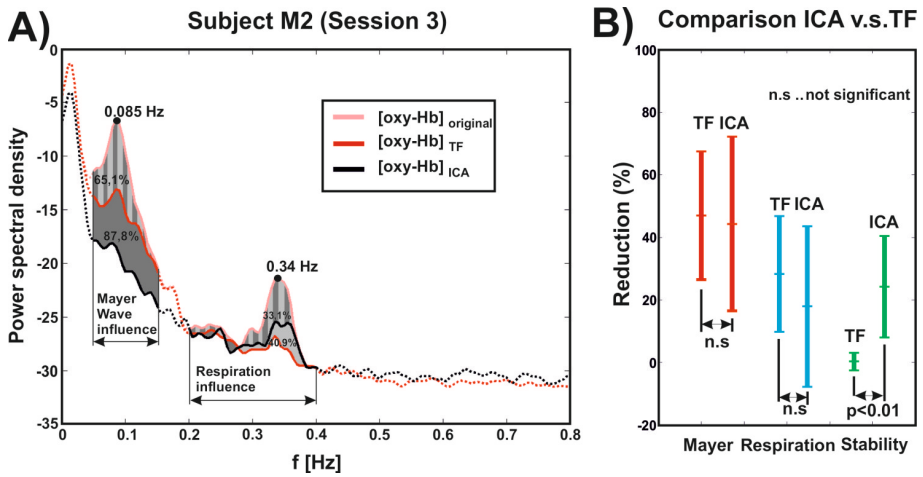

Figure 2.10: A) Example power spectral density illustrating percentage reduction in Mayer wave and respiratory rhythms via ICA and TFs on a representative subject. B) General comparison between ICA and TF. (Modified from [6].)

Both, ICA and TFs, are seen to produce large reductions in Mayer wave and respiratory influences on the [oxy-Hb] signals (Figure 2.10). However, while TFs induce only small changes in non-artifactual signal components ICA induces much larger changes. This suggests that TFs are the most suitable choice for artifact reduction. However, TFs require a large amount (around 60s) of data to estimate the coefficients before they can be applied. By contrast ICA does not require any previous measures of the signal. Hence, while TFs seem to be more suitable for offline analysis in neuroscientific studies ICA may be more suitable for online artifact removal and use in an oBCI.

Table 2.1: Percentage reduction of physiological influences (blood pressure (BP) and respiration (resp.)) and the power reduction in the non-influenced bands (stab.) via ICA and TF approaches.

	Transfer function approach						ICA approach					
	Session 2			Session 3			Session 2			Session 3		
Subj.	BP	resp.	stab.	BP	resp.	stab.	BP	resp.	stab.	BP	resp.	stab.
	%	%	%	%	%	%	%	%	%	%	%	%
M1	48.1	45.4	1.5	37.3	45.0	3.4	36.4	31.9	6.9	32.9	26.8	29.5
M2	68.3	31.2	1.5	65.1	40.9	0.7	67.6	52.4	7.6	87.8	33.1	43.7
M3	45.3	32.4	0.3	11.5	9.4	0.2	59.9	16.7	25.7	2.9	-32.2	5.4
M4	80.1	10.1	0.9	72.5	24.7	0.6	86.7	25.7	35.1	86.9	30.6	20.7
M5	25.5	-0.5	0.1	20.2	3.8	0.1	11.5	8.3	17.0	36.0	14.2	19.2
M6	70.6	17.6	1.2	55.4	12.9	1.1	31.2	30.4	34.8	61.8	18.5	22.3
M7	36.5	45.7	0.5	45.6	48.4	1.6	27.8	-27.3	51.6	-13.4	-5.8	-12.9
M8	69.2	47.1	0.5	17.7	37.5	0.0	45.6	-36.3	22.0	41.3	27.7	30.3
M9	35.1	45.7	2.0	50.6	56.0	1.3	43.0	45.4	39.8	31.0	54.2	11.7
M10	59.6	13.7	0.4	25.1	-0.4	-11.4	75.8	27.6	23.8	33.8	16.5	51.8
mean	53.8	28.8	0.9	40.1	27.8	-0.2	48.5	17.5	26.4	40.0	18.3	21.8
SD	18.3	17.5	0.6	21.1	20.3	4.1	23.5	28.9	14.2	32.1	23.5	18.1

	Overall					
	BP	resp.	stab.	BP	resp.	stab.
	%	%	%	%	%	%
mean	46.9	28.3	0.3	44.3	17.9	24.3
SD	20.5	18.5	2.9	27.8	25.7	16.2

2.2.2 Feature extraction

After the raw signals have been preprocessed, in the next step, features describing important signal properties are extracted from the data. The goal of this step is to find an appropriate representation of the signals and to simplify the signal information for classification.

Genres of features

Different genres of features, e.g. amplitude measures (concentration values of one or more channels at a specific time point or duration), slope (signal slope over a predifined time window), laterality (differences in activity between two spatial measurement positions) and variance (measure of signal spread) are useable. Furthermore, there are four strategies to calculate these features. The first strategy is to use the raw NIR light intensity, the second is to calculate [oxy-Hb] and [deoxy-Hb] signals and use one of these signals alone. The third strategy is to use [oxy-Hb] and [deoxy-Hb] signals together, and the last one is to use total hemoglobin ([Hbtot] = [oxy-HB] + [deoxy-Hb]) signals.

For example, in [9, 36, 100, 155] concentration values of [oxy-Hb] and [deoxy-Hb] are used. Whereas, in [139] only the amplitude measures of NIR light intensity are used. Other studies use, the slope [140] or combine different genres of features [112, 164]. In this thesis amplitude measures of [oxy-Hb] (chapter 3.3, 4.1 and 4.2) as well as [deoxy-Hb], [Hbtot] and pairs of [oxy-Hb] and [deoxy-Hb] (chapter 3.3) are used as features.

Feature selection

After a set of features has been extracted from the signals the next step is to reduce the number of features (too many features lead to a poor generalization of the classification model) and select only those features which are important for detection or which contribute most to a good online separation of the different classes. Normally this step is done offline, whereby different methods to find a suitable subset of features are usable.

An optimal, but time-consuming, approach is to search in all possible feature combinations and choose a subset of features which yields the best result. This approach is known as "exhaustive search" or "brute search" and was used in chapter 3.3 to identify the best performing antagonistic feature combination.

In addition to the exhaustive search, other search strategies (exponential, sequential and randomized algorithms) are suitable if the feature set is too

large. The most popular algorithm, used in many BCI studies, is the so-called sequential floating forward selection (SFFS, for details on this algorithm see [141]).

2.2.3 Classification

Provided features from the feature extraction block are used to assign the brain signal to a category. Several classification schemes are usable. Popular classifiers investigated for use in fNIRS based oBCI systems are Fisher's linear discriminant analysis (LDA [46] used e.g. in [9, 100, 140, 164]), the quadratic discriminant analysis (QDA, used in [140]), support vector machines (SVM [172] used in [155, 164]) and Hidden Markov models (HMM [142] used in [139, 155]).

As Fisher's LDA is used in this thesis, a short description of this classification scheme is given. The LDA is a technique for reducing the dimensionality of the data and identifies a linear hyperplane to discriminate between two different classes (C_1 and C_2, for more than two classes several classifiers can be combined). The hyperplane is chosen in such a way that the distance between the means of the classes is maximized whereas the interclass variance is minimized. Therefore an optimal weight vector $\mathbf{w}$ has to be found from training samples, which optimally separates the two different classes by using a discriminant function y. This function can be written as follows

$$y = \mathbf{w}^T\mathbf{x} + b_0 \tag{2.5}$$

where y is the calculated output value for a candidate feature subset x of an unknown class and b_0 is the bias or threshold. If y is greater than zero the data can be classified as class C_1 or class C_2 if y is less than zero.

Chapter 3

Investigations on the potential feasibility of using simple mental arithmetic for controlling an oBCI

In recent years, the potential feasibility of using functional near-infrared spectroscopy (fNIRS) technology alternatively to (e.g. [36, 118, 155, 164]) or in combination with electroencephalography (EEG) [54, 128] for brain computer interface systems (optical and hybrid BCIs) was investigated. In particular, a number of studies could show that various mental tasks, such as motor imagery [35, 36, 82, 153, 154, 155] as well as mental arithmetic (MA) and mental singing [118, 139, 140] or other higher cognitive tasks [3, 100, 121, 164, 171] are suitable for optical BCI (oBCI) applications. Whereas the use of motor imagery requires optode placement over the motor cortex the use of higher cognitive tasks which are associaded with prefrontal cortex (PFC) activity seems to be more practical and user-friendly (easy and fast optode placement) and suitable for application outside of the lab. In addition a frontal optode placement avoids signal attenuation and motion artifacts caused by hair [36].

It is known that the frontal cortex plays a major role in solving an MA task. Previous neuroimaging studies using functional magnetic resonance imaging (fMRI) exploring arithmetic tasks revealed left-sided and/or bilateral activation of the ventrolateral (VLPFC) and dorsolateral (DLPFC) prefrontal cortex [86, 145, 107] during simple arithmetic operations like one-digit addition, subtraction and multiplication tasks. Furthermore, several neuroscientific studies using fNIRS have also demonstrated the implication of the PFC during MA [72, 76, 77, 165].

This chapter investigates the concept of using hemodynamic responses caused by performing MA tasks as a control signal for an oBCI system and is based mainly on three publications [8, 9, 130]:

- **G. Bauernfeind**, R. Leeb, S. C. Wriessnegger, and G. Pfurtscheller. Development, set-up and first results for a one-channel near-infrared spectroscopy system. *Biomed Tech (Berl)*, 53(1):36-43, 2008.
- G. Pfurtscheller, **G. Bauernfeind**, S. C. Wriessnegger, and C. Neuper. Focal frontal (de)oxyhemoglobin responses during simple arithmetic. *Int J Psychophysiol*, 76(3):186-92, 2010.
- **G. Bauernfeind**, R. Scherer, G. Pfurtscheller, and C. Neuper. Single-trial classification of antagonistic oxyhemoglobin responses during mental arithmetic. *Med Biol Eng Comput*, 49(9):979-984, 2011.

3.1 Study 1: Development, set-up and first results for a one-channel near-infrared spectroscopy system

Different mental arithmetic (MA) experiments were carried out as part of the presented study [8]. All experiments were in compliance with the World Medical Association Declaration of Helsinki. The aim of these experiments was to measure hemodynamic changes in [oxy-Hb] and [deoxy-Hb] caused by different MA tasks to identify stable and reproducible activation patterns and to identify reactive optode positions which could be used for further oBCI experiments.

3.1.1 Materials and methods

Experiment 1

A group of five subjects (S1 to S5; 3 males and 2 females, all right-handed) aged 28.4 ± 6.3 years (mean ± SD) participated in this study using the custom-made one-channel system (for a detailed description of the system see chapter 2.1). For artifact reduction (pulse and respiration related effects) a 0.09 Hz low-pass Butterworth filter of order 4 with 60 dB in the stop band was used. The effects of Mayer waves were not removed with this filter (for further details see chapter 2.2). In addition, a 0.01-Hz highpass filter was

used to remove baseline drift. The subjects were seated in a comfortable armchair. The sources and the detector were placed above the medial area of the anterior prefrontal cortex, 1.5 cm to the left and right of position FP1 (Figure 3.1A), respectively, according to the international 10-20 system for EEG recording [74]. During the task, subjects had to perform an arithmetic operation. In detail, after a visual cue, the subjects had to subtract two three-figure numbers presented on a monitor within 10 s (e.g., 793-247), after that a pause of 30 s followed. One recording session consisted of six trials and lasted approximately 4.3 min. The timing of the experiment is shown in Figure 3.2. Each subject performed four recordings on two days, resulting in 24 trials, except for subject S1, who performed 42 trials (seven recordings in 3 days). From this data the mean task-related concentration changes of [oxy-Hb] and [deoxy-Hb] referred to a 10 s baseline interval prior to the task (seconds -10 to 0) were calculated in the unit of μM.

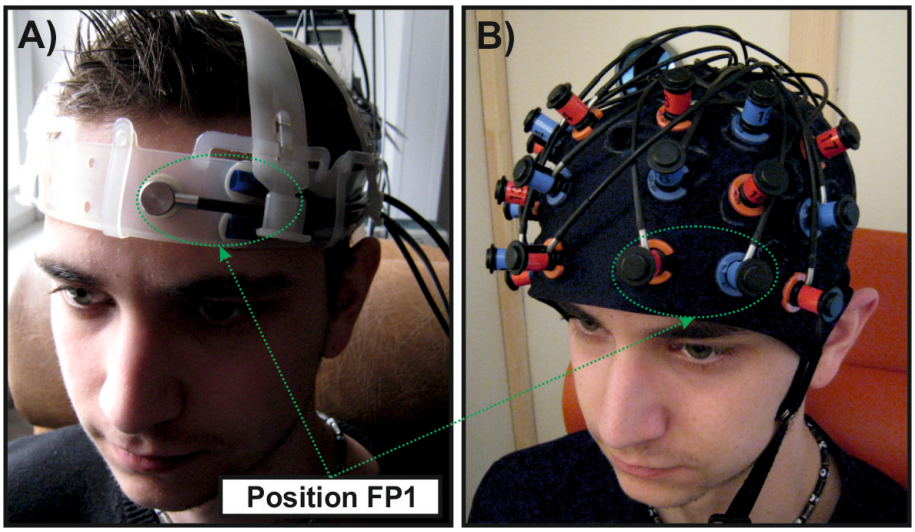

Figure 3.1: A) Optode placement of the one-channel custom-made system (two light emitting diodes, one detector) and B) multi-channel fNIRS-system. The multi-channel array was arranged in such a way that channel 2 was placed over the FP1 position, similar to the one channel-system. (Modified from [8]; Picture with written permission of the subject.)

Experiment 2

Measurements were made for a group of 10 subjects (S1, S5 and S6 to S13; 5 males and 5 females, all right-handed) aged 26.6 $\pm$ 3 years using the one-

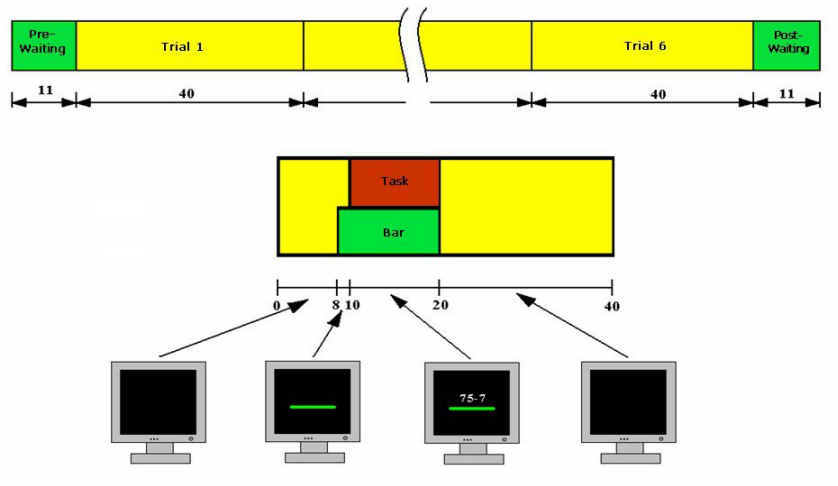

Figure 3.2: Time course of the MA tasks. After a waiting period of 11 s, six trials were performed. The time course of one of these trials is shown separately. 2 seconds before the task started, a green bar appeared. After the cue (e.g., 793-274 for experiment 1 or 78-7 for experiments 2 and 3) the subject had to perform subtractions (repetitively for experiments 2 and 3) for 10 s until the green bar disappeared, which was followed by a pause of 30 s. (Modified from [8].)

channel system. The experimental set-up was the same as for experiment 1, but the task differed. Instead of performing a single subtraction, subjects had to perform repetitive subtractions within a time slot of 10 s (e.g., 97-4=93, 93-4=89, 89-4=85,...; Figure 3.2). For each subject, seven recordings were made on one day, resulting in 42 trials each. Afterwards the mean task-related concentration changes of [oxy-Hb] and [deoxy-Hb] referenced to a 10 s baseline interval prior to the task (seconds -10 to 0) were calculated for each subject.

Experiment 3

To evaluate the results obtained, additional measurements of four subjects (S1, S5, S9, S12) from the group of experiment 2 were performed using a commercial multi-channel fNIRS system (ETG-4000, Hitachi Medical Corporation, Osaka, Japan; for a detailed description of the system see chapter 2.1). The same paradigm was used as in experiment 2. The 24 channel array (a detailed drawing is given in Figure 3.5B) of this system was arranged the way

that channel 2 was placed over the FP1 position, similar to the one-channel system (see Figures 3.1 and 3.5A). The distance between the source and the detector is the same as in the one-channel system ($d = 3$ cm).

The data of experiment 2 (recalculated in mM mm) and 3 were compared with a cross-correlation based on equation 3.1 of the averaged [oxy-Hb] and [deoxy-Hb] responses of channel FP1 of both systems. The data of the whole trial time was used. The Pearson correlation coefficient r_{xy} and the p-values for the hypothesis that both signals are the same, are calculated by:

$$r_{xy} = \frac{s_{xy}}{s_x s_y} = \frac{n\sum x_i y_i - \sum x_i \sum y_i}{\sqrt{n\sum x_i^2 - (\sum x_i)^2}\sqrt{n\sum y_i^2 - (\sum y_i)^2}} \tag{3.1}$$

with n being the length of the signals x and y, s_x and s_y being the standard deviation and s_{xy} the covariance of the two signals. So the correlation coefficients $r_{[oxy-Hb]}$ and $r_{[deoxy-Hb]}$ can be calculated by inserting the one-channel time course as x and the corresponding channel of the multi-channel-recording as y in the above equation.

The significance of the correlation was calculated by testing the null hypothesis that the "product-moment correlation coefficient" is zero using Student's t-test on the statistic $t = r \cdot \frac{\sqrt{n-2}}{\sqrt{1-r^2}}$.

3.1.2 Results

Experiment 1

Mean changes in [oxy-Hb] and [deoxy-Hb] based on 24 trials for five subjects, with the exception of subject S1 (42 trials), are displayed in Figure 3.3. The MA task was always performed between $t = 0$ and 10 s (marked as the shaded area in Figure 3.3). All subjects showed a similar activation pattern involving a decrease in [oxy-Hb] and an increase in [deoxy-Hb].

Experiment 2

The results for seven out of ten subjects based on 42 trials each are shown in Figure 3.4. Owing to exceptionally high intra-record variability caused by fitful breathing during the experimental epoch (e.g., a cessation of breathing when solving the MA task), three subjects did not deliver comparable results and were excluded. The plots reveal the same significant decrease in [oxy-Hb] and increase in [deoxy-Hb] in each subject, as found in experiment 1 (see Figure 3.3), except for S9, who exhibited a decrease in [deoxy-Hb].

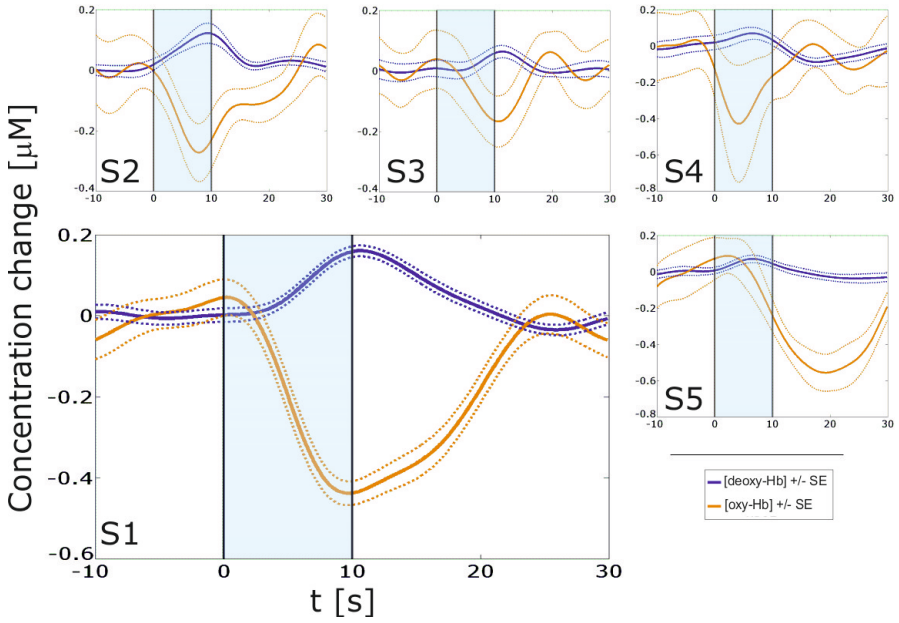

Figure 3.3: Mean concentration changes (mean ± SE) for subjects S1 (enlarged image) and S2 to S5 during mental arithmetic experiment 1 (N = 42). The shaded area indicates the time period of the MA task. [oxy-Hb] is plotted in orange and [deoxy-Hb] in blue. (Modified from [8].)

Experiment 3

The results for four of the subjects who took part in experiment 2 (S1, S5, S9 and S12) are reported in this section and the result for one of these subjects (S1) is shown in Figure 3.5C. The large image shows channel 2, which was placed over position FP1, similar to the experiments with the one-channel system. To compare signals measured with the one-channel system and the multi-channel system, the result from experiment 2 (recalculated in mM mm) is included in the large image. Cross-correlation of [oxy-Hb] and [deoxy-Hb] data for both systems were performed and revealed a highly significant ($p<0.001$ for [oxy-Hb] and [deoxy-Hb]) correlation for all subjects (detailed values are given in Table 3.1). It could be demonstrated that, independently of the fNIRS system used, the same time course of [oxy-Hb] and [deoxy-Hb] changes could be obtained.

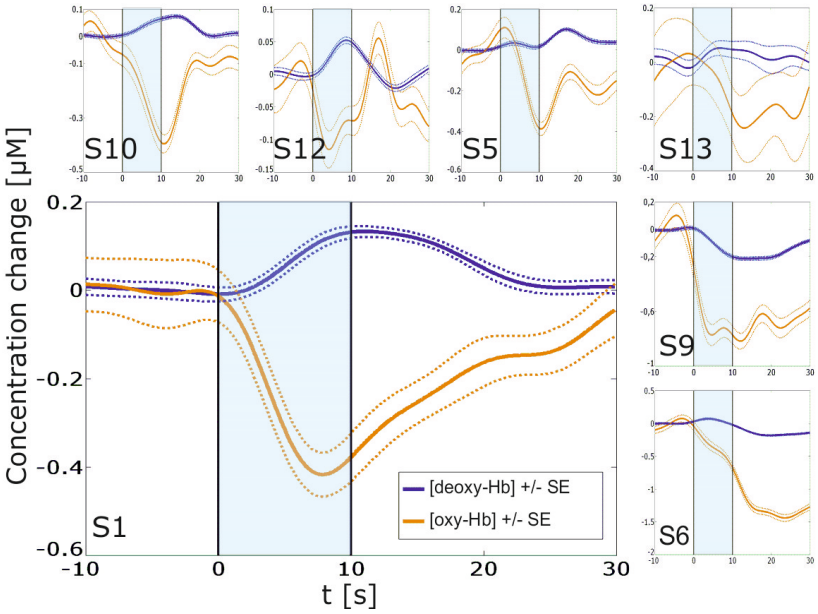

Figure 3.4: Concentration changes (mean ± SE) for 7 subjects (enlarged image, subject S1) during mental arithmetic experiment 2 (based on 42 trials for each subject). (Modified from [8].)

3.1.3 Discussion

The experiments with slightly different MA tasks (one subtraction for experiment 1 and repetitive subtractions within the task for experiments 2 and 3) revealed relatively reproducible results independent of the system used (custom-made one-channel system and commercial multi-channel fNIRS system). Of special interest are the unexpected [oxy-Hb] and [deoxy-Hb] responses during the MA task. In all experiments, with both fNIRS systems, [oxy-Hb] decreased and [deoxy-Hb] increased. This is in contrast to other results reported (e.g. [165] or [187]). For example, Tanida and colleagues investigated the relationship between asymmetry of the prefrontal cortex activity and the automatic nervous system (ANS) response during MA [165]. They found increases of [oxy-Hb] and total hemoglobin (=[oxy-Hb]+[deoxy-Hb]) associated with decreases of [deoxy-Hb] in the bilateral PFC. On the other hand, Hoshi and colleagues [76] found in 9 of 33 healthy subjects the same decrease in [oxy-Hb] and increase in [deoxy-Hb] over frontal regions of the dominant hemisphere during MA tasks performance as reported in this study. However, the remaining 24 subjects showed an increase in [oxy-Hb] and a decrease in [deoxy-Hb].

In principle, one reason for such unexpected [oxy-Hb] and [deoxy-Hb] re-

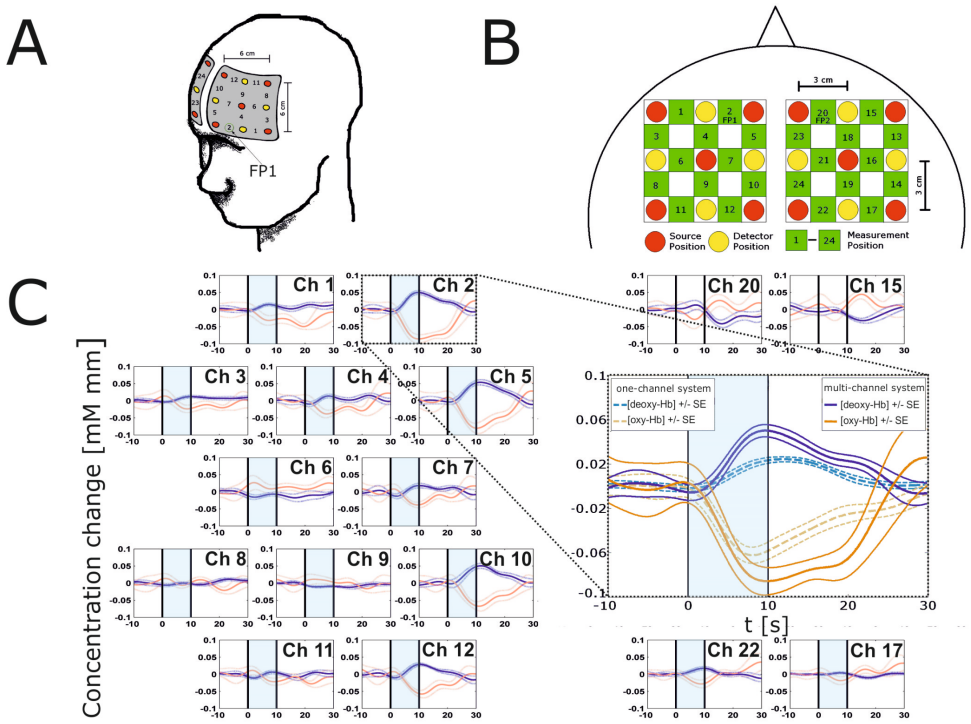

Figure 3.5: A) Schematic illustration of the bilateral positioning of the two 3x3 arrays. B) Positional layout (2x3x3) of the sources and detectors. C) Mean concentration changes (mean ± SE) of 24 channels for subject S1 (42 trials) during the MA task in experiment 3. The enlarged image shows channel 2, which was placed over the FP1 position, similar to the one-channel system. For comparison, the curve shape from experiment 2 is included in the enlarged image. (Modified from [8].)

sponses could be that extracortical (scalp) effects dominate the results, but for a source-detector spacing greater than 20 mm the intensely sensitive region is concentrated to the gray matter [62, 122] and a considerable amount of the signal changes originates from hemodynamic changes at the surface of the brain and in the gray matter [123]. Another argument supporting the assumption that the present data are cerebral signals is that the tissue permeated by the NIR light showed a clear vascular and metabolic response to the experimental task. This conclusion is confirmed by the results of experiment 3, which demonstrated that, independently of the fNIRS system used, the same task-dependent time course for [oxy-Hb] and [deoxy-Hb] changes could be obtained (Figure 3.5C). Another reason for the unexpected responses con-

Table 3.1: Cross-correlation (r) results of the averaged [oxy-Hb] and [deoxy-Hb] responses between both systems during experiments 2 and 3. Highly significant values ($p<0.001$) are marked with a **.

subject ID	$r_{[oxy-Hb]}$	$r_{[deoxy-Hb]}$
S1	0.770 **	0.973 **
S5	0.647 **	0.404 **
S9	0.770 **	0.748 **
S12	0.698 **	0.892 **

cerns the task chosen, since neuronal activation might be more complicated during MA.

The neural networks involved in mental arithmetic operations are distributed over the frontal cortex, the inferior parietal lobule and other areas [41, 86, 107, 145] and are not located exactly under the optodes placed over the frontal brain. Some evidence for this hypothesis can be found in the data of subject S1 in experiment 3 (Figure 3.5C). The signals in channels 5, 10 and 12 were similar to that in channel 2 (FP1 position); in contrast, the channels around channel 6, which corresponds roughly to the dorsolateral prefrontal cortex [125], exhibited different signals. Thus, the frontal [oxy-Hb] decrease and [deoxy-Hb] increase may be explained as a surround effect of an [oxy-Hb] increase and [deoxy-Hb] decrease in areas not yet covered with the measurement grid. Such a surround effect was already reported during EEG recordings and is known as "focal event-related desynchronization / surround event-related synchronization" [162], but has also been observed in blood flow studies [45].

However, the relatively low intra-subject variability in the time course of the hemodynamic response measured over the FP1 position during the MA task and the reproducibility of the response within different MA experiments provide evidence that an MA task is suitable for designing an fNIRS-based oBCI system using only a single channel [36]. Nevertheless, online signal detection with an optical BCI could be relatively easier with antagonistic activation patterns, which means that the hemodynamic responses displaying an opposite polarity (e.g. [oxy-Hb] increase and decrease) at different optode locations. But this needs further inquiry involving a more detailed investigation on the spatial and temporal characteristics of activation patterns caused by the performance of a simple MA task.

3.2 Study 2: Focal frontal (de)oxyhemoglobin responses during simple arithmetic

As stated in the discussion of study 1 (section 3.1), the spatial and temporal characteristics of activation patterns caused by the performance of a simple MA task need further inquiry. Therefore, the purpose of the present study [130] was to examine the changes of [oxy-Hb] and [deoxy-Hb] during the performance of a simple mental arithmetic task over the prefrontal cortex using a commercial multi-channel fNIRS system. A further goal of this study was to determine whether a simple arithmetic task can elicit focal changes of [oxy-Hb] and [deoxy-Hb] over prefrontal cortex locations which can be used for future optical BCI systems.

3.2.1 Material and methods

Subjects and experimental procedure

The investigations were carried out on a group of ten paid University students (five males and five females, all right-handed) aged between 26.1 ± 2.7 years (mean ± SD). The subjects abstained from caffeine before recording, were seated in a comfortable armchair, and gave written informed consent before the experiment. The study was approved by the ethics committee of the Medical University of Graz.

The subjects were asked to serially subtract a one-digit number from a two-digit number (e.g. 97-4; the same task as in experiment 2 and 3 in section 3.1). Prior to each task a 10 s baseline interval was recorded. During the task the subjects had to sequentially subtract a one-digit number from a two-digit number (e.g., 97-4=93, 93-4=89, ...; the initial subtraction was presented visually on a monitor) as quickly as possible for 12 seconds; afterwards, a 28 s resting period followed, resulting in a total trial length of 40 s. During the pause, the subjects were instructed not to move and to stay relaxed by just looking at the black screen. In sum 24 trials were collected. To avoid enhancement of 3^{rd} order BP waves (so called Mayer waves, [40, 87]) or their sub-harmonics, an experimental paradigm with 12 s activity phase and 28 s pause was chosen. It is very important to control these waves since they have large magnitudes and can mask task-related changes [8, 34, 51] (for further details see chapter 2.2).

Data acquisition and processing

A continuous wave system (ETG-4000, Hitachi Medical Corporation, Osaka, Japan; for a detailed description of the system see chapter 2.1) was used to record brain oxygenation. The used optode probeset consists of 16 photo-detectors and 17 light emitters (3x11 grid), resulting in a total of 52 channels. The sampling rate was set to 10 Hz. The distance between source and detector was 3 cm. The lowest line of channels was arranged along the FP1-FP2 line of the international EEG 10-20 system [74], with channel 48 exactly at the FP1 position (Figure 3.6A). In order to allow a probabilistic reference to cortical areas underlying the measurement channels a procedure which projects topographical data based on skull landmarks into a 3D reference frame (MNI-space, Montreal Neurological Institute) optimized for fNIRS analysis [152] was used. So for each fNIRS channel position (Figure 3.6B), a set of MNI coordinates (x, y, and z) was calculated together with an error estimate (SD). The centers of the circle regions represent the locations of the most likely MNI coordinates for the fNIRS channel projected on the cortical surface. The edges represent the boundaries defined by the standard deviation. Furthermore this procedure allows comparison of the results to results provided by similar fMRI studies (e.g. [86, 107, 145]). For further details on the corresponding anatomical structures see [125].

After a visual inspection of the raw fNIRS data, channels with poor signal quality were marked (in three subjects; two, four and nine channels respectively). Afterwards, a common average reference (CAR) spatial filter (for details see chapter 2.2) was used to remove global influences (e.g. changes in heart rate or respiratory influences). Therefore, for every time point, the mean of all non-marked channels was calculated and subtracted from each channel. For artifact reduction, a 0.09 Hz low pass Butterworth filter of order 4 with 60 dB in the stop band was designed. Additionally, a 0.01 Hz high pass filter was used to remove baseline drifts. For further details, see [8]. The subject with nine marked channels displayed too many artifacts and was removed from further analysis, and a second subject showed no stable pattern and was also omitted.

Calculation of task-related changes and topographic distribution

The mean task-related changes of [oxy-Hb] and [deoxy-Hb] referred to a 10 s baseline interval prior to the task (seconds -10 to 0) were calculated for each non-marked channel. For the marked channels, the changes were calculated by interpolating the surrounding channels.

The topographic distributions during the tasks are further visualized by plotting the [oxy-Hb] and [deoxy-Hb] values at their corresponding spatial position. A 2-D interpolation on a fine Cartesian grid was used to generate a scalp distribution. Two different points in time are illustrated. The first point between 0 and 2 s corresponds to the cue presentation and start of the task; the second point between 10 and 12 s corresponds to the end of the task. [oxy-Hb] and [deoxy-Hb] are visualized in different plots, but use the same scale. Increases are plotted in blue and decreases in red (no activation is plotted in white). Examples of the hemodynamic responses at all 52 channels are displayed in Figure 3.7 and 3.8.

Statistical analysis

Two 3x5 repeated measures of analyses (ANOVA) were performed separately for [oxy-Hb] and [deoxy-Hb]. The two factors, "REGIONS OF INTEREST" (ROI: frontal, left, right), and "TIME" (baseline, seconds 8-10, seconds 10-12, seconds 12-14, and seconds 14-16), were used as within-subject variables. The MNI coordinates and anatomical locations of the included channels are given in Table 3.2 and Figure 3.6B. Additionally the effect size measures (η^2) were calculated to obtain information on how strong the effects are [30] and we checked our data for outliers [159]. No outliers were found.

Table 3.2: ROI, channel numbers, MNI coordinates, composite standard deviations for the estimation on the cortical surface (SD) and related Brodmann and anatomical areas.

ROI		Channel	MNI-space correspondence				Cortical areas	
			x	y	z	SD	BA	
1	APFC	46	23	72	8	4	10	SFG
		47	-8	73	6	5	10	MeFG
		48	-31	66	3	5	10	MFG
2	Left DLPFC	18	-51	23	41	5	9	MFG
		28	-47	39	28	6	46	MFG
		29	-61	11	28	6	9	IFG
2	Right DLPFC	13	48	31	42	5	9	MFG
		23	57	26	29	5	46	MFG
		24	45	62	29	5	46	MFG

BA, Brodmann area; SFG, superior frontal gyrus; MFG, middle frontal gyrus IFG, inferior frontal gyrus; MeFG, medial frontal gyrus.

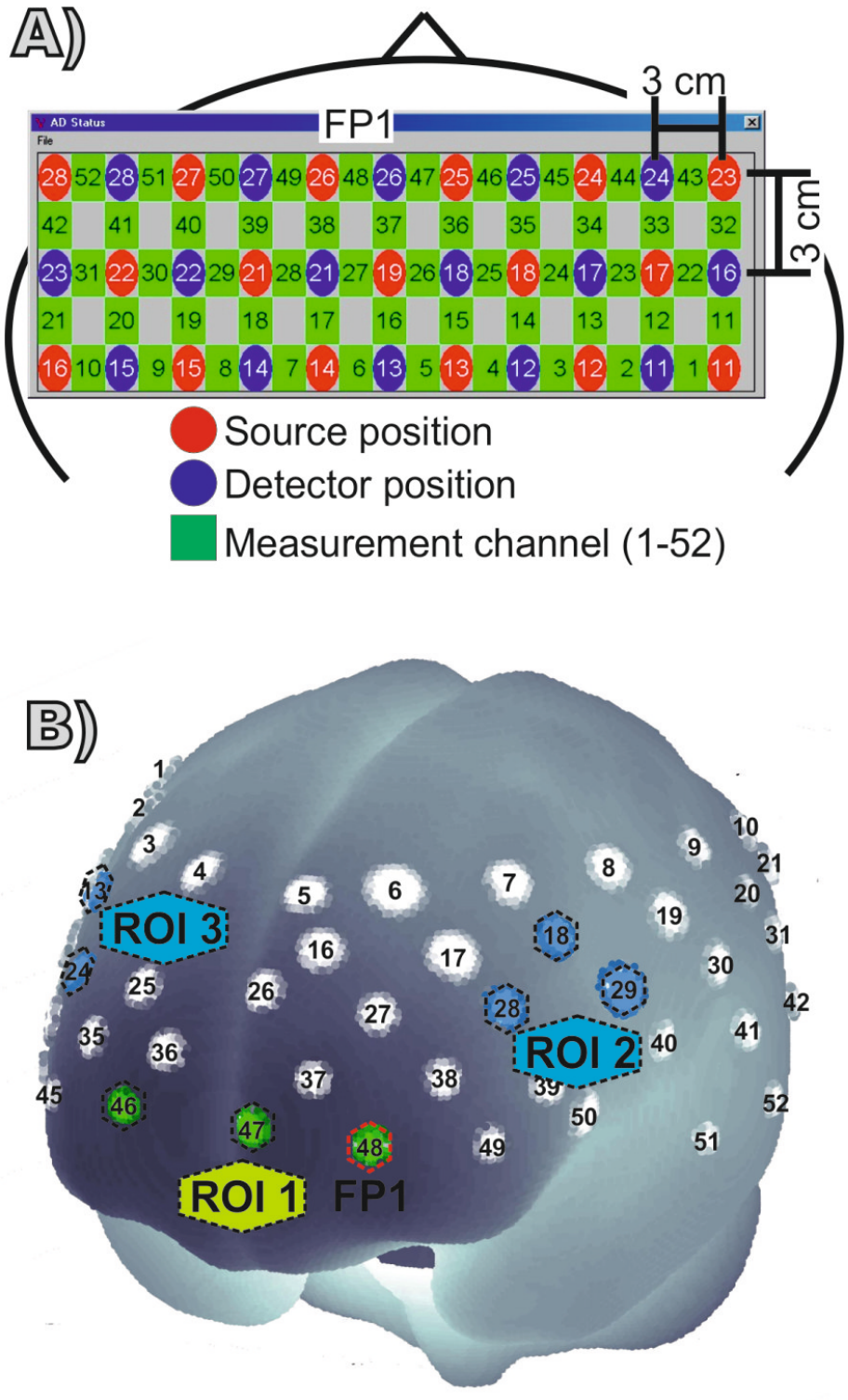

Figure 3.6: A) Schematic illustration of the multi-channel array (52 channels, 3x11 grid). B) Projections of the fNIRS channel positions on the cortical surface. Positions are overlaid on an MNI-152 compatible canonical brain which is optimized for fNIRS analysis [152]. The lowest line of channels was arranged along the FP1-FP2 line of the international EEG 10-20 system, with channel 48 exactly at the FP1 position. (Modified from [130].)

3.2.2 Results

Eight out of ten subjects displayed a relative focal bilateral increase of [oxy-Hb] accompanied by a [deoxy-Hb] decrease in the DLPFC (marked by gray broken line ellipses in the right upper panel of Figure 3.7B). In parallel, they showed a decrease of [oxy-Hb], accompanied by a [deoxy-Hb] increase, in most channels overlaying the medial area of the anterior prefrontal cortex (APFC) (Figure 3.7B, marked by a black broken line ellipsis).

Figure 3.7A presents the grand average hemodynamic responses ([oxy-Hb], [deoxy-Hb]) during the task. The largest and thus most stable [oxy-Hb] decreases in the map are localized at channels 48 (FP1 position) and 37 (3 cm posterior to FP1). The largest [oxy-Hb] increases can be found in the left hemisphere at channel 28 and in the right hemisphere at channel 24. Furthermore a peak latency of the hemodynamic responses in the MA task at second 15, and a delay of the onset of the [oxy-Hb] decrease in the order of 2 s, was found.

For statistical analysis, the averages of 3 channels of each ROI (ROI_1: APFC, ch 46, 47 and 48; ROI_2: left DLPFC, ch 18, 28 and 29; ROI_3: right DLPFC, ch 13, 23 and 24) were calculated. The results of the 3x5 analysis of variance (ANOVA) revealed the following significant findings: for [oxy-Hb] the main effect of ROI revealed significance ($F_{(2,14)}=27.93$; $p<0.01$; $\eta^2 = 0.80$). Furthermore the interaction ROI x time showed significance ($F_{(8,56)}=24.37$; $p<0.01$; $\eta^2=0.78$). The Bonferroni posttest showed a significant change of [oxy-Hb] over left and frontal sites for all time periods compared to the baseline (Figure 3.7A, lower panels). For [deoxy-Hb] no significant main effect of ROI: ($F_{(2,14)}=2.61$; $p<0.11$; $\eta^2=0.27$) could be found. Although the interaction ROI x TIME showed significance ($F_{(8,56)}=3.29$; $p<0.01$; $\eta^2=0.32$) the Bonferroni posttest showed no significant changes of [deoxy-Hb] compared to the baseline. Only in the later time periods significant differences between the frontal and the left and right ROI could be found.

Figure 3.8 shows the hemodynamic responses for a representative subject. This subject also shows a relative focal bilateral increase of [oxy-Hb] in the DLPFC in parallel with a decrease of [oxy-Hb] in the medial area of the APFC. The largest [oxy-Hb] decrease is localized at channel 37 (3 cm posterior to FP1, Figure 3.8, lower panel left), the largest [oxy-Hb] increases can be found in the right hemisphere at channel 24 (Figure 3.8, lower panel right). Note that neighboring channels (ch 27 and 28; ch 24 and 25, marked by broken line ellipses) display significant [oxy-Hb] responses with opposite polarity, which underlines the focal increase/decrease of [oxy-Hb] and [deoxy-Hb] in frontal areas.

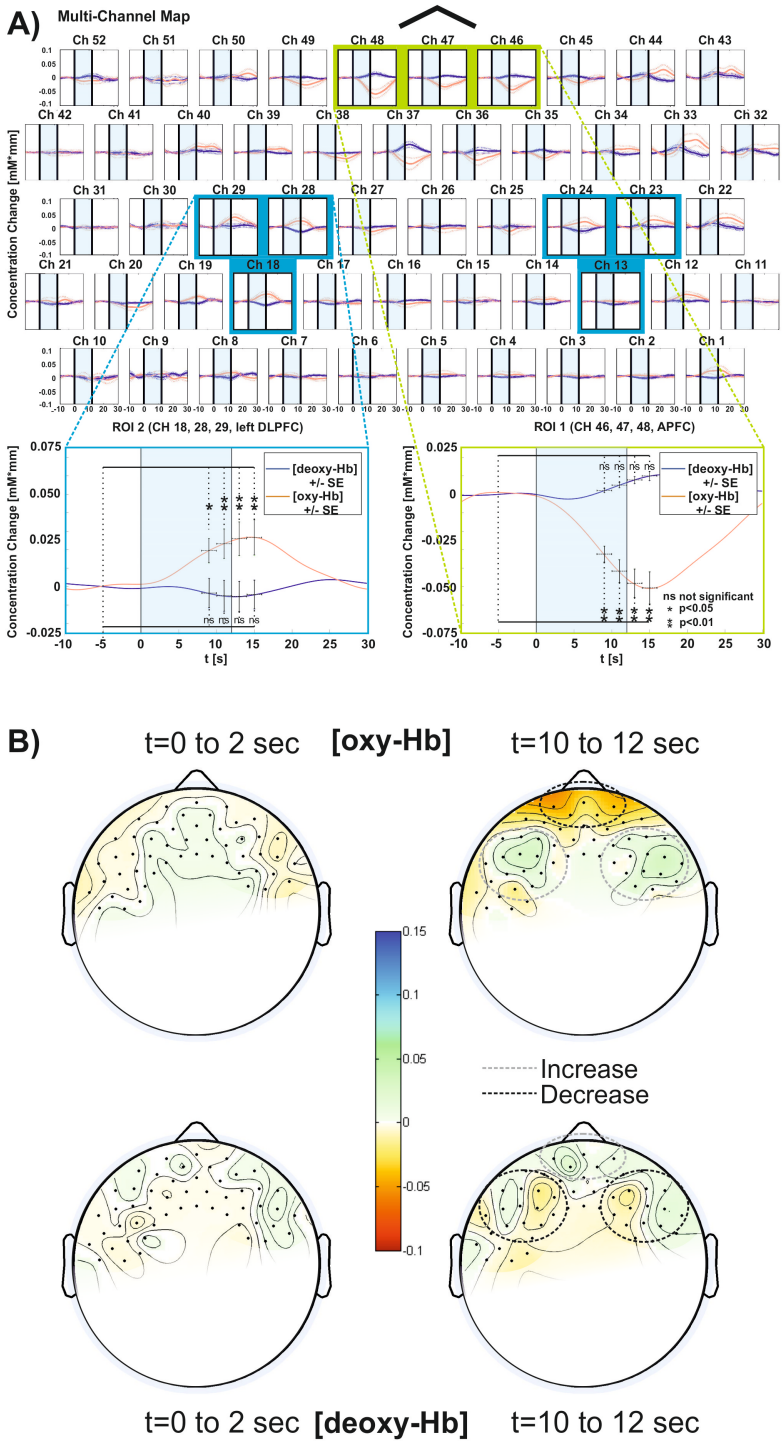

Figure 3.7: A) Grand average (8 subjects) changes (mean ± SE) of [oxy-Hb] and [deoxy-Hb]. The focal bilateral increase of [oxy-Hb] in the DLPFC in parallel with a decrease of [oxy-Hb] in the medial area of the APFC is marked by gray and black broken line ellipses respectively. B) Topographic distributions during the tasks at two different points in time (second 0-2; second 10-12). (Modified from [130].)

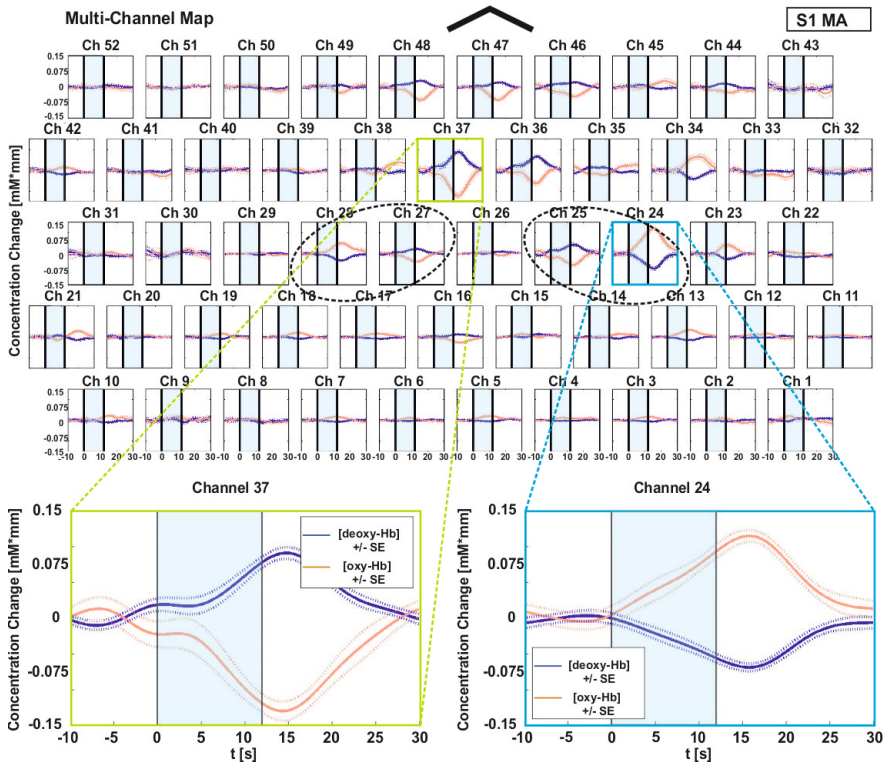

Figure 3.8: Mean concentration changes (mean ± SE) during MA of a representative subject (S1). This subject also shows a relative focal bilateral increase of [oxy-Hb] in the DLPFC in parallel with a decrease of [oxy-Hb] in the medial area of the APFC. The largest [oxy-Hb] decrease is localized at channel 37 (around 3 cm posterior to FP1, lower panel left), the largest [oxy-Hb] increases can be found on the right hemisphere at channel 24 (lower panel, right). (Modified from [130].)

3.2.3 Discussion

The purpose of the study was to investigate the spatio-temporal patterns of hemodynamic responses during a simple MA task in prefrontal brain regions. In most of the subjects a relative focal bilateral increase (with a left hemispheric dominance) of [oxy-Hb] accompanied by a [deoxy-Hb] decrease in the DLPFC was found. In parallel, a response displaying an opposite polarity (decrease of [oxy-Hb] accompanied by a [deoxy-Hb] increase in most channels overlaying the medial area of the APFC) was found. While the [oxy-Hb] changes revealed significance in both areas, the [deoxy-Hb] changes were not significant. The reason for the latter could be the small amplitude of the [deoxy-Hb] response. Theories of the hemodynamic response (e.g. [25]) predict the [oxy-Hb] response to be larger than [deoxy-Hb], usually by a factor of 2 or more. Missing significant [deoxy-Hb] effects might be simply explained by the smaller amplitude of [deoxy-Hb]-responses, even when [deoxy-Hb] is better for localizing functions, and may correspond more closely to the BOLD response [157]. Therefore, it is not surprising that no significant [deoxy-Hb] responses were observed. For example, Hofmann et al. [73] recently reported large [oxy-Hb] and small [deoxy-Hb] responses in a visual word recognition task and Herrmann et al. [67] large [oxy-Hb] and small [deoxy-Hb] responses during enhanced alertness.

First, as speculated in study 1 (see chapter 3.1) a significant simultaneous [oxy-Hb] increase and [oxy-Hb] decrease in different prefrontal areas during simple MA occured, which can be explained in the context of "focal activation/surround deactivation". Antagonistic activation patterns have been already described by brain activation studies using fMRI and EEG. For example Ehrsson and colleagues [49] reported, in a foot movement execution and imagination task, a positive BOLD signal in the foot area and a negative BOLD in the hand area with slightly greater magnitude during real movements. This can be interpreted as "focal activation (positive BOLD) /surround deactivation (negative BOLD)". Furthermore Pfurtscheller and Neuper [136] observed in their EEG study that the event-related desynchronisation (ERD) of alpha band activity does not occur in isolation, but is often accompanied by an increase in synchronization (ERS) in neighboring areas that correspond to the same or other modalities of information processing [133]. This phenomenon was called "focal ERD/surround ERS" [162]. So, for example, foot movement or foot motor imagery results in a focal ERD at electrodes overlaying the foot representation area and/or the supplementary motor area, and in an ERS at electrodes overlaying the hand representation area. Additionally antagonistic hemodynamic responses were also reported

by Franceschini [60] and colleagues in a study using fNIRS. They investigated the contra- and ipsilateral hemodynamic response of the sensorimotor cortex to unilateral voluntary movements, tactile, and electrical stimulation. For electrical stimulation, but not for voluntary movements and tactile stimulation, they observed an ipsilateral deactivation pattern in parallel with a contralateral activation pattern. They interpreted the absent deactivation in the ipsilateral side during voluntary movement and tactile stimulation by the insufficient subtraction of systemic changes due to the increase of heart rate. So the deactivation pattern caused by inhibition or decrease in activity of certain brain areas that do not pertain to the attended process may sometimes be canceled out by systemic changes. Hence it is appropriate to remove these systemic influences by different signal processing approaches (for example using a CAR spatial filter as done in our study) to uncover the deactivation pattern. In addition, assuming that not every cognitive process must necessarily lead to an increase in heart rate and therewith result in higher [oxy-Hb] in the brain, an alternative explanation might be the fact that [oxy-Hb] must be drained from one part of the brain (deactivation) to be delivered to another region (activation).

Second, the results reported are in line with fMRI studies that found bilateral activation of the VLPFC and DLPFC and the inferior and superior parietal cortex, primarily in the left hemisphere, during the performance of different arithmetic tasks [86, 107, 145]. For example Kawashima and colleagues [86] examined brain areas involved in simple arithmetic (addition, subtraction and multiplication) in eight children and eight adults, respectively. In the adult group they found a left lateralized activation (peak activation in the inferior frontal gyrus; Figure 3.9B) during the subtraction task which corresponds to the findings in the present fNIRS-study (Figure 3.9A).

Although the study revealed interesting results concerning hemodynamic changes in the prefrontal cortex during MA, some limitations should also be mentioned. First of all, the small sample (N=10) of subjects. Although statistically significant [oxy-Hb] changes in 8 out of 10 subjects were found, a bigger sample is needed to clarify some individual changes of [oxy-Hb] increase/decrease during MA.

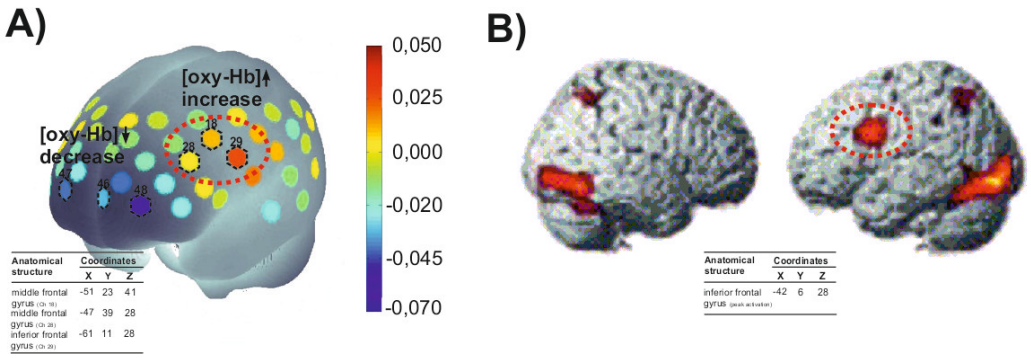

Figure 3.9: A) Grand average (8 subjects) change of [oxy-Hb] (averaged between 10 and 12 s) plotted into a 3D reference frame. The focal increase of [oxy-Hb] in the DLPFC in parallel with a decrease of [oxy-Hb] in the medial area of the APFC is marked. B) Surface projections of color-coded statistical parametric maps (subtraction vs. baseline control; modified from [86]). The MNI coordinates and anatomical locations of the activated brain areas are included for both studies.

In summary, the study demonstrated that significant [oxy-Hb] increases and [oxy-Hb] decreases can be found at optodes placed over the prefrontal cortex even during simple MA. Furthermore, there is evidence that the antagonistic hemodynamic response pattern during MA may be suitable in an optical BCI with good performance, and that only 2 prefrontal fNIRS channels may be necessary to realize such an oBCI system.

3.3 Study 3: Single trial classification of antagonistic oxyhemoglobin responses during mental arithmetic

A robust single-trial detection of brain activity is one relevant issue for all types of BCIs that are based on classification. The identification of brain patterns that naïve users can reliably generate and that are stable over time may significantly contribute to more accurate discrimination. With antagonistic activation patterns, as found for the simple mental arithmetic (MA) task in study 2 (see chapter 3.2), an improved online classification for optical BCIs using MA should become possible. For this investigation the data from the previous study was used. In that study antagonistic activation patterns (focal bilateral increase of [oxy-Hb] in the dorsolateral prefrontal cortex in parallel with a [oxy-Hb] decrease in the medial area of the anterior prefrontal cortex) in eight subjects were found. The [oxy-Hb] responses were used to search for the best antagonistic feature combination and compared to individual features from the same regions. Additionally the use of antagonistic [deoxy-Hb], total hemoglobin [Hbtot] and pairs of [oxy-Hb] and [deoxy-Hb] features, as well as the existence of a group-related feature sets, was investigated.

3.3.1 Materials and methods

Subjects, experimental paradigm and data collection

In [130] the investigations were carried out on a group of ten paid University students, five males and five females, all right-handed and aged 26.1 ± 2.7 years. The study was approved by the Medical University of Graz Institutional Review Board. Subjects were without medical conditions, compensated for participation, and gave written informed consent after the aim of the study had been explained to them. For the investigations presented in this paper the data of eight subjects (three male, five female, aged 26.0 ± 2.8 years) which showed a relative focal bilateral increase of [oxy-Hb] in the DLPFC in parallel with a decrease in the medial area of the APFC was used.

Data analysis

After removing baseline drifts by using a 0.01 Hz high pass filter, the task-related changes of [oxy-Hb] referred to a 10 s baseline interval prior to the

task (seconds -10 to 0) were calculated (For further details see [5] and [130]). To capture the antagonistic [oxy-Hb] patterns three regions of interest (ROI) were defined: ROI_1 consisted of channels 46, 47 and 48 over APFC, ROI_2 of channels 18, 28 and 29 over left DLPFC and ROI_3 of channels 13, 23 and 24 over right DLPFC (Figure 3.6B).

For classification Fisher's linear discriminant analysis (LDA) classifier was used. To evaluate the LDA generalization, data recorded from each subject was split into a training and evaluation set. The former, consisting of 10 or 16 trials respectively, was used to train and test the discriminative power of [oxy- Hb] feature combinations selected from the different ROIs. The best performing features were selected and used to train the LDA. The evaluation set, composed of the last eight trials, was then used to assess the performance of the trained LDA.

Changes of the [oxy-Hb] response at second 10, 11, 12, 13 and 14 (tm; $\pm$ 2 s around the end of the MA task, to cover also delayed task related parts of the response) were labeled as class MA. Samples at second 26, 27, 28, 29 and 30 (tr; lying in between two MA tasks) were labeled as class REST. Features consist of an individual [oxy-Hb] value of one channel at a fixed time (tm or tr). In Table 3.3 and 3.4 the positions of the channels (channel number as well as underlying Brodmann and anatomical areas) and the corresponding time points are indicated. For each subject, independent LDAs were trained and validated (leave-one-out cross validation) with individual [oxy-Hb] responses for each possible combination (ROI_i, tm_j, tr_k) with i=1,2,3; j=1,2, ..., 5, k=1, 2, ..., 5. Exhaustive Search, i.e., all possible feature combinations were evaluated, was used in the above procedure to identify the best performing antagonistic feature combination (ROI_1, ROI_2, tm_j, tr_k) or (ROI_1, ROI_3, tm_j, tr_k) with j=1,2, ..., 5 and k=1,2, ..., 5.

The same procedure was applied also to the antagonistic [deoxy-Hb], antagonistic total hemoglobin [Hbtot] = [oxy-HB] + [deoxy-Hb] and to tuples of ([oxy-Hb], [deoxy-Hb]). Additionally, antagonistic [oxy-Hb] changes that perform best over all subjects were investigated (group-related [oxy-Hb] pattern). In the latter the most commonly selected features over all subjects at the averaged time points of tm and tr were identified.

3.3.2 Results

Off-line simulation

The best performing classifiers, calculated from the training-set, were used to compute an off-line simulation with the evaluation set (8 trials per class, summarized in Table 3.3 and Table 3.4). Six out of the 8 subjects (75 %)

performed better than the chance level (71.9 % (α=0.05) for 8 trials [116]) when antagonistic patterns are used (Table 3.3).

Table 3.3: Classification accuracies (acc.; bold numbers indicate classification accuracies above the chance level (71.9% for 8 trials)) and used features (pos.$_i$, indicating the underlying Brodmann and anatomical areas; tm and tr, corresponding time points) for the antagonistic [oxy-Hb] patterns for all subjects.

Sub.	Antagonistic [oxy-Hb] pattern								
	acc.	pos.$_1$			pos.$_2$			tm	tr
	%	Ch.	BA.	Anat.	Ch.	BA.	Anat.	(s)	(s)
S1	68.75	46[a]	10	SFG	24[b]	46	MFG	10	29
S2	**87.50**	47[a]	10	MeFG	24[b]	46	MFG	13	30
S3	**75.00**	48[a]	10	MFG	29[c]	9	IFG	12	29
S4	**87.50**	48[a]	10	MFG	29[c]	9	IFG	14	28
S5	**81.25**	47[a]	10	MeFG	28[c]	46	MFG	13	26
S6	68.75	46[a]	10	SFG	28[c]	46	MFG	10	26
S7	**87.50**	47[a]	10	MeFG	18[c]	9	MFG	10	29
S8	**81.25**	47[a]	10	MeFG	28[c]	46	MFG	12	26
mean	79.69							11.75	27.88
SD	8.01							1.58	1.64

[a] APFC
[b] r. DLPFC
[c] l. DLPFC

BA, Brodmann area; SFG, superior frontal gyrus; MFG, middle frontal gyrus; IFG, inferior frontal gyrus; MeFG, medial frontal gyrus

Only one subject performed better than random when using individual features from ROI_1, ROI_2 or ROI_3, respectively (see Table 3.4). An analysis of variance (ANOVA) and a Newman-Keuls post test revealed that antagonistic features perform significantly better than individual features ($F_{(3/21)}$=8.74; p<0.001; Figure 3.10). Figure 3.10 depicts the significant contrasts of the classification accuracy between the antagonistic and individual features. The Y-axis indicates the mean classification accuracy over all subjects for the use of antagonistic feature combinations and individual features from ROI_1, ROI_2 or ROI_3 (see also Table 3.3 and Table 3.4).

Table 3.4: Classification accuracies (in %) for individual [oxy-Hb] features for all subjects. Bold numbers indicate classification accuracies above the chance level of 71.9%.

Sub.	ROI_1 [oxy-Hb]						ROI_2 [oxy-Hb]						ROI_3 [oxy-Hb]					
	acc.	pos.			tm	tr	acc.	pos.			tm	tr	acc.	pos.			tm	tr
	(%)	Ch.	BA	Anat.	(s)	(s)	(%)	Ch.	BA	Anat.	(s)	(s)	(%)	Ch.	BA	Anat.	(s)	(s)
S1	62.50	46[a]	10	SFG	11	29	56.25	18[c]	9	MFG	10	26	56.25	24[b]	46	MFG	10	30
S2	62.50	47[a]	10	MeFG	10	26	50.00	28[c]	46	MFG	11	30	62.50	24[b]	46	MFG	14	26
S3	62.50	46[a]	10	SFG	11	27	50.00	29[c]	9	IFG	11	26	68.75	24[b]	46	MFG	12	27
S4	**81.25**	48[a]	10	MFG	13	29	50.00	29[c]	9	IFG	10	27	62.50	24[b]	46	MFG	13	26
S5	50.00	47[a]	10	MeFG	12	26	68.75	28[c]	46	MFG	11	27	56.25	24[b]	46	MFG	11	30
S6	62.50	46[a]	10	SFG	10	26	50.00	28[c]	46	MFG	10	26	62.50	24[b]	46	MFG	10	26
S7	62.50	46[a]	10	SFG	13	28	**81.25**	18[c]	9	MFG	10	29	62.50	23[b]	46	MFG	12	28
S8	62.50	48[a]	10	MFG	10	26	68.75	28[c]	46	MFG	12	26	**75.00**	23[b]	46	MFG	14	27
mean	63.28				11.25	27.13	59.38				10.63	27.13	63.28				12.00	27.50
SD	8.48				1.28	1.36	12.05				0.74	1.55	6.19				1.6	1.69

[a] APFC
[b] r. DLPFC
[c] l. DLPFC

BA, Brodmann area; SFG, superior frontal gyrus;
MFG, middle frontal gyrus; IFG, inferior frontal gyrus;
MeFG, medial frontal gyrus

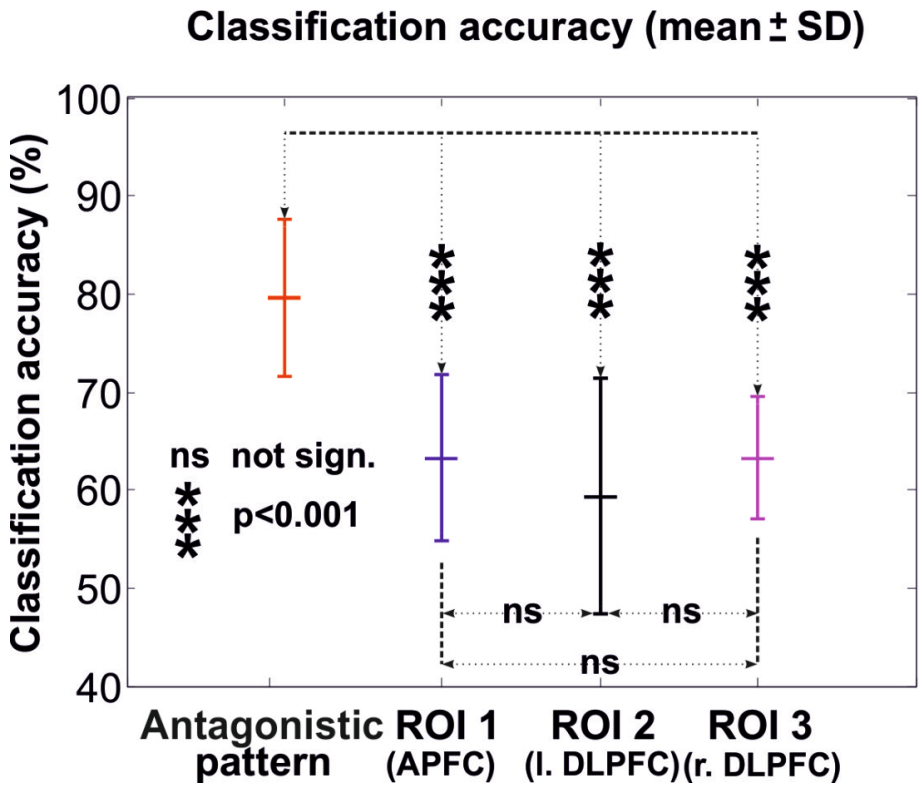

Figure 3.10: Significant contrasts of the classification accuracy between the antagonistic and individual features. (Modified from [9].)

Comparison of antagonistic [oxy-Hb], [deoxy-Hb], [Hbtot] and pairs of [oxy-Hb] and [deoxy-Hb]) features

An off-line simulation with the evaluation set using the best performing antagonistic [deoxy-Hb], [Hbtot] and ([oxy-Hb], [deoxy-Hb]) features (Table 3.5) was computed. By using antagonistic [deoxy-Hb] only two subjects performed better than random. An ANOVA and a Newman-Keuls posttest revealed that antagonistic [oxy-Hb] features perform significantly better than antagonistic [deoxy-Hb] features ($F_{(4/28)}$=2.81; $p<0.05$). No significant differences between antagonistic [oxy-Hb], antagonistic [Hbtot] as well as ([oxy-Hb], [deoxy-Hb]) tuples were found. In the case of [Hbtot] four and in the case of ([oxy-Hb], [deoxy-Hb]) three out of the 8 subjects, respectively, performed significantly better than random.

Table 3.5: Classification accuracies (in %) for antagonistic [deoxy-Hb], [Hbtot] and tuples of [oxy-Hb] and [deoxy-Hb] features for all subjects. Additionally the classification accuracies using a group-related set of antagonistic [oxy-Hb] features are shown.

Subj.	Antagonistic pattern				
	[oxy-Hb]	[deoxy-Hb]	[Hbtot]	[deoxy-Hb] and [oxy-Hb]	group-related
S1	68.75	68.75	50.00	68.75	68.75
S2	**87.50**	62.50	**81.25**	68.75	**75.00**
S3	**75.00**	62.50	56.30	**75.00**	68.75
S4	**87.50**	**81.25**	**93.75**	**81.25**	**87.50**
S5	**81.25**	50.00	68.75	68.75	62.50
S6	68.75	56.25	56.25	62.50	50.00
S7	**87.50**	62.25	**93.75**	68.75	**75.00**
S8	**81.25**	**87.50**	**81.25**	**93.75**	**75.00**
mean	79.69	66.38	72.66	73.44	70.31
SD	8.01	12.48	17.33	9.88	10.95

Stability of antagonistic [oxy-Hb] features

According to the findings of the feature selection and off-line simulation most commonly selected features of all subjects (Ch. 47, APFC and Ch. 28, l. DLPFC at the averaged time points of tm and tr (tm=12 s, tr=28 s; Table 3.3)) were used. The group-related [oxy-Hb] features set achieved on average a classification accuracy of 70.3% over all subjects (Table 3.5). No significant differences were found between the use of subject-specific antagonistic features and the above group-related feature set. Four out of the eight subjects performed better than chance level (mean 78.1%).

3.3.3 Discussion

The aim of the study was to investigate the usefulness of antagonistic [oxy-Hb] patterns in the context of single trial classification for oBCI. The results show that two fNIRS channels placed over predefined brain areas, i.e., left or right DLPFC and APFC, respectively, may significantly increase the performance of optical BCIs compared to the more common approach to use only one channel (e.g. [118, 148]).

In the feature selection process the best performing antagonistic and individual features, respectively, were investigated. To account for the low number of trials available for evaluating the performance, we adapted the

chance level of classification to guarantee the correct comparison [116]. By using the best antagonistic [oxy-Hb] features performing an off-line simulation mean classification accuracy (%) of 79.69 ± 8.01 (mean ± SD, Table 3.3) was computed. Individual features performed worse (classification accuracies (%) of 63.28 ± 8.48 (ROI_1), 59.38 ± 12.05 (ROI_2) and 63.28 ± 6.19 (ROI_3), Table 3.4). In each case only one subject reached accuracies above the chance level. In contrast, with the antagonistic features 6 of the 8 subjects (75%) performed accuracies (mean 83.3%) above the chance level. So the use of antagonistic [oxy-Hb] features, compared to individual [oxy-Hb] features from ROI_1, ROI_2 and ROI_3, significantly increased the classification accuracy (Tables 3.3 and 3.4, Figure 3.10).

In addition antagonistic [oxy-Hb] features were compared with antagonistic [deoxy-Hb] and [Hbtot] features as well as ([oxy-Hb], [deoxy-Hb]) tuples. [deoxy-Hb], [Hbtot] and tuples of [oxy-Hb] and [deoxy-Hb] performed worse (classification accuracies (%) of 63.38 ± 12.48 ([deoxy-Hb]), 72.66 ± 17.33 ([Hbtot]) and 73.44 ± 9.88 ([oxy-Hb] and [deoxy-Hb]), Table 3.5) whereby only [deoxy-Hb] exhibits significant difference to the use of [oxy-Hb]. These lower classification accuracies may be simply explained by the fact that [deoxy-Hb] changes are smaller in amplitude, usually by a factor two or more (e.g. [72, 101]), and higher in variance than [oxy-Hb] changes, more susceptible to noise and therefore less suitable as feature for single trial classification.

The performance comparison between the use of subject-specific versus group-related features surprisingly revealed no significant differences. This supports the hypothesis that MA generates focal and rather well defined metabolic response patterns. For the realization of optical BCIs this means that the considered features are spatially focused, task-related and valid for several users.

Antagonistic activation patterns known as "focal activation/surround deactivation" have been described in different studies. So e.g. "focal ERD/ surround ERS" was reported during hand and foot movement execution or imagination in EEG [136, 162] and "positive BOLD/negative BOLD" in fMRI ([49, 79]. The usability of this phenomenon for classification in motor imagery based BCI-systems (ERD/ERS) is well documented [135]. So far, however, it had been unknown that this phenomenon is also present in fNIRS data [130], and this study showed for the first time the usefulness of this phenomenon for fNIRS data classification.

Although the study revealed significant results, some limitations should also be mentioned. First of all, the number of subjects is low. However, concerning the significant increase of the classification accuracy using antagonistic [oxy-Hb] changes instead of individual features only from one single region, our findings suggest that the use of antagonistic patterns may be a

suitable control strategy for optical BCIs. However, to clarify this in more detail, especially in an online study, a bigger sample is needed. Another limitation is the temporal resolution of the hemodynamic response - in the range of several seconds - which limits the information transfer rates achievable for BCI-based communication. In [130] a delay of the onset and a peak latency of the hemodynamic responses in the order of 2 to 3 s was found. With the paradigm, classification approach and analysis windows used for this study in mind, around 12 s (MA) to 16 s (REST) (Table 3.3) would be needed to classify the task reasonably well. By shortening the baseline interval prior to the task to 5 s this might lead to a maximal achievable information transfer rate of around 3 to 3.5 bits/min (comparable with results in [36]). To increase this transfer rate further basic research is necessary, e.g. investigating the use of fast optical signals [65, 83, 181].

In summary, this study suggests that the use of antagonistic [oxy-Hb] features may significantly increase the classification accuracy. The off-line simulation results confirmed the hypothesis made in study 2 (chapter 3.2) that two prefrontal fNIRS channels can capture antagonistic hemodynamic patterns during a mental arithmetic task that can be detected reasonably well without the need of time consuming user-adaptation. In combination with the self paced paradigm the use of antagonistic patterns may be an important contribution for simple and cheap optical BCI systems which are currently under development.

Chapter 4

Online oBCI studies with operand conditioning

During the past years neurofeedback has become more and more important in neuroscience. Research over the past two decades showed that various parameters like heart rate and blood pressure as well as brain activity can be brought under voluntary control after training with feedback. The field of applications ranges from caregiving to hyperactive children [56, 93] and epilepsy prevention [48, 176] via stroke therapy [10, 180] through to communication and control support for paralyzed patients [17, 88, 132, 185]. The required methods are normally based on electroencephalography (EEG). Besides EEG, such systems have been also realized with functional magnetic resonance imaging (fMRI) [177, 179] and magnetoencephalography (MEG) [106, 161]. Additionally to these established techniques functional near-infrared spectroscopy (fNIRS) seems to be also a suitable method.

The fNIRS signal consists of slow hemodynamic responses (changes in [oxy-Hb] and [deoxy-Hb]), which are in the order of seconds. Similar slowly varying bio-signal changes are addressed in the analysis of slow cortical potentials (SCP) in the EEG. SCPs are potential shifts of neuronal assemblies of the cerebral cortex lasting up to several seconds [15, 16].

Inspired by the work of Prof. Birbaumer's group in Tuebingen [17, 88] who used such slow bio-signals to implement a BCI for locked-in patients this work describes the realization and evaluation of a real-time feedback system based on a one-channel fNIRS-system (for a detailed description of the system see chapter 2.1) for usage as an oBCI. This chapter also includes a case study on using the oBCI system in combination with a steady-state visual evoked potentials (SSVEP)-based BCI applications as a "hybrid" BCI [128]. Large parts of the work presented in this chapter already appeared at poster presentations and in conference proceedings as well as a book section and a

peer-reviewed journal publication [114, 128]:

- **G. Bauernfeind**, R. Leeb, P. Linortner, C. Neuper, and G. Pfurtscheller. Using Near-Infrared Spectroscopy (NIRS) to realize an optical BCI. *Proceedings of the Neuromath Workshop 2009*.
- G. Pfurtscheller, B. Z. Allison, **G. Bauernfeind**, C. Brunner, S. Solis Escalante, R. Scherer, T. O. Zander, G. R. Müller-Putz, C. Neuper, and N. Birbaumer. The hybrid BCI *Front Neurosci*, 4:42, 2010.
- G. R. Müller-Putz, R. Leeb, J. D. Millan, P. Horki, A. Kreilinger, **G. Bauernfeind**, B. Z. Allison, C. Brunner, and R. Scherer. Principles of Hybrid Brain-Computer Interfaces. In *Toward Practical BCIs: Bridging the Gap from Research to Real-World Applications*, 2012, in press.

4.1 Study 1: Using functional near-infrared spectroscopy (fNIRS) to realize an optical BCI (oBCI)

The aim of this work was to implement a real-time fNIRS-feedback system (optical BCI (oBCI)) based on a one-channel NIRS system (chapter 2.1). For evaluation of the system a case study with five subjects was performed. The subjects were trained to influence their prefrontal [oxy-Hb] volitionally. The experimental procedure included the following steps: a strategy finding phase where the subjects should find a method to control the oxygenation, a training phase to consolidate the strategy and a test phase to evaluate the performance.

4.1.1 Materials and methods

oBCI system

The real-time feedback system is based on the one-channel fNIRS-system described in chapter 2.1 (Figure 2.1). To implement the real-time system (Figure 4.1B) a standard PC was used. Data acquisition (sampling frequency 250 Hz), signal processing, control of the feedback-system and the generation of the output signal (sampling frequency 10 Hz) were implemented in MATLAB and Simulink (Figure 4.2A). The feedback loop was closed by displaying the output on a monitor. During the signal processing the following

steps were carried out. After calculating the relative changes of [oxy-Hb] and [deoxy-Hb] (implementation of equation 1.6 in section 1.3.2) in the unit of μM, a digital 3 Hz low pass filter of order 5 with an attenuation of 30 dB in the stop band was used to enable down sampling to 10 Hz (see Figure 4.2C). Further baseline drifts are removed by subtracting a 10 s moving average. Additionally a 0.75 s moving average was used to smooth the signal (minimize pulse artifacts, see Figure 4.2B). The processed [oxy-Hb] change, referred to a 4 second baseline interval (mean concentration of the last 4 seconds prior the task), was used as a visual feedback for the subjects. Different types of feedback are possible. In the strategy finding and training phase a feedback bar and in the test phase a moving ball was used (the length of the bar and the position of the ball on the screen, respectively were proportional to the [oxy-Hb]).

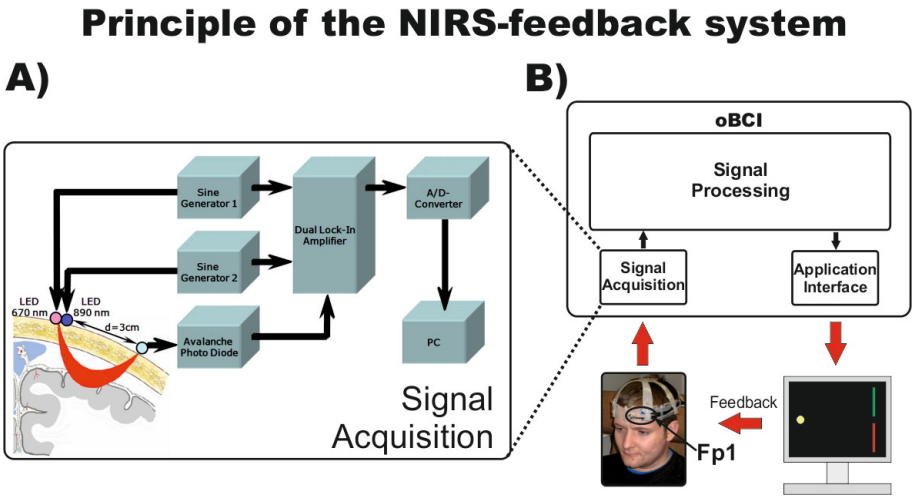

Figure 4.1: A) Components of the one-channel fNIRS-system (chapter 2.1). B) Flow chart of the implemented fNIRS-feedback system with optode placement on the frontal cortex 1.5 cm to the left and right of position FP1. (Image reprinted with permission of the subject)

Subjects and experimental procedure

The presented experiment focused on fNIRS-based feedback-training, consisting of three different phases: First strategy finding, second training and third test phase. The phases can be subdivided into sessions, trials and tasks. Five subjects (A1 to A5; three females and two males) aged between 25 and 30 years (27.2 $\pm$ 1.9; mean $\pm$ SD) were recruited for participation. All subjects had normal or corrected to normal vision and were right-handed

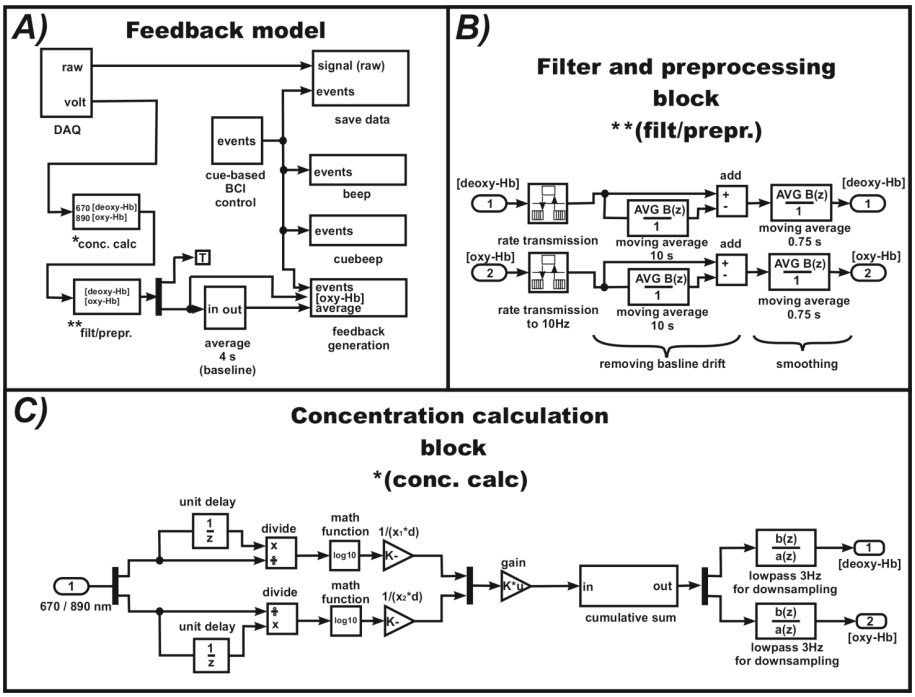

Figure 4.2: A) Simulink feedback model with blocks for C) concentration calculation (implementation of equation 1.6 in section 1.3.2) and B) filter/preprocessing (remove baseline drift and smoothing).

(handedness was investigated by the HDT-test [158]). After the successful completion of a phase the subjects were entitled to participate in the next phase. All experiments were in compliance with the World Medical Association Declaration of Helsinki. The subjects gave written informed consent before the experiment. The aim of this experiment was to train subjects to volitionally control their prefrontal [oxy-Hb].

Strategy finding phase: Within two to four sessions over up to four weeks subjects were required to find a mental strategy for controlling the oxygenation (oxy-Hb concentration) over the PFC. The PFC receives and sends commands to nearly all cortical motor and sensory systems, as well as many sub-cortical structures and plays a major role in various higher cognitive tasks (for review see e.g. [111]). So we decided to leave the type of strategy (quoted hereafter as activation) to be used to the subjects. The subjects were seated in a comfortable armchair. The sources and detector were placed over the frontal cortex 1.5 cm to the left and right of position FP1 (Figure 4.1B) according to the international 10-20 system for EEG recording [74]. So the measurement

position is overlaying Brodmann's area 10. For further details on the corresponding anatomical structure see [125]. One session consisted of 40 activation tasks with a duration of 8 s. The start of such an activation task was indicated by a beep tone, the appearance of a green cross and the occurrence of a feedback bar. As already mentioned the feedback bar represents the current oxygenation level referred to a 4 second baseline interval prior to the task. The end of the activation task was indicated by a low-pitched beep after which a pause of 8 s (black screen) followed, so one trial lasted 16 s. After such a trial a random time interval (between 5 to 10 s) was implemented. The timing of the strategy finding session is shown in Figure 4.3A. Subjects were asked to perform not more than three different self-chosen activation tasks in one session to manipulate the feedback bar. After finding a stable activation task, a final session with the chosen task was performed. Afterwards the subjects switched to the next phase.

Training phase: During the training phase (up to five weeks) subjects performed one or two training sessions per week. In these sessions an additional rest condition was added (subjects were told to try to increase the length of the feedback bar in the course of the session). The start of the rest condition was indicated by a double beep and the appearance of a green cross. In contrast to the activation task no feedback was given. During the rest condition the subjects had to stay relaxed. The end of the rest condition was indicated like the end of the activation task, by a low-pitched beep. Independent of the task a pause of 8 s, followed by a random time interval (intertrial interval, 5 to 10 s) was given afterwards. One session consisted of 20 activation and 20 rest trials which occurred in a random order. The timing of a training session is shown in Figure 4.3B.

Test phase (basket game): In this phase subjects received feedback in form of a basket game [99]. A green ball started at a predefined position and the subjects had to reach a green basket area. Therefore the screen was splitted into two regions, an upper and a lower half. The subjects had to reach the target area by relaxing or performing the activation task. The timing was equal to the timing in the training phase (Figure 4.3C). Each session consisted of 20 upper and 20 lower half trials which occurred in a random order. So two outcomes are possible: The subjects reached the green basket and executed a correct response or missed the basket and performed an incorrect response. The performance of each session was evaluated by the ratio of the number of total

correct responses (maximum 20 each class) to the number of trials per session (40 trials).

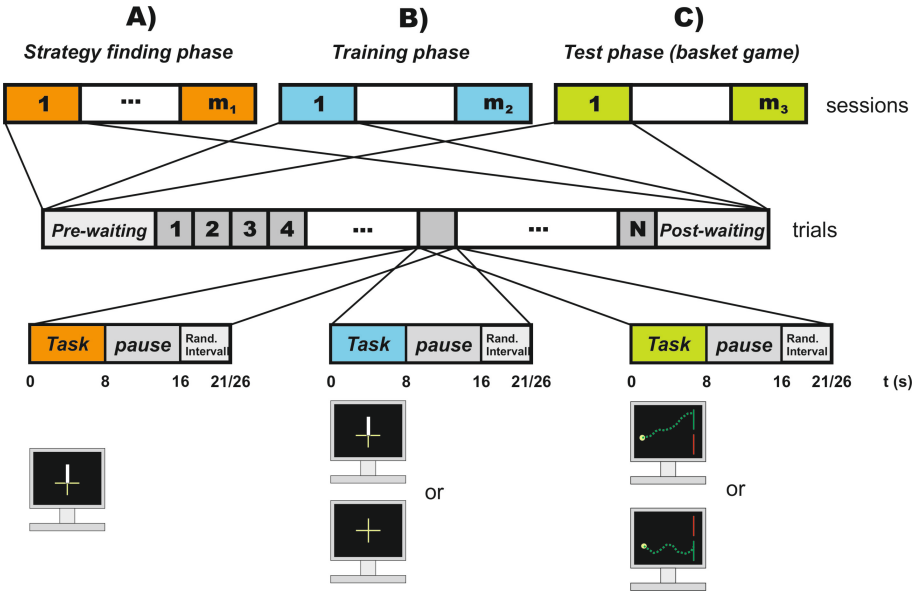

Figure 4.3: Time flow of A) strategy finding, B) training and C) test phase. One session consists of 40 trials with duration of 16 s (8 s task duration and 8 s pause). Between the trials an intertrial interval of 5 to 10 s was implemented. In the lowest part a conceptual screenshot is given.

4.1.2 Results

Strategy finding phase: A list of the tested activation tasks of all subjects who found a stable activation pattern, including the moving direction of the bar while performing the finally chosen activation tasks, is shown in Table 4.1. Subject A5 was highly motivated but was not able to find a stable activation pattern within the sessions. In contrast to subjects A1, A3 and A4, who showed similar activation patterns, a decrease of [oxy-Hb], subject A2 selected a task that increased the frontal oxygenation.

Training phase: Four subjects (A1, A2, A3, A4) entered the training phase. As mentioned before, subject A5 was not able to find a stable brain pattern and therefore never reached the training phase. In the training phase, all subjects were able to improve their [oxy-Hb] change. For each subject the mean changes of [oxy-Hb] of the final training

session, based on 20 trials each class, are displayed in Figure 4.4. Unfortunately subjects A3 and A4 were not able to exhibit significant differences between rest and activation (A3: $t_{(19)}$=-2.006, p=0.059; A4: $t(19)$=-0.007, p=0.994; the mean concentration between second 7 to second 8 was used to calculate the statistic) and therefore not able to participate in the test phase. For this reason both subjects were excluded from further measurements. Only subjects A1 and A2 (A1: $t_{(19)}$=-4.395, p<0.001; A2: $t_{(19)}$=4.756, p<0.001) were able to produce significant differences between rest and activation.

Test phase (basket game): Only subjects A1 and A2 entered the test phase and used the basket game as feedback scenario. Subject A1 performed three sessions in this phase and achieved a hit rate of 57.5%, 52.5% and 55%, which does not differ significantly from a random performance [116]. Subject A2 performed four sessions in the test phase and achieved hit rates of 67.5%, 70%, 75% and 80%, which is significantly better than a random performance [116]. For each subject and each test session, the average responses and standard errors (in [μM]) at the end of the feedback period and the number of times of occurrence of each outcome are given in Table 4.2. The responses of subject A2 in the final test session are displayed in Figure 4.5. In this Figure the mean "hit" (target reached) changes of [oxy-Hb] is based on 17 trials for activation condition and 15 trials for rest condition respectively.

4.1.3 Discussion

In this work a simple implementation of an oBCI system based on a custom-built one-channel fNIRS-system is presented. Up to now only a few publications on online realizations of such systems exist [36, 118, 156]. Furthermore, some studies only investigated the use of realtime fNIRS feedback without oBCI application [82, 90]. Comparing these above mentioned studies, in four of them the optodes (52 channels in [82], 24 channels in [90], two channels in [156] and one channel in [36]) were placed above the motor cortex. As described in [36] it is important to maintain a proper and stable connection with the scalp. Additionally hair can attenuate the signal and cause motion artifacts [5, 34] so that a high effort is necessary to establish a stable connection. In contrast a single channel placement over the forehead and PFC respectively [118] seems to be more practical and user-friendly and able to overcome this problem.

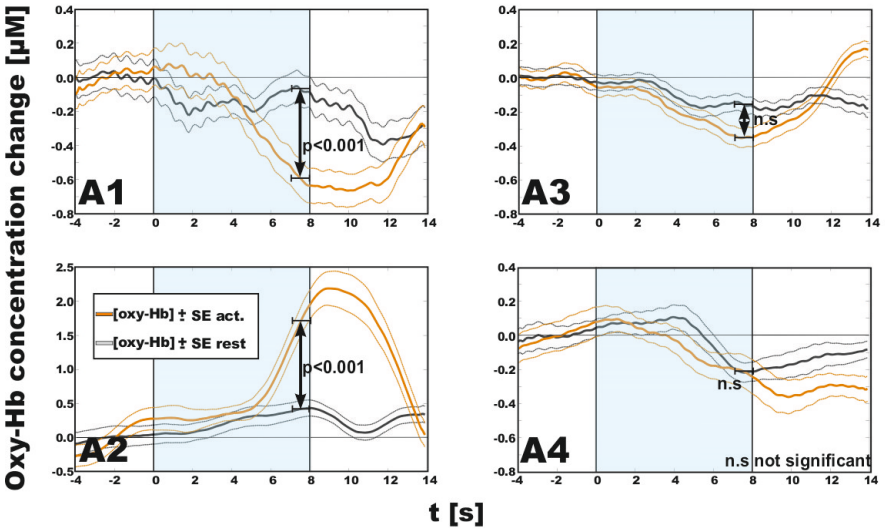

Figure 4.4: Mean concentration changes (mean ± SE) of rest and activation class for 4 subjects during the last training session (based on 20 trials for each class). The rest class is plotted in gray and the activation class is plotted in orange. The shaded area indicates the time period of the task.

The results of the first two phases indicate that subjects can learn to control their prefrontal [oxy-Hb] with the presented system. With the aid of feedback 4 subjects could find stable strategies. Three subjects (A1, A3, A4) chose strategies which showed similar activation patterns, a decrease of [oxy-Hb], while subject A2 chose a task which increased the frontal oxygenation (the selected strategies are shown in Table 4.1). An explanation of the different "activation" patterns (increase or decrease of [oxy-Hb]) of the subjects could be the activation and deactivation of different neural networks of the PFC involved in the chosen strategy. These networks are distributed over the frontal cortex or other areas, and are not located exactly under the optodes. Thus, a frontal [oxy-Hb] decrease may be explained as a surround effect of activation (increase of [oxy-Hb]) in other areas [5, 130]. Such a decrease in prefrontal [oxy-Hb] was reported by Shimada et al. during visual feedback of the moving hand in a reaching task and interpreted in terms of prefrontal "deactivation" [151]. Additionally bidirectionally modulated networks were also determined by fMRI [79]. The bidirectionality was represented in this work by positive (activation) and negative (inhibition) blood oxygen level dependent (BOLD) changes. Also during self-regulation of SCPs significant deactivations (negative BOLD responses) were found in parietal, frontal and

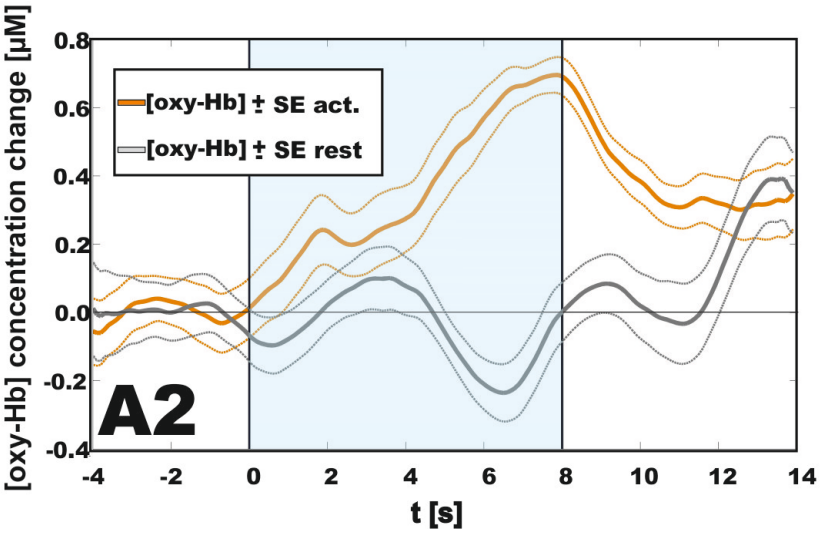

Figure 4.5: Mean "hit" concentration changes of oxy-Hb (mean ± SE) of rest and activation class based on 17 trials for activation class and 15 trials for rest class (session 4). The rest class is plotted in gray and the activation class is plotted in orange. The shaded area indicates the time period of the task.

prefrontal areas [69]. However, all subjects could raise their activation pattern significantly during the training phase (up to eight training sessions within five weeks). Unfortunately two subjects were not able to achieve significant differences between rest and activation. So only two subjects entered the final test phase and used the feedback scenario. Subject A2 performed four sessions in the test phase and could improve the performance from 67.5% in the first session to a hit rate of 80% in the fourth session. In contrast, subject A1 performed three sessions in the test phase and achieved a hit rate of around 55%, which doesn't differ significantly from a random performance [116]. Nevertheless it seems that subject A1 could achieve control with further training. The results indicate that subjects can learn to voluntarily influence their prefrontal [oxy-Hb] after some training sessions with the described system. However not all subjects were able to achieve suitable results in the given training time.

In summary, this study demonstrates that subjects can learn to volitionally control their prefrontal [oxy-Hb]. Further the feasibility of a single channel oBCI system with optode placement over the PFC was shown, but additional research is needed to investigate its further potential and applicability.

Table 4.1: List of tested activation tasks of all subjects including the moving direction of the bar during performing the finally chosen activation tasks.

Subject	Session 1	Session 2	Session 3	Session 4
A1	Mental arithmetic Repeat path in mind -	Touching the nose alternatingly with the index finger of both hands Perform a complex motor imagery (finger movement) Pad on toes	Touching the nose alternatingly with the index finger of both hands ↓ in mind - -	- - -
A2	Playing categories (game) Repeat path in mind Sing a song in mind	Playing categories (game) Perform hand tapping in mind -	Perform hand tapping in mind - -	Perform a complex motor imagery ↑ (finger movement) - -
A3	Perform a right hand motor imagery Sing a song in mind	Sing a song in mind ↓ -	- -	- -
A4	Perform foot motor imagery Sing a song in mind Emotions	Sing a song in mind Perform foot motor imagery Emotions	Dancing to a song in mind Sing a song in mind -	Dancing to a song in mind ↓ - - -
A5	Subject A5 was not able to find a stable activation pattern within the sessions			

Table 4.2: Hits and miss during basket game sessions. Each experimental session consists of 40 trials (20 each class). For each subject and each test session, the average responses in [μM] and standard errors at the end of the feedback and the number of times of occurrence of each outcome are given.

Test phase (basket game)		Upper basket targeted		Lower basket targeted		Performance
session		hit	miss	hit	miss	%
A1						
1	mean	0.21	-1.06	-0.79	0.57	
	SE	0.14	0.16	0.09	0.14	
	No.	8	12	15	5	57.5
2	mean	-0.09	-0.71	-0.88	0.09	
	SE	0.13	0.14	0.13	0.14	
	No.	11	9	10	10	52.5
3	mean	0.00	-0.56	-0.45	0.22	
	SE	0.08	0.11	0.09	0.08	
	No.	15	5	7	13	55.0
A2						
1	mean	1.85	x	-0.39	0.88	
	SE	0.17	x	0.13	0.27	
	No.	20	x	7	13	67.5
2	mean	0.69	0.15	0.01	0.49	
	SE	0.10	0.14	0.11	0.09	
	No.	15	5	13	7	70.0
3	mean	0.39	0.08	0.09	0.34	
	SE	0.06	0.08	0.04	0.12	
	No.	13	7	17	3	75.0
4	mean	0.69	0.10	0.00	0.41	
	SE	0.05	0.17	0.09	0.22	
	No.	17	3	15	5	80.0

4.2 Study 2: Self-activation of an SSVEP-based orthosis control using fNIRS

Self-activation is an important factor for BCI systems to become more practical and user-friendly devices [150]. This means that the user should be able to switch the system on or offautonomously. In this preliminary study, the worldwide first realization of an asynchronous hybrid BCI system [128], which is composed of two different BCIs, was investigated. In this study the oBCI system (for details see chapter 4.1) was used to turn on and off an electrical hand orthosis controlled by an EEG-based steady-state visual evoked potential (SSVEP)-BCI application.

4.2.1 Materials and methods

Hybrid BCI system

The hybrid system (Figure 4.6) consists of the oBCI system introduced in chapter 4.1.1 and an SSVEP orthosis control system (for details see [95]). SSVEPs are time- and phase-locked responses in the EEG which occur over the visual cortex if stimuli are presented in a rapid sequence. If more than one stimulus is presented, and the subjet focuses on one specific stimulus, the corresponding frequency can be picked up in the EEG. With this method multi-class BCIs can be realized. In the presented study the EEG to measure the SSVEPs was recorded bipolarly from electrodes placed over the occipital cortex (electrode position O1, 2.5 cm inter-electrode distance, ground Fz, Figure 4.6B).

Subjects and experimental procedure

One subject, familiar with fNIRS (subject participated in the study described in chapter 4.1) but naive using SSVEP, performed 4 runs with the hybrid system. In each run, the subject had to open and close (one activation block contained positions 1-2-3-4-3-2-1) the orthosis (Figure 4.6D) three times, each at self paced intervals, with 60 second breaks between the blocks (resting periods). To open the orthosis, the subject had to focus on an 8 Hz flickering LED. To close the orthosis, the subject had to pay attention to a 13 Hz flickering LED (Figure 4.6C). Only if the whole open/close sequence had been finished, the resting period was initiated.

Prior to the first block, the subject had to self-initiate the SSVEP orthosis control using the fNIRS system as a "brain switch" [128]. To this end, the fNIRS measurement was split up into 8 second periods. A prewaiting

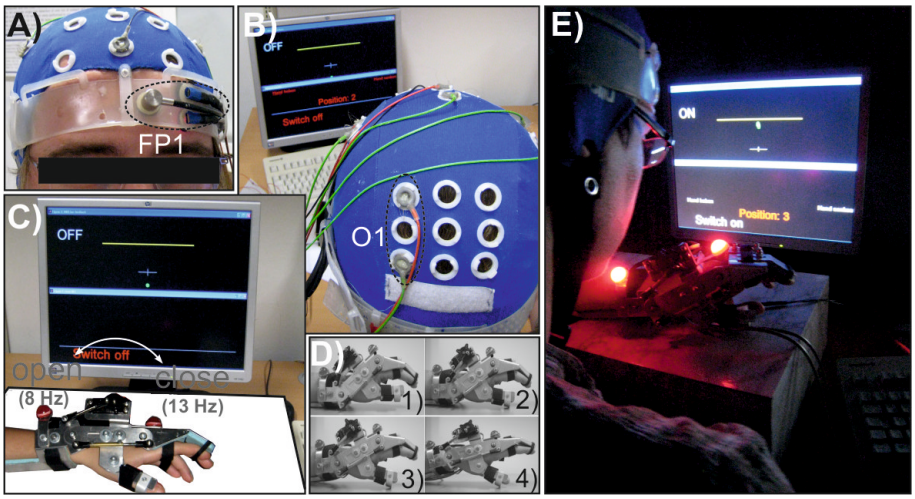

Figure 4.6: A) One channel fNIRS placement over FP1. B) EEG recording to measure SSVEPs (electrode position O1, 2.5 cm inter-electrode distance, ground Fz). C) Hybrid BCI system. Orthosis in front of the presentation screen. The upper part of the presentation screen displays the ball position, which represents the varying concentration change. The bold horizontal yellow line in the window indicates the on/off toggle switch threshold. In the lower part of the screen, the current status of the SSVEP orthosis control (on/off) and the detected command were shown. D) Stepwise SSVEP orthosis control. E) Experimental setup. (Modified from [114, 128].)

period was included prior to the first segment, which started at second 18. Within the periods, the relative [oxy-Hb] change (measured over position FP1, Figure 4.6A) was used as a visual feedback (green ball). The measured concentration change, referred to a 4 second baseline interval (mean concentration of the last 4 seconds prior to the period), represents the ball position on the screen. If the change exceeded a subject-specific threshold, indicated as a yellow bar on the screen (Figure 4.6C), an on/off (off/on) state switch of the orthosis control was triggered. The threshold for the first run was selected from previous fNIRS measurements of the subject (chapter 4.1) and adapted after the first run to minimize false positives (FP). After each switch, no other switch command was accepted for a period of 8 seconds (refractory period, black screen). During the resting periods and after the last activation block, the subject was instructed to switch off the SSVEP orthosis control system by using the brain switch again to avoid FP SSVEP activations.

4.2.2 Results

During the first two runs, FPs were detected in the activation as well as in the resting period (fNIRS and SSVEP, Figure 4.7). In the third run the subject displayed a perfect performance with the fNIRS switch and only two FP detections occurred during the SSVEP orthosis control (for run 3 also the corresponding [oxy-Hb] signal is shown). In the last run, the subject displayed a perfect performance with 100% accuracy, meaning only true positive (TP) activations in the fNIRS and SSVEP control, respectively. Table 4.3 summarizes these results.

Table 4.3: True positive (TP) and false positive (FP) detections in self-paced orthosis and fNIRS control. The parameters are given for the activation (AP) as well as the resting (RP) period.

	activation period				resting period			time		
	fNIRS		SSVEP		fNIRS		SSVEP	AP	RP	total
	TP	FP	TP	FP	TP	FP	FP			
run	-	-	(min^{-1})	(min^{-1})	-	-	(min^{-1})	(s)	(s)	(s)
1	7	4	5.4	0.0	9	6	4.0	201.6	180.0	381.6
2	3	0	7.7	0.4	7	4	1.3	140.6	180.0	320.6
3	3	0	6.4	0.7	3	0	0.0	162,6	180.0	347.8
4	3	0	6.6	0.0	3	0	0.0	162.6	180.0	342.6
mean	4.0	1.0	6.5	0.3	5.5	2.5	1.2	168.1	180.0	348.1
SD	2.0	2.0	1.0	0.4	3.0	3.0	1.9	25.2	0.0	25.2

4.2.3 Discussion

This feasibility study presented the first implementation of a hybrid BCI system combining an oBCI with an EEG-based SSVEP BCI. In general there are several reasons to combine two different BCI approaches into one hybrid BCI, e.g. to improve classification accuracy or bit rate [23], or to avoid application specific limitations of the single BCIs. For example, a major limitation for solely fNIRS-based approaches is the temporal resolution of the hemodynamic response - in the range of several seconds - which limits the information transfer rates achievable for BCI-based communication or control. In contrast, SSVEP-based BCIs provide one of the fastest communication approaches for non-invasive BCI systems [13]; however, a major drawback of such systems is a high FP-rate for asynchronous applications (unintended commands during resting periods) [137].

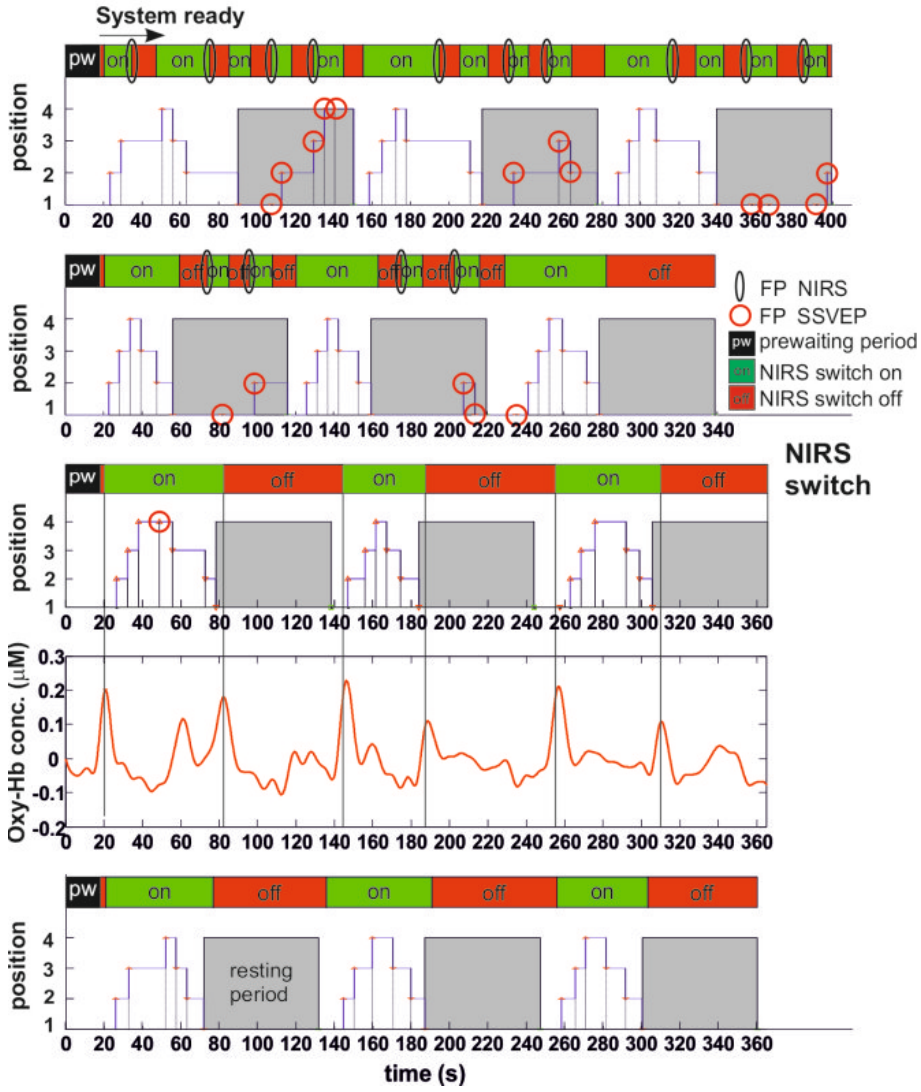

Figure 4.7: Timing of the 4 runs, green areas indicate an activated SSVEP control. The gray areas indicate resting periods. Red circles indicate FPs in SSVEP control, black ellipses in fNIRS. The black areas at the beginning of each run indicate a prewaiting period. For run 3 the [oxy-Hb] level in μM is shown. (Modified from [114, 128].)

The presented hybrid BCI approach avoids the limitation of the SSVEP approach by using the oBCI as an on/off switch. One important feature of such a brain switch is that unintended activations (FPs) should not occur. However, in the first run FPs of the brain switch were detected in the activation as well as in the resting period. These FPs were caused by the fact that the subject-specific threshold for the first run was selected from previous fNIRS measurements of the subject. After adjusting the threshold, no further FPs occured in run 3 and run 4, and therefore no false orthosis movements were detected in the resting periods because the SSVEP orthosis control was not activated.

In summary the preliminary results provide evidence that the combination of fNIRS and SSVEP within a hybrid BCI system may be a suitable control interface, and the promising results encourage further hybrid BCI research with a larger group of subjects.

Chapter 5

Summary and Conclusion

Several years ago fNIRS was proposed as a novel approach in the field of brain-computer interface (BCI) research. Since that time, only a few research groups have investigated different concepts using fNIRS alternatively to EEG-based systems for BCI communication. When this thesis was started, only hemodynamic responses caused by the performance of motor imagery were used as a control signal for the so-called optical BCI (oBCI) systems. However, it was known from different neuroscientific studies that also other mental tasks, such as mental arithmetic (MA) or mental singing, can induce hemodynamic changes which can be measured with the fNIRS technique and therefore may be suitable control strategies for oBCI systems.

Therefore the main focus in this thesis was placed on exploring the usefulness of MA as a control strategy for oBCI systems. In the first study on this subject special emphasis was put on the spatio-temporal investigation of hemodynamic brain patterns caused by the performance of a simple MA task. The results of the first study, performing different experiments with slightly different MA tasks (single and repetitive subtractions), revealed reproducible results independent of the fNIRS system used. Although the results provided evidence that MA is a suitable control strategy for oBCI systems, the findings of a decrease in [oxy-Hb] and increase in [deoxy-Hb] over the anterior prefrontal cortex (APFC) were in contrast to other studies which reported an opposite polarity. It was speculated that the frontal [oxy-Hb] decrease and [deoxy-Hb] increase may be explained as a surround effect of an [oxy-Hb] increase and [deoxy-Hb] decrease in areas not investigated during the measurements. To investigate this hypothesis in more detail a second study on a group of 10 subjects measuring hemodynamic brain patterns on larger cortical areas was performed. The results revealed the same hemodynamic responses as found in the first study. However, in addition a relative focal bi-

lateral increase (with a left hemispheric dominance) of [oxy-Hb] accompanied by a [deoxy-Hb] decrease in the dorsolateral PFC (DLPFC) was found. The results were also in line with fMRI studies which found the same bilateral activation of the DLPFC. It was further speculated that such antagonistic patterns, a simultaneous [oxy-Hb] increase and [oxy-Hb] decrease in different prefrontal areas, may be suitable in an oBCI, and that only two prefrontal fNIRS channels may be necessary to realize such a system. Therefore, in a third study a single trial classification of the antagonistic hemodynamic responses was performed. For this investigation the data of the previous study was used to search for the best antagonistic feature combination and compared to individual features from the same regions. Additionally the use of antagonistic [deoxy-Hb], total hemoglobin [Hbtot] and pairs of [oxy-Hb] and [deoxy-Hb] features as well as the existence of a group-related feature set was investigated. The results showed that two fNIRS channels placed over predefined brain areas, i.e., left or right DLPFC and APFC, respectively, significantly ($p<0.001$) increase the performance, from 63.3 to 79.7%, of oBCIs compared to the use of only one channel over the APFC or DLPFC. Furthermore, the performance comparison between the use of subject-specific versus group-related features revealed no significant differences. This supports the hypothesis that MA generates focal and rather well defined metabolic response patterns. For practical optical BCIs this means that the considered features are spatially focused, task-related and valid for several users. Summarizing all three studies it was shown that the performance of an MA task is a suitable control strategy for oBCI systems and that only two prefrontal fNIRS channels are necessary to capture and classify an MA task reasonably well without the need of time consuming user-adaptation. In combination with a self paced paradigm the use of antagonistic pattern may be an important contribution for simple and cheap oBCI systems which are currently under development.

A further focus was laid on the realization and evaluation of a real-time fNIRS feedback system for usage as an oBCI. Five subjects were trained to influence their prefrontal [oxy-Hb] volitionalyl and use it finally as a control signal for an oBCI. Although all subjects could raise their hemodynamic pattern significantly during training only two subjects were able to achieve suitable results in the given training time. However, the results indicate that subjects can learn to voluntarily influence their prefrontal [oxy-Hb] after some training sessions. Further, the feasibility of a single channel oBCI system was shown, but additional research is needed to investigate its full potential and applicability. Out of these investigations, in a preliminary feasibility study the worldwide first realization of an asynchronous fNIRS based hybrid BCI

system was shown. Therefore the above mentioned real-time fNIRS feedback system was combined with a traditional EEG-based BCI system to control an electrical hand orthosis. The usability of the hybrid system was finally evaluated with a single subject which gained perfect control (100% accuracy) after a short period of training. This result provides evidence that also the combination of an oBCI and an EEG-based BCI within a hybrid BCI system may be a suitable control interface.

Publications

Journal articles

2012

B. Z. Allison, R. Leeb, C. Brunner, G. R. Müller-Putz, **G. Bauernfeind**, J. W. Kelly, and C. Neuper. Toward smarter BCIs: extending BCIs through hybrid BCIs and intelligent control. *J Neural Eng*, 9(1):013001, 2012.

G. Litscher, **G. Bauernfeind**, G. R. Müller-Putz, and C. Neuper. Laser-induced evoked potentials in the brain after non-perceptible optical stimulation at the Neiguan acupoint? A preliminary report. *Evid Based Complement Alternat Med*, 2012, in press.

G. Pfurtscheller, **G. Bauernfeind**, C. Neuper, and F. H. Lopes da Silva. Does conscious intention to perform a motor act depend on slow prefrontal (de)oxyhemoglobin oscillations in the resting brain? *Neurosci Lett*, 508(2):89-94, 2012.

2011

G. Bauernfeind, R. Scherer, G. Pfurtscheller, and C. Neuper. Single-trial classification of antagonistic oxyhemoglobin responses during mental arithmetic. *Med Biol Eng Comput*, 49(9):979-984, 2011.

G. Bauernfeind, V. Kaiser, T. Kaufmann, A. Kreilinger, A. Kübler, and C. Neuper. Cortical effects of BCI training measured with fNIRS. *Int J Bioelectromag*, 13:66-67, 2011.

V. Kaiser, **G. Bauernfeind**, T. Kaufmann, A. Kreilinger, A. Kübler, and C. Neuper. Cortical Effects of User Learning in a Motor-Imagery BCI Training. *Int J Bioelectromag*, 13(2):60-61, 2011.

G. Litscher, **G. Bauernfeind**, X. Gao, G. Müller-Putz, L. Wang, W. Anderle, I. Gaischek, D. Litscher, C. Neuper, and R. C. Niemtzow. Battlefield Acupuncture and Near-Infrared Spectroscopy - Miniaturized Computer-Triggered Electrical Stimulation of Battlefield Ear Acupuncture Points and 50-Channel Near-Infrared Spectroscopic Mapping. *Med Acup*, 23(4):263-270, 2011.

G. Pfurtscheller, D. Klobassa, C. Altstätter, **G. Bauernfeind**, and C. Neuper. About the stability of phase-shifts between slow oscillations around 0.1 Hz in cardiovascular and cerebral systems. *IEEE Trans Biomed Eng*, 58(7):2064-2071, 2011.

G. Pfurtscheller, D. Klobassa, **G. Bauernfeind**, and C. Neuper. Cardiovascular responses after brisk finger movement and their dependency on the eigenfrequency of the baroreflex loop. *Neurosci Lett*, 490(1):31-35, 2011.

2010

G. Pfurtscheller, **G. Bauernfeind**, S. C. Wriessnegger, and C. Neuper. Focal frontal (de)oxyhemoglobin responses during simple arithmetic. *Int J Psychophysiol*, 76(3):186-92, 2010.

G. Pfurtscheller, B. Z. Allison, **G. Bauernfeind**, C. Brunner, S. Solis Escalante, R. Scherer, T. O. Zander, G. R. Müller-Putz, C. Neuper, and N. Birbaumer. The hybrid BCI *Front Neurosci*, 4:42, 2010.

G. Pfurtscheller, R. Ortner, **G. Bauernfeind**, P. Linortner, and C. Neuper. Does conscious intention to perform a motor act depend on slow cardiovascular rhythms? *Neurosci Lett*, 468(1):46-50, 2010.

2008

G. Bauernfeind, R. Leeb, S. C. Wriessnegger, and G.Pfurtscheller. Development, set-up and first results for a one-channel near-infrared spectroscopy system. *Biomed Tech (Berl)*, 53(1):36-43, 2008.

K. Pfurtscheller, **G. Bauernfeind**, G. R. Müller-Putz, B. Urlesberger, W. Müller, and G. Pfurtscheller. Correlation between EEG burst-to-burst intervals and HR acceleration in preterm infants. *Neurosci Lett*, 437(2):103-106, 2008.

Proceedings

2012

G. Bauernfeind, I. Daly, and G. R. Müller-Putz. On the removal of physiological artifacts from fNIRS. *Proceedings of the 3rd TOBI Workshop 2012*, 24-25, 2012.

2011

G. Bauernfeind, R. Scherer, G. Pfurtscheller, and C. Neuper. Classication of Focal Frontal Oxyhemoglobin Responses During Mental Arithmetic. *Proceedings of the 5th International Brain-Computer Interface Conference 2011*, 264-267, 2011.

G. Pfurtscheller, **G. Bauernfeind**, and C. Neuper. Slow Phase-related Oscillations of Prefrontal (De)oxyhemoglobin and Central EEG Alpha and Beta Power in the Resting Brain. *Proceedings of the 5th International Brain-Computer Interface Conference 2011*, 340-342, 2011.

2010

G. Bauernfeind, S. C. Wriessnegger, G. Pfurtscheller, and C. Neuper. Fokale frontale (De)oxyhmoglobin-nderung whrend einfacher arithmetischer Aufgaben: Anmerkungen zur Verwendung als Steuersignale für optische Gehirn-Computer-Interface (oBCI)-Anwendungen. *Kongress 5 Jahre INGE St.*, 30-30, 2010.

G. Bauernfeind, K. Schweizer, S. C. Wriessnegger, S. Kober, G. Pfurtscheller, and C. Neuper. Neural correlates of the execution and inhibition of well learned foot and finger movements: an NIRS study. *Proceedings of the 1st TOBI Workshop 2010*, 38-38, 2010.

2009

G. Bauernfeind, R. Leeb, P. Linortner and G. Pfurtscheller. Using Near-Infrared Spectroscopy (NIRS) to realize an optical BCI. *Proceedings of the Neuromath Workshop 2009*, 35-35, 2009.

2008

G. Bauernfeind, R. Leeb, C. Neuper, and G. Pfurtscheller. Reducing the blood pressure influence on characteristic hemodynamic responses: a preliminary NIRS study. *Proceedings of the 4th International Brain-Computer Interface Workshop and Training Course 2008*, 309-314, 2008.

2007

G. Bauernfeind, K. Pfurtscheller, G.R. Müller-Putz, B. Urlesberger, W. Müller, and G. Pfurtscheller. Cortico-cardiac coupling and maturation aspects in preterm infants at 36 weeks of conceptional age. *Proceedings of the Neuromath Workshop 2007*, 11-22, 2007.

G. Bauernfeind, R. Leeb, S. C. Wriessnegger, V. Kaiser, and G. Pfurtscheller. Electrical and optical recording of neural activity during mental task. *Proceedings of the 1st Workgroups Meeting*, 99-99, 2007.

G. R. Müller-Putz, R. Leeb, **G. Bauernfeind**, K. Pfurtscheller, B. Urlesberger, and G. Pfurtscheller. Cortico-cardiac coupling in preterm infants and adults. *Proceedings of the 1st Workgroups Meeting*, 38-38, 2007.

2006

G. Bauernfeind, R. Leeb, S. C. Wriessnegger, H. Scharfetter, and G. Pfurtscheller. Setup of the NIRS based Graz-BCI. *Proceedings of the 3rd International Brain-Computer Interface Workshop and Training Course 2006*, 102-103, 2006.

R. Leeb, **G. Bauernfeind**, S. C. Wriessnegger, H. Scharfetter, and G. Pfurtscheller. First steps towards the NIRS-based Graz-BCI. *Proceedings der Gemeinsame Jahrestagung der Deutschen, der Österreichischen und der Schweizerischen Gesellschaften für Biomedizinische Technik*, 1-2, 2006.

Book chapters

2012

G. R. Müller-Putz, R. Leeb, J. D. Millan, P. Horki, A. Kreilinger, **G. Bauernfeind**, B. Z. Allison, C. Brunner, and R. Scherer. Principles of Hybrid Brain-Computer Interfaces. In *Toward Practical BCIs: Bridging the Gap*

from Research to Real-World Applications, 2012, in press.

Bibliography

[1] P. M. Arenth, J. H. Ricker, and M. T. Schultheis. Applications of functional near-infrared spectroscopy (fNIRS) to Neurorehabilitation of cognitive disabilities. *Clin Neuropsychol*, 21(1):38–57, 2007.

[2] S. R. Arridge, M. Cope, and D. T. Delpy. Theoretical basis for the determination of optical pathlengths in tissue: temporal and frequency analysis. *Physics Med Biol*, 37(7):1531–1560, 1992.

[3] H. Ayaz, M. Izzetoglu, S. Bunce, T. Heiman-Patterson, and B. Onaral. Detecting cognitive activity related hemodynamic signal for brain computer interface using functional near infrared spectroscopy. *Proc. IEEE EMBS 2007*, pages 342–345, 2007.

[4] G. Bauernfeind. *Entwicklung eines Nah-Infrarot-Spektroskopie-Systems für die Verwendung als optisches Brain-Computer Interface*. PhD thesis, Graz University of Technology, Austria, 2006.

[5] G. Bauernfeind. *Nah-Infrarot-Spektroskopie am Menschen*. VDM Verlag, 2008.

[6] G. Bauernfeind, I. Daly, and G. R. Müller-Putz. On the removal of physiological artifacts from fNIRS. *Proceedings of the 3rd TOBI Workshop 2012*, pages 24–25, 2012.

[7] G. Bauernfeind, V. Kaiser, T. Kaufmann, A. Kreilinger, A. Kbler, and C. Neuper. Cortical effects of BCI training measured with fNIRS. *Int J Bioelect*, 13(2):66–67, 2011.

[8] G. Bauernfeind, R. Leeb, S. Wriessnegger, and G. Pfurtscheller. Development, set-up and first results of a one-channel near-infrared spectroscopy system. *Biomed Tech (Berl)*, 53(1):36–43, 2008.

[9] G. Bauernfeind, R. Scherer, G. Pfurtscheller, and C. Neuper. Single trial classification of antagonistic oxyhemoglobin responses during mental arithmetic. *Med Biol Eng Comput*, 49(9):979–984, 2011.

[10] T. S. Bearden, J.E. Cassisi, and M. Pineda. Neurofeedback training for a patient with thalamic and cortical infarctions. *Appl Psychophysiol Biofeedback*, 28(3):241–253, 2003.

[11] A. Belouchrani, K. Abed-Meraim, J. Cardoso, and E. Moulines. A blind source seperation technique using second-order statistics. *IEEE Trans Sig Proc*, 45(2):434–444, 1997.

[12] H. Berger. Über das Elektrenkephalogramm des Menschen. *Archiv für Psychiatrie und Nervenkrankheiten*, 87:527–570, 1929.

[13] G. Bin, X. Gao, Z. Yan, B. Hong, and S. Gao. An online multi-channel SSVEP-based brain-computer interface using a canonical correlation analysis method. *J Neural Eng*, 6(4):046002, 2009.

[14] N. Birbaumer. Breaking the silence: brain-computer interfaces (BCI) for communication and motor control. *Psychophysiology*, 43(6):517–532, 2006.

[15] N. Birbaumer, T. Elbert, A.G. Canavan, and B. Rockstroh. Slow potentials of the cerebral cortex and behavior. *Physiol Rev*, 70(1):21–41, 1990.

[16] N. Birbaumer, T. Elbert, B. Rockstroh, and W. Lutzenberger. Biofeedback of event-related slow potentials of the brain. *Int J Psychol*, 16(4):389–415, 1981.

[17] N. Birbaumer, N. Ghanayim, T. Hinterberger, I. Iversen, B. Kotchoubey, A. Kübler, J. Perelmouter, E. Taub, and H. Flor. A spelling device for the paralyzed. *Nature*, 398:297–298, 1999.

[18] N. Birbaumer and R. F. Schmidt. *Biologische Psychologie*. Springer Verlag, 1999.

[19] N. Birbaumer, C. Weber, C. Neuper, E. Buch, K. Haapen, and L. Cohen. Physiological regulation of thinking: brain-computer interface (BCI) research. *Prog Brain Res*, 159:369–391, 2006.

[20] B. Blankertz, G. Dornhege, M. Krauledat, K. R. Müller, V. Kunzmann, F. Losch, and G. Curio. The Berlin brain-computer interface: EEG-based communication without subject training. *IEEE Trans Neural Syst Rehabil Eng*, 14(2):147–152, 2006.

[21] F. P. Bolin, L. E. Preuss, R. C. Taylor, and R. J. Ference. Refractive index of some mammalian tissues using a fiber optic cladding method. *Appl Opt*, 28(12):2297–2303, 1989.

[22] J. E. Brazy, D.V. Lewis, M. H. Mitnick, and F. F. Jöbsis. Noninvasive monitoring of cerebral oxygenation in preterm infants: preliminary observations. *Pediatrics*, 75(2):217–225, 1985.

[23] C. Brunner, B. Z. Allison, C. Altstätter, and C. Neuper. A comparison of three brain-computer interfaces based on event-related desynchronization, steady state visual evoked potentials, or a hybrid approach using both signals. *J Neural Eng*, 8(2):025010, 2011.

[24] R. B. Buxton. The Elusive Initial Dip. *Neuroimage*, 13(6):953–958, 2001.

[25] R. B. Buxton, K. Uludag, D. J. Dubowitz, and T. T. Liu. Modeling the hemodynamic response to brain activation. *Neuroimage*, 23 Suppl 1:S220–S233, 2004.

[26] S. Chakravarti, S. Srivastava, and A. J. C. Mittnacht. Near Infrared Spectroscopy (NIRS) in Children. *Semin Cardiothorac Vasc Anesth*, 12(1):70–79, 2008.

[27] B. Chance, M. Cope, E. Gratton, N. Ramanujam, and B. Tromberg. Phase measurement of light absorption and scatter in human tissue. *Rev Sci Instrum*, 69(10):3457–3481, 1998.

[28] B. Chance, J. S. Leigh, H. Miyake, D.S. Smith, S. Nioka, R. Greenfeld, M. Finander, K. Kaufmann, W. Levy, M. Young, P. Cohen, H. Yoshioka, and R. Boretsky. Comparison of time-resolved and -unresolved measurements of deoxyhemoglobin in brain. *Proc Natl Acad Sci U S A*, 85(14):4971–4975, 1988.

[29] D. D. Clark and L. Sokoloff. Circulation and Energy Metabolism of the Brain. In G. J. Siegel, B. W. Agranoff, R. W. Albers, S. K. Fisher, and M. D. Uhler, editors, *Basic Neurochemistry: Molecular, Cellular and Medical Aspects*, pages 637–670. Lippincott, Philadelphia, 1999.

[30] J. Cohen. *Statistical Power Analysis for the Behavioral Sciences*. Lawrence Erlbaum Associates, Hillsdale, NJ, 1988.

[31] M. Cope. *The Application of Near Infrared Spectroscopy to Non Invasive Monitoring of Cerebral Oxygenation in the Newborn Infant*. PhD thesis, University College London, England, 1991.

[32] M. Cope and D. T. Delpy. A system for the long-term measurement of cerebral blood and tissue oxygenation in newborn infants by near infrared transillumination. *Med Biol Eng Comput*, 26(3):289–294, 1988.

[33] S. Coyle. *Near-Infrared Spectroscopy for Brain Computer Interfacing*. PhD thesis, National University of Ireland, Ireland, 2005.

[34] S. Coyle, T. Ward, and C. Markham. Physiological noise in near-infrared spectroscopy: implications for optical brain computer interfacing. *Conf Proc IEEE Eng Med Biol Soc*, 6:4540–4543, 2004.

[35] S. Coyle, T. E. Ward, C. Markham, and G. McDarby. On the suitability of near-infrared (NIR) systems for next-generation brain-computer interfaces. *Physiol Meas*, 25(4):815–822, 2004.

[36] S. Coyle, T. E. Ward, and C. M. Markham. Brain-computer interface using a simplified functional near-infrared spectroscopy system. *J Neural Eng*, 4(3):219–226, 2007.

[37] X. Cui, S. Bray, D. M. Bryant, G. H. Glover, and A. L. Reiss. A quantitative comparison of NIRS and fMRI across multiple cognitive tasks. *Neuroimage*, 54(4):2808–2821, 2011.

[38] D. Cyranoski. Neuroscience: Thought experiment. *Nature*, 469(7329):148–149, 2011.

[39] F. H. Lopes da Silva. Neural mechanisms underlying brain waves: from neural membranes to networks. *Electroenceph clin Neurophysiol*, 79(2):81–93, 1991.

[40] R. W. De Boer, J. M. Karemaker, and J. Strackee. On the spectral analysis of blood pressure variability. *Am J Physiol*, 251(3 Pt 2):H685–H687, 1986.

[41] S. Dehaene, N. Molko, L. Cohen, and A. J. Wilson. Arithmetic and the brain. *Curr Opin Neurobiol*, 14(2):218–224, 2004.

[42] D. T. Delpy and M. Cope. Quantification in tissue near-infrared spectroscopy. *Philos Trans R Soc Lond B Biol Sci*, 352(1354):649–659, 1997.

[43] D. T. Delpy, M. Cope, P. van der Zee, S. Arridge, S. Wray, and J. Wyatt. Estimation of optical pathlength through tissue from direct time of flight measurement. *Phys Med Biol*, 33(12):1433–1442, 1988.

[44] I. M. Devonshire, N. G. Papadakis, M. Port, J. Berwick, A. J. Kennerley, J. E. Mayhew, and P. G. Overton. Neurovascular coupling is brain region-dependent. *Neuroimage*, 59(3):1997–2006, 2012.

[45] W. C. Drevets, H. Burton, T. O. Videen, A. Z. Snyder, J. R. Simpson, and M. E. Raichle. Blood flow changes in human somatosensory cortex during anticipated stimulation. *Nature*, 373(6511):249–252, 1995.

[46] R. O. Duda, P. E. Hart, and D. G. Stork. *Pattern Classification*. Wiley-Interscience, 2000.

[47] A. Duncan, J. H. Meek, M. Clemence, C. E. Elwell, L. Tyszczuk, M. Cope, and D.T. Delpy. Optical pathlength measurements on adult head, calf and forearm and the head of the newborn infants using phase resolved optical spectroscopy. *Phys Med Biol*, 40(2):295–304, 1995.

[48] T. Egner and M. B. Sterman. Neurofeedback treatment of epilepsy: from basic rationale to practical application. *Expert Rev Neurother*, 6(2):247–257, 2006.

[49] H. H. Ehrsson, S. Geyer, and E. Naito. Imagery of voluntary movement of fingers, toes, and tongue activates corresponding body-part-specific motor representations. *J Neurophysiol*, 90(5):3304–3316, 2003.

[50] C. E. Elwell, M. Cope, A. D. Edwards, J. S. Wyatt, E. O. Reynolds, and D. T. Delpy. Measurement of cerebral blood flow in adult humans using near infrared spectroscopy - methodology and possible errors. *Adv Exp Med Biol*, 317:235–245, 1993.

[51] C. E. Elwell, R. Springett, and E. Hillman. Oscillations in cerebral haemodynamics - Implications for functional activation studies. *Adv Exp Med Biol*, 471:57–65, 1999.

[52] U. E. Emir, C.B. Akgul, A. Akin, A. Ertuzun, B. Sankur, and K. Harmanci. Wavelet denoising vs. ICA denoising for functional optical imaging. *Proc 1st Int IEEE EMBS Conf Neural Eng*, pages 5384 –5387, 2003.

[53] L. A. Farwell and E. Donchin. Talking off the top of your head: toward a mental prosthesis utilizing event-related brain potentials. *Electroencephalogr Clin Neurophysiol*, 70(6):510–523, 1988.

[54] S. Fazliand, J. Mehnert, J. Steinbrink, G. Curio, A. Villringer, K. R. Müller, and B. Blankertz. Enhanced performance by a hybrid NIRS-EEG brain computer interface. *Neuroimage*, 59(1):519–529, 2011.

[55] G. Florian, A. Stancak, and G. Pfurtscheller. Cardiac response induced by voluntary self-paced finger movement. *Int J Psychophysiol*, 28(3):273–283, 1998.

[56] D. J. Fox, D. F. Tharp, and L. C. Fox. Neurofeedback: an alternative and efficacious treatment for Attention Deficit Hyperactivity Disorder. *Appl Psychophysiol Biofeedback*, 30(4):365–373, 2005.

[57] E. Fox, F. F. Jöbsis, and M. H. Mitnick. Monitoring cerebral oxygen sufficiency in anaesthesia and surgery. *Adv Exp Med Biol*, 191:849–854, 1985.

[58] P. T. Fox and M. E. Raichle. Focal physiological uncoupling of cerebral blood flow and oxidative metabolism during somatosensory stimulation in human subjects. *Proc Natl Acad Sci U S A*, 83(4):1140–1144, 1986.

[59] P. T. Fox, M. E. Raichle, M. A. Mintun, and C. Dence. Nonoxidative glucose consumption during focal physiologic activity. *Science*, 241(4864):462–464, 1988.

[60] M. A. Franceschini, S. Fantini, J. H. Thompson, J. P. Culver, and D. A. Boas. Hemodynamic evoked response of the sensorimotor cortex measured noninvasively with near-infrared optical imaging. *Psychophysiology*, 40(4):548–560, 2003.

[61] M. Fukuda. *Psychiatric Disorders and NIRS*. Nakayama Shoten Co. Ltd., 2009.

[62] Y. Fukuiy, Y. Ajichi, and E. Okada. Monte Carlo prediction of near-infrared light propagation in realistic adult and neonatal head models. *Applied Optics*, 42(16):2881–2887, 2003.

[63] B. Graimann. *Movement-related patterns in ECoG and EEG: Visualization and detection*. PhD thesis, Graz University of Technology, Austria, 2002.

[64] G. Gratton and P. M. Corballis. Removing the heart from the brain: compensation for the pulse artifact in the photon migration signal. *Psychophysiology*, 32(3):292–299, 1995.

[65] G. Gratton and M. Fabiani. Shedding light on brain function: the event-related optical signal. *Trends Cogn Sci*, 5(8):357–363, 2001.

[66] M. J. Herrmann, A. C. Ehlis, A. Wagener, C. P. Jacob, and A. J. Fallgatter. Near-infrared optical topography to assess activation of the parietal cortex during a visuo-spatial task. *Neuropsychologia*, 43(12):51713–1720, 2005.

[67] M. J. Herrmann, T. Huter, M. M. Plichta, A. C. Ehlis, G. W. Alpers, A. Mühlberger, and A. J. Fallgatter. Enhancement of activity of the primary visual cortex during processing of emotional stimuli as measured with event-related functional near-infrared spectroscopy and event-related potentials. *Hum Brain Mapp*, 29(1):28–35, 2008.

[68] D. K. Hill and R. D. Keynes. Opacity changes in stimulated nerve. *J Physiol*, 108(3):278–281, 1949.

[69] T. Hinterberger, R. Veit, U. Strehl, T. Trevorrow, M. Erb, B. Kotchoubey, H. Flor, and N. Birbaumer. Brain areas activated in fMRI during self-regulation of slow cortical potentials (SCPs). *Exp Brain Res*, 152(1):113–122, 2003.

[70] S. R. Hintz. Near-infrared spectroscopy: Neonatal and Perinatal Applications. *NeoReviews*, 2:22–28, 2001.

[71] L. R. Hochberg, M. D. Serruya, G. M. Friehs, J. A. Mukand, M. Saleh, A. H. Caplan, A. Branner, D. Chen, R. D. Penn, and J. P. Donoghue. Neuronal ensemble control of prosthetic devices by a human with tetraplegia. *Nature*, 442(7099):164–171, 2006.

[72] C. Hock, F. Müller-Spahn, S. Schuh-Hofer, M. Hofmann, U. Dirnagl, and A. Villringer. Age dependency of changes in cerebral hemoglobin oxygenation during brain activation: a near-infrared spectroscopy study. *J Cereb Blood Flow Metab*, 15(6):1103–1108, 1995.

[73] M. J. Hofmann, M. J. Herrmann, I. Dan, H. Obrig, M. Conrad, L. Kuchinke, A. M. Jacobs, and A. J. Fallgatter. Differential activation of frontal and parietal regions during visual word recognition: an optical topography study. *Neuroimage*, 40(3):1340–1349, 2008.

[74] R. W. Homan, J. Herman, and P. Purdy. Cerebral location of international 10-20 system electrode placement. *Electroencephalogr Clin Neurophysiol*, 66(4):376–382, 1987.

[75] Y. Hoshi. Functional near-infrared optical imaging: utility and limitations in human brain mapping. *Psychophysiology*, 40(4):511–520, 2003.

[76] Y. Hoshi, H. Onoe, Y. Watanabe, J. Andersson, M. Bergström, A. Lilja, B. Löngström, and M. Tamura. Non-synchronous behaviour of neuronal activity, oxidative metabolism and blood supply during mental tasks in man. *Neurosci Lett*, 172(1-2):129–133, 1994.

[77] Y. Hoshi and M. Tamura. Detection of dynamic changes in cerebral oxygenation coupled to neuronal function during mental work in man. *Neurosci Lett*, 150(1):5–8, 1993.

[78] Y. Hoshi and M. Tamura. Dynamic multichannel near-infrared optical imaging of human brain activity. *J Appl Physiol*, 75(4):1842–1846, 1993.

[79] F. Hummel, R. Saur, S. Lasogga, C. Plewnia, M. Erb, D. Wildgruber, W. Grodd, and C. Gerloff. To act or not to act. Neural correlates of executive control of learned motor behavior. *Neuroimage*, 23(4):1391–1401, 2004.

[80] F. F. Jöbsis. Noninvasive, infrared monitoring of cerebral and myocardial oxygen sufficiency and circulatory parameters. *Science*, 198(4323):1264–1267, 1977.

[81] M. Kameyama, M. Fukuda, Y. Yamagishi, T. Sato, T. Uehara, M. Ito, T. Suto, and M. Mikuni. Frontal lobe function in bipolar disorder: a multichannel near-infrared spectroscopy study. *Neuroimage*, 29(1):172–184, 2006.

[82] S. Kanoh, Y. M. Murayama, K. Miyamoto, T. Yoshinobu, and R. Kawashima. A NIRS-based brain-computer interface system during motor imagery: system development and online feedback training. *Conf Proc IEEE Eng Med Biol Soc 2009*, pages 594–597, 2009.

[83] T. Kato. Principle and technique of NIRS-imaging for human brain FORCE: fast-oxygen response in capillary event. *Int Cong Ser*, 1270:85–90, 2004.

[84] T. Kato, A. Kamei, S. Takashima, and T. Ozaki. Human visual cortical function during photic stimulation monitoring by means of nearinfrared spectroscopy. *J Cereb Blood Flow Metab*, 13(3):516–520, 1993.

[85] L. Kauhanen, T. Nykopp, J. Lehtonen, P. Jylänki, J. Heikkonen, P. Rantanen, H. Alaranta, and M. Sams. EEG and MEG brain-computer interface for tetraplegic patients. *IEEE Trans Neural Syst Rehabil Eng*, 14(2):190–193, 2006.

[86] R. Kawashima, M. Taira, K. Okita, K. Inoue, N. Tajima, H. Yoshida, T. Sasaki, M. Sugiura, J. Watanabe, and H. Fukuda. A functional MRI study of simple arithmetic - a comparison between children and adults. *Brain Res Cogn Brain Res*, 18(3):225–231, 2004.

[87] H. P. Koepchen. Physiology of rhythms and control systems: An integrative approach. In H. Haken and H. P. Koepchen, editors, *Rhythms in physiological systems: An integrative approach*, pages 3–20. Springer, 1991.

[88] A. Kübler, B. Kotchoubey, T. Hinterberger, N. Ghanayim, J. Perelmouter, M. Schauer, C. Fritsch, E. Taub, and N. Birbaumer. The thought translation device: a neurophysiological approach to communication in total motor paralysis. *Exp Brain Res*, 124(2):223–32, 1999.

[89] A. Kübler and K. R. Müller. An Introduction to Brain-Computer Interfacing. In G. Dorhegen, J. R. Millan, T. Hinterberger, D. J. McFarland, and K. R. Müller, editors, *Toward Brain-Computer Interfacing*, pages 1–25. MIT Press, 2007.

[90] J. Kurzman, S.C. Wriessenegger, and C. Neuper. Implementation of a realtime feedback system based on multichannel near-infrared spectroscopy. *Proceedings of the 4th International Brain-Computer Interface Workshop and Training Course*, pages 309–314, 2008.

[91] W. Kuschinsky and O. B. Paulson. Capillary circulation in the brain. *Cerebrovasc Brain Metab Rev*, 4(3):261–286, 1992.

[92] M. Lebedev and M. A. L. Nicolelis. Brain-machine interfaces: past, present and future. *Trends Neurosci*, 29(9):536–546, 2006.

[93] U. Leins, G. Goth, T. Hinterberger, C. Klinger, N. Rumpf, and U. Strehl. Neurofeedback for children with ADHD: a comparison of SCP and Theta/Beta protocols. *Appl Psychophysiol Biofeedback*, 32(2):73–88, 2007.

[94] E. C. Leuthardt, G. Schalk, J. R. Wolpaw, J. G. Ojemann, and D. W. Moran. A brain-computer interface using electrocorticographic signals in humans. *J Neural Eng*, 1(2):63–71, 2004.

[95] P. Linortner, R. Ortner, G.R. Müller-Putz, C. Neuper, and G. Pfurtscheller. Self -paced control of a hand orthosis using SSVEP-based bci. *Proceedings of the13th International Conference on Human-Computer Interaction 2009*, 2009.

[96] G. Litscher and G. Schwarz. *Transcranial Cerebral Oximetry*. Pabst Science Publishers, 1997.

[97] H. Lüthy. Die Ultraviolettabsorption der lebenden Nervenfaser. *Helv Physiol Pharmacol Acta*, 4(C):20–22, 1946.

[98] H. Lüthy. *Helv Physiol Pharmacol Acta*, 6(1):28–30, 1948.

[99] W. Lutzenberger, T. Elbert, B. Rockstroh, and N. Birbaumer. The effects of self-regulation of slow cortical potentials on performance in a signal detection task. *Int J Neurosci*, 9(3):175–183, 1979.

[100] S. Luu and T. Chau. Decoding subjective preference from single-trial near-infrared spectroscopy signals. *J Neural Eng*, 6(1):016003, 2009.

[101] A. Maki, Y. Yamashita, Y. Ito, E. Watanabe, Y. Mayanagi, and H. Koizumi. Spatial and temporal analysis of human motor activity using noninvasive NIR topography. *Med Phys*, 22(12):1997–2005, 1995.

[102] D. Malonek, U. Dirnagl, U. Lindauer, K. Yamada, I. Kanno, and A. Grinvald. Vascular imprints of neuronal activity: relationships between the dynamics of cortical blood flow, oxygenation, and volume changes following sensory stimulation. *Proc Natl Acad Sci U S A*, 94(26):14826–14831, 1997.

[103] D. Malonek and A. Grinvald. Interactions between electrical activity and cortical microcirculation revealed by imaging spectroscopy: implications for functional brain mapping. *Science*, 272(5261):551–554, 1996.

[104] F. Matthews, B. A. Pearlmutter, T. E. Ward, C. Soraghan, and C. Markham. Hemodynamics for Brain-Computer Interfaces. *IEEE Sig Process*, 25(1):87–94, 2008.

[105] E. M. Maynard, C. T. Nordhausen, and R. A. Normann. The Utah intracortical Electrode Array: a recording structure for potential brain-computer interfaces. *Electroencephalogr Clin Neurophysiol*, 102(3):228–239, 1997.

[106] J. Mellinger, G. Schalk, C. Braun, H. Preissl, W. Rosenstiel, N. Birbaumer, and A. Kübler. An MEG-based brain-computer interface (BCI). *Neuroimage*, 36(3):581–593, 2007.

[107] V. Menon, S. M. Rivera, C. D. White, G. H. Glover, and A. L. Reiss. Dissociating prefrontal and parietal cortex activation during arithmetic processing. *Neuroimage*, 12(4):357–365, 2000.

[108] M. Middendorf, G. McMillan, G. Calhoun, and K. S. Jones. Brain-computer interfaces based on the steady-state visual-evoked response. *IEEE Trans Rehabil Eng*, 8(2):211–214, 2000.

[109] M. Mihara, H. Yagura, M. Hatakenaka, N. Hattori, and I. Miyai. Clinical application of functional near-infrared spectroscopy in rehabilitation medicine. *Brain Nerve*, 62(2):125–132, 2010.

[110] J. del R. Millán. Brain-computer interfaces. In M. A. Arbib, editor, *The handbook of brain theory and neural networks: the second edition*. MIT Press, 2002.

[111] E. K. Miller and J.D. Cohen. An integrative theory of prefrontal cortex function. *Annu Rev Neurosci*, 24:167–202, 2001.

[112] S. Moghimi, A.Kushki, S. Power, A.M. Guerguerian, and T. Chau. Automatic detection of a prefrontal cortical response to emotionally-rated music using multi-channel near-infrared spectroscopy. *J Neural Eng*, 9(2):026022, 2012.

[113] G. Morren, U. Wolf, P. Lemmerling, M. Wolf, J. H. Choi, E. Gratton, L. De Lathauwer, and S. Van Huffel. Detection of fast neuronal signals in the motor cortex from functional near infrared spectroscopy measurements using independent component analysis. *Med Biol Eng Comput*, 42(1):92–9, 2004.

[114] G. R. Müller-Putz, R. Leeb, J. D. Millan, P. Horki, A. Kreilinger, G. Bauernfeind, B. Z. Allison, C. Brunner, and R. Scherer. Principles of Hybrid Brain-Computer Interfaces. In *Toward Practical BCIs: Bridging the Gap from Research to Real-World Applications*. Springer, 2012, in press.

[115] G. R. Müller-Putz, R. Scherer, C. Brauneis, and G. Pfurtscheller. Steady-state visual evoked potential (SSVEP)-based communication: impact of harmonic frequency components. *J Neural Eng*, 2(4):123–130, 2005.

[116] G. R. Müller-Putz, R. Scherer, R. Leeb, and G. Pfurtscheller. Better than random? A closer look on BCI results. *Int J Bioelectromagn*, 10:52–55, 2008.

[117] G. R. Müller-Putz, R. Scherer, C. Neuper, and G. Pfurtscheller. Steady-state somatosensory evoked potentials: suitable brain signals for brain-computer interfaces? *IEEE Trans Neural Syst Rehabil Eng*, 14(1):30–37, 2006.

[118] M. Naito, Y. Michioka, K. Ozawa, Y. Ito, M. Kiguchi, and T. Kanazawa T. A communication means for totally locked-in ALS patients based on changes in cerebral blood volume measured with near-infrared light. *IEICE Trans Inf Syst E*, 90(D):1028–1037, 2007.

[119] M. A. L. Nicolelis. Actions from thoughts. *Nature*, 409(6818):403–407, 2001.

[120] E. Niedermeyer. The normal EEG of the waking adult. In E. Niedermeyer and F. H. Lopes da Silva, editors, *Electroencephalography: basic principles, clinical applications and related fields*. Lippincott Williams & Wilkins, 2005.

[121] H. Ogata, T. Mukai, and T. Yagi. A study on the frontal cortex in cognitive tasks using near-infrared spectroscopy. *Conf Proc IEEE Eng Med Biol Soc 2007*, pages 4731–4734, 2007.

[122] E. Okada and D. T. Delpy. Near-infrared light propagation in an adult head model. II. Effect of superficial tissue thickness on the sensitivity of near-infrared spectroscopy signal. *App Opt*, 42(16):2915–2922, 2003.

[123] E. Okada, M. Firbank, and D. T. Delpy. The effect of overlying tissue on the spatial sensitivity profile of near-infrared spectroscopy. *Phys Med Biol*, 40(12):2093–2108, 1995.

[124] E. Okada, M. Firbank, M. Schweiger, S. R. Arridge, M. Cope, and D. T. Delpy. Theoretical and experimental investigation of near-infrared light propagation in a model of the adult head. *App Opt*, 36(1):21–31, 1997.

[125] M. Okamoto, H. Dan, K. Sakamoto, K. Takeo, K. Shimizu, S. Kohno, I. Oda, S. Isobe, T. Suzuki, K. Kohyama, and I. Dan. Three-dimensional probabilistic anatomical cranio-cerebral correlation via the international 10-20 system oriented for transcranial functional brain mapping. *Neuroimage*, 21(1):99–111, 2004.

[126] M. S. Patterson, B. Chance, and B.C. Wilson. Time resolved reflectance and transmittance for the non-invasive measurement of tissue optical properties. *Appl Opt*, 28(12):2331–2336, 1989.

[127] G. Pfurtscheller. Graphical display and statistical evaluation of event-related desynchronization (ERD). *Electroencephalogr Clin Neurophysiol*, 43(5):757–760, 1977.

[128] G. Pfurtscheller, B. Z. Allison, G. Bauernfeind, C. Brunner, S. Solis Escalante, R. Scherer, T. O. Zander, G. R. Müller-Putz, C. Neuper, and N. Birbaumer. The hybrid BCI. *Front Neurosci*, 4:42, 2010.

[129] G. Pfurtscheller and A. Aranibar. Event-related cortical desynchronization detected by power measurements of scalp EEG. *Electroencephalogr Clin Neurophysiol*, 42(6):817–826, 1977.

[130] G. Pfurtscheller, G. Bauernfeind, S. C. Wriessnegger, and C. Neuper. Focal frontal (de)oxyhemoglobin responses during simple arithmetic. *Int J Psychophysiol*, 76(3):186–192, 2010.

[131] G. Pfurtscheller and A. Berghold. Patterns of cortical activation during planning of voluntary movement. *Electroencephalogr Clin Neurophysiol*, 72(3):250–258, 1989.

[132] G. Pfurtscheller, D. Flotzinger, M. Pregenzer, J. R. Wolpaw, and D. McFarland. EEG-based brain computer interface (BCI). search for optimal electrode positions and frequency components. *Med Prog Technol*, 21(3):573–576, 1995.

[133] G. Pfurtscheller and F. H. Lopes da Silva. Event-related EEG/MEG synchronization and desynchronization: basic principles. *Clin Neurophysiol*, 110(11):1842–1857, 1999.

[134] G. Pfurtscheller, H. Maresch, and S. Schuy. Inter- and intrahemispheric differences in the peak frequency of rhythmic activity within the alpha band. *Electroencephalogr Clin Neurophysiol*, 42(6):77–83, 1977.

[135] G. Pfurtscheller, G. R. Müller-Putz, A. Schlögl, B. Graimann, R. Scherer, R. Leeb, C. Brunner, C. Keinrath, F. Y. Lee, G. Townsend, C. Vidaurre, and C. Neuper. 15 years of BCI research at Graz University of Technology: current trends. *IEEE Trans Neural Syst Rehabil Eng*, 14(2):205–210, 2006.

[136] G. Pfurtscheller and C. Neuper. Event-related synchronization of mu rhythm in the EEG over the cortical hand area in man. *Neurosci Lett*, 174(1):93–96, 1994.

[137] G. Pfurtscheller, T. Solis-Escalante, R. Ortner, P. Linortner, and G. R. Müller-Putz. Self-paced operation of an SSVEP-based orthosis with and without an imagery-based "brain switch": a feasibility study towards a hybrid BCI. *IEEE Trans Neural Syst Rehabil Eng*, 18(4):409–414, 2010.

[138] T. W. Picton, M. S. John, A. Dimitrijevic, and D. Purcell. Human auditory steady-state responses. *Int J Audiol*, 42(4):177–219, 2003.

[139] S. D. Power, T. H. Falk, and T. Chau. Classification of prefrontal activity due to mental arithmetic and music imagery using hidden markov models and frequency domain near-infrared spectroscopy. *J Neural Eng*, 7(2):26002, 2010.

[140] S. D. Power, A. Kushi, and T. Chau. Towards a system-paced near-infrared spectroscopy brain-computer interface: differentiating prefrontal activity due to mental arithmetic and mental singing from the no-control state. *J Neural Eng*, 8(6):066004, 2011.

[141] P. Pudil, J. Novovičová, and J. Kittler. Floating search methods in feature selection. *Pattern Recognit Lett*, 15 (1994):1119–1125, 1994.

[142] L. R. Rabiner. A Tutorial on Hidden Markov Models and Selected Applications in Speech Recognition. *Proc IEEE*, 77(2):257–286, 1989.

[143] M. E. Raichle and D. A. Gusnard. Appraising the brain's energy budget. *Proc Natl Acad Sci U S A*, 99(16):10237–10239, 2002.

[144] D. Regan. Some characteristics of average steady-state and transient responses evoked by modulated light. *Electroencephalogr Clin Neurophysiol*, 20(3):238–248, 1966.

[145] T. C. Rickard, S. G. Romero, G. Basso, C. Wharton, S. Flitman, and J. Grafman. The calculating brain: an fMRI study. *Neuropsychologia*, 38(3):325–335, 2000.

[146] C. S. Roy and C. S. Sherrington. On the regulation of the blood-supply of the brain. *J Physiol*, 11(1-2):85–108, 1890.

[147] rtsBCI. Graz brain-computer interface real-time open source package. *Available online at http://sourceforge.net/projects/biosig/*, 2004-2011.

[148] K. Sagara, K. Kido, and K. Ozawa. Portable single-channel NIRS-based BMI system for motor disabilities' communication tools. *Conf Proc IEEE Eng Med Biol Soc*, pages 602–605, 2009.

[149] G. Schalk, J. Kubánek, K. J. Miller, N. R. Anderson, E. C. Leuthardt, J. G. Ojemann, D. Limbrick, D. Moran, L. A. Gerhardt, and J. R. Wolpaw. Decoding two-dimensional movement trajectories using electrocorticographic signals in humans. *J Neural Eng*, 4(3):264–275, 2007.

[150] R. Scherer, G. R. Müller-Putz, and G. Pfurtscheller. Self-initiation of EEG-based brain-computer communication using the heart rate response. *J Neural Eng*, 4(4):L23–L29, 2007.

[151] S. Shimada, K. Hiraki, G. Matsuda, and I. Oda. Decrease in prefrontal haemoglobin oxygenation during reaching tasks with delayed visual feedback: a near-infrared spectroscopy study. *Brain Res Cogn Brain Res*, 20(3):480–490, 2004.

[152] A. K. Singh, M. Okamoto, H. Dan, V. Jurcak, and I. Dan. Spatial registration of multichannel multi-subject fNIRS data to MNI space without MRI. *Neuroimage*, 27(4):842–851, 2005.

[153] R. Sitaram, A. Caria, and N. Birbaumer. Hemodynamic brain-computer interfaces for communication and rehabilitation. *Neural Netw*, 22(9):1320–1328, 2009.

[154] R. Sitaram, Y. Hoshi, and C. Guan. Near infrared spectroscopy based brain-computer interface. *Proc SPIE*, 5852:434–442, 2005.

[155] R. Sitaram, H. Zhang, C. Guan, M. Thulasidas, Y. Hoshi, A. Ishikawa, K. Shimizu, and N. Birbaumer. Temporal classification of multichannel near-infrared spectroscopy signals of motor imagery for developing a brain-computer interface. *Neuroimage*, 34(4):1416–1427, 2007.

[156] C. J. Soraghan, F. Matthews, D. Kelly, C. Markham, B. A. Pearlmutter, and R. O'Neill. A Dual-Channel Optical Brain-Computer Interface in a Gaming Environment. *CGAMES 2006 - 9th International Conference on Computer Games: AI, Animation, Mobile, Educational and Serious Games*, 2006.

[157] J. Steinbrink, A. Villringer, F. Kempf, D. Haux, S. Boden, and H. Obrig. Illuminating the BOLD signal: combined fMRI-fNIRS studies. *Magn Reson Imaging*, 24(4):495–505, 2006.

[158] H. Steingruber and G. Lienert. *Hand-Dominanz-Test.* Hogrefe, Göttingen, 1971.

[159] J. Stevens. *Applied multivariate statistics for the social sciences*. Erlbaum, Mahwah, New Jersey, 2002.

[160] G. Strangman, J. P. Culver, J. H. Thompson, and D. A. Boas. A quantitative comparison of simultaneous BOLD fMRI and NIRS recordings during functional brain activation. *Neuroimage*, 17(2):719–731, 2002.

[161] G. Sudre, L. Parkkonen, E. Bock, S. Baillet, W. Wang, and D. J. Weber. rtMEG: a real-time software interface for magnetoencephalography. *Comput Intell Neurosci*, page 327953, 2011.

[162] P. Suffczynski, J. P. Pijn, G. Pfurtscheller, and F. H. Lopes da Silva. Event-related dynamics of alpha band rhythm: A neuronal network model of focal ERD/surrounded ERS. In G. Pfurtscheller and F.H. Lopes da Silva, editors, *Event-Related Desynchronization. Handbook of Electroencephalography and Clinical Neurophysiology. Revised Edition Vol. 6.*, pages 67–85. Elsevier, 1999.

[163] S. Sutton, M. Braren, J. Zubin, and E.R. John. Evoked-potential correlates of stimulus uncertainty. *Science*, 150(3700):1187–1188, 1965.

[164] K. Tai and T. Chau. Single-trial classification of NIRS signals during emotional induction tasks: towards a corporeal machine interface. *J Neuroeng Rehabil*, 6(1):39, 2009.

[165] M. Tanida, S. Sakatani, R. Takano, and K. Tagai. Relation between asymmetry of prefrontal cortex activities and the autonomic nervous system during a mental arithmetic task: near infrared spectroscopy study. *Neurosci Lett*, 369(1):69–74, 2004.

[166] N. Tax, G. Pichler, K. Grossauer, M. Pocivalnik, H. Zotter, W. Raith, W. Müller, and B. Urlesberger. Tilting the Head Changes Cerebral Haemodynamics in Neonates. *Neonatology*, 100(3):253–259, 2011.

[167] R. Turner and A. Grinvald. Direct visualization of patterns of deoxygenation and reoxygenation in monkey cortical vasculature during functional brain activation. *Proc Soc Magn Reson*, 1:430, 1994.

[168] K. Uludag, J. Steinbrink, A. Villringer, and H. Obrig. Separability and cross talk: optimizing dual wavelength combinations for near-infrared spectroscopy of the adult head. *Neuroimage*, 22(2):583–589, 2004.

[169] B. Urlesberger, E. Kratky, T. Rehak, M. Pocivalnik, A. Avian, J. Czihak, W. Müller, and G. Pichler. Regional Oxygen Saturation of the

Brain during Birth Transition of Term Infants: Comparison between Elective Cesarean and Vaginal Deliveries. *J Pediatr*, 159(3):404–408, 2011.

[170] B. Urlesberger, F. Reiterer, and W. Müller. Cerebral oximetry in pediatrics. In G. Litscher and G. Schwarz, editors, *Transcranial Cerebral Oximetry*. Pabst Science Publishers, 1997.

[171] K. Utsugi, A. Obata, H. Sato, T. Katsura, K. Sagara, A. Maki, and H. Koizumi. Development of an optical brain-machine interface. *Conf Proc IEEE Eng Med Biol Soc 2007*, pages 5338–5341, 2007.

[172] V. N. Vapnik. *The nature of statistical learning theory*. Springer-Verlag, 2000.

[173] J. J. Vidal. Toward direct brain-computer communication. *Annu Rev Biophys Bioeng*, 2:157–180, 1973.

[174] A. Villringer and U. Dirnagl. Coupling of brain activity and cerebral blood flow: basis of functional neuroimaging. *Cerebrovasc Brain Metab Rev*, 7(3):240–276, 1995.

[175] A. Villringer, J. Planck, C. Hock, L. Schleinkofer, and U. Dirnagl. Near infrared spectroscopy (NIRS): a new tool to study hemodynamic changes during activation of brain function in human adults. *Neurosci Lett*, 154(1-2):101–104, 1993.

[176] J. E. Walker and G. P. Kozlowski. Neurofeedback treatment of epilepsy. *Child Adolesc Psychiatr Clin N Am*, 14(1):163–176, 2005.

[177] N. Weiskopf. Real-time fMRI and its application to neurofeedback. *Neuroimage*, 2011, in press.

[178] N. Weiskopf, K. Mathiak, S. W. Bock, F. Scharnowski, R. Veit, W. Grodd, R. Goebel, and N. Birbaumer. Principles of a brain-computer interface (BCI) based on real-time functional magnetic resonance imaging (fMRI). *IEEE Trans Biomed Eng*, 51(6):966–970, 2004.

[179] N. Weiskopf, R. Veit, M. Erb, K. Mathiak, W. Grodd, R. Goebel, and N. Birbaumer. Physiological self-regulation of regional brain activity using real-time functional magnetic resonance imaging (fMRI): methodology and exemplary data. *Neuroimage*, 19(3):577–586, 2003.

[180] K. Wing. Effect of neurofeedback on motor recovery of a patient with brain injury: a case study and its implications for stroke rehabilitation. *Top Stroke Rehabil*, 8(3):45–53, 2001.

[181] M. Wolf, U. Wolf, V. Toronov, A. Michalos, L. A. Paunescu, J. Choi, and E. Gratton. Different time evoluion of oxyhemoglobin and deoxyhemoglobin concentration changes in visual and motor cortices during functional stimulation: A near-infrared spectroscopy study. *Neuroimage*, 16(3 Pt 1):704–712, 2002.

[182] A. J. Wolfberg and A. J. du Plessis. Near-infrared spectroscopy in the fetus and neonate. *Clin Perinatol*, 33(3):707–728, 2006.

[183] J. Wolpaw, D. J. McFarland, T. M. Vaughan, and G. Schalk. The Wadsworth Center brain-computer interface (BCI) research and development program. *IEEE Trans Neural Syst Rehabil Eng*, 11:204–207, 2003.

[184] J. R. Wolpaw, N. Birbaumer, D. J. McFarland, G. Pfurtscheller, and T. M. Vaughan. Brain-computer interfaces for communication and control. *Clin Neurophysiol*, 113:767–791, 2002.

[185] J. R. Wolpaw and D. J. McFarland. Multichannel EEG-based brain-computer communication. *Electroencephalogr Clin Neurophysiol*, 90(6):444–449, 1994.

[186] S. C. Wriessnegger, J. Kurzmann, and C. Neuper. Spatio-temporal differences in brain oxygenation between movement execution and imagery: a multichannel near-infrared spectroscopy study. *Int J Psychophysiol*, 67(1):54–63, 2008.

[187] H. Yang, Y. Wang, Z. Zhou, H. Gong, Q. Lou, Y. Wang, and Z. Lu. Sex differences in prefrontal hemodynamic response to mental arithmetic as assessed by near-infrared spectroscopy. *Gend Med*, 6(4):565–574, 2009.

[188] Q. Zhang, D. H. Brooks, M. A. Franceschini, and D. A. Boas. Eigenvector-based spatial filtering for reduction of physiological interference in diffuse optical imaging. *J Biomed Opt*, 10(1):11014, 2005.

[189] Q. Zhang, G. E. Strangman, and G. Ganis. Adaptive filtering to reduce global interference in non-invasive NIRS measures of brain activation: how well and when does it work? *Neuroimage*, 45(3):788–794, 2009.